IEC PAS 63184

Edition 1.0 2021-05

PUBLICLY AVAILABLE SPECIFICATION

PRE-STANDARD

colour inside

Assessment methods of the human exposure to electric and magnetic fields from wireless power transfer systems – Models, instrumentation, measurement and numerical methods and procedures (frequency range of 1 kHz to 30 MHz)

IEC PAS 63184:2021-05(en)

IEC Central Office
3, rue de Varembé
CH-1211 Geneva 20
Switzerland

Tel.: +41 22 919 02 11
info@iec.ch
www.iec.ch

About the IEC
The International Electrotechnical Commission (IEC) is the leading global organization that prepares and publishes International Standards for all electrical, electronic and related technologies.

About IEC publications
The technical content of IEC publications is kept under constant review by the IEC. Please make sure that you have the latest edition, a corrigendum or an amendment might have been published.

IEC publications search - webstore.iec.ch/advsearchform
The advanced search enables to find IEC publications by a variety of criteria (reference number, text, technical committee, …). It also gives information on projects, replaced and withdrawn publications.

IEC Just Published - webstore.iec.ch/justpublished
Stay up to date on all new IEC publications. Just Published details all new publications released. Available online and once a month by email.

IEC Customer Service Centre - webstore.iec.ch/csc
If you wish to give us your feedback on this publication or need further assistance, please contact the Customer Service Centre: sales@iec.ch.

IEC online collection - oc.iec.ch
Discover our powerful search engine and read freely all the publications previews. With a subscription you will always have access to up to date content tailored to your needs.

Electropedia - www.electropedia.org
The world's leading online dictionary on electrotechnology, containing more than 22 000 terminological entries in English and French, with equivalent terms in 18 additional languages. Also known as the International Electrotechnical Vocabulary (IEV) online.

IEC PAS 63184

Edition 1.0 2021-05

PUBLICLY AVAILABLE SPECIFICATION

PRE-STANDARD

colour inside

Assessment methods of the human exposure to electric and magnetic fields from wireless power transfer systems – Models, instrumentation, measurement and numerical methods and procedures (frequency range of 1 kHz to 30 MHz)

INTERNATIONAL
ELECTROTECHNICAL
COMMISSION

ICS 17.220.20

ISBN 978-2-8322-9542-7

Warning! Make sure that you obtained this publication from an authorized distributor.

CONTENTS

INTERNATIONAL ELECTROTECHNICAL COMMISSION

_____

ASSESSMENT METHODS OF THE HUMAN EXPOSURE TO ELECTRIC AND MAGNETIC FIELDS FROM WIRELESS POWER TRANSFER SYSTEMS – MODELS, INSTRUMENTATION, MEASUREMENT AND NUMERICAL METHODS AND PROCEDURES (FREQUENCY RANGE OF 1 kHz TO 30 MHz)

FOREWORD

1) The International Electrotechnical Commission (IEC) is a worldwide organization for standardization comprising all national electrotechnical committees (IEC National Committees). The object of IEC is to promote international co-operation on all questions concerning standardization in the electrical and electronic fields. To this end and in addition to other activities, IEC publishes International Standards, Technical Specifications, Technical Reports, Publicly Available Specifications (PAS) and Guides (hereafter referred to as "IEC Publication(s)"). Their preparation is entrusted to technical committees; any IEC National Committee interested in the subject dealt with may participate in this preparatory work. International, governmental and non-governmental organizations liaising with the IEC also participate in this preparation. IEC collaborates closely with the International Organization for Standardization (ISO) in accordance with conditions determined by agreement between the two organizations.
2) The formal decisions or agreements of IEC on technical matters express, as nearly as possible, an international consensus of opinion on the relevant subjects since each technical committee has representation from all interested IEC National Committees.
3) IEC Publications have the form of recommendations for international use and are accepted by IEC National Committees in that sense. While all reasonable efforts are made to ensure that the technical content of IEC Publications is accurate, IEC cannot be held responsible for the way in which they are used or for any misinterpretation by any end user.
4) In order to promote international uniformity, IEC National Committees undertake to apply IEC Publications transparently to the maximum extent possible in their national and regional publications. Any divergence between any IEC Publication and the corresponding national or regional publication shall be clearly indicated in the latter.
5) IEC itself does not provide any attestation of conformity. Independent certification bodies provide conformity assessment services and, in some areas, access to IEC marks of conformity. IEC is not responsible for any services carried out by independent certification bodies.
6) All users should ensure that they have the latest edition of this publication.
7) No liability shall attach to IEC or its directors, employees, servants or agents including individual experts and members of its technical committees and IEC National Committees for any personal injury, property damage or other damage of any nature whatsoever, whether direct or indirect, or for costs (including legal fees) and expenses arising out of the publication, use of, or reliance upon, this IEC Publication or any other IEC Publications.
8) Attention is drawn to the Normative references cited in this publication. Use of the referenced publications is indispensable for the correct application of this publication.
9) Attention is drawn to the possibility that some of the elements of this IEC Publication may be the subject of patent rights. IEC shall not be held responsible for identifying any or all such patent rights.

A PAS is an intermediate specification made available to the public and needing a lower level of consensus than an International Standard to be approved by vote (simple majority).

IEC PAS 63184 has been processed by IEC technical committee 106: Methods for the assessment of electric, magnetic and electromagnetic fields associated with human exposure.

The text of this PAS is based on the following document:	This PAS was approved for publication by the P-members of the committee concerned as indicated in the following document
Draft PAS	**Report on voting**
106/529/DPAS	106/532/RVDPAS

Following publication of this PAS, which is a pre-standard publication, the technical committee or subcommittee concerned may transform it into an International Standard.

This PAS shall remain valid for an initial maximum period of 2 years starting from the publication date. The validity may be extended for a single period up to a maximum of 2 years, at the end of which it shall be published as another type of normative document, or shall be withdrawn.

IMPORTANT – The "colour inside" logo on the cover page of this document indicates that it contains colours which are considered to be useful for the correct understanding of its contents. Users should therefore print this document using a colour printer.

INTRODUCTION

The scope of this document falls under the IEC work item "development of standard for measurement and calculation methods used to assess human exposure to electric, magnetic and electromagnetic fields." Wireless power transfer (WPT) is the transmission of electrical power from a transmitter to a receiver without current-carrying wires. This technology is increasingly being implemented in a wide range of applications at different frequency ranges from consumer electronics (e.g. mobile phones, tablet PCs) to automotive (electric vehicles (EVs)). The human exposure is limited to avoid hazardous nerve effects (< 10 MHz) and thermal effects (> 100 kHz). An ITU-R published report (ITU-R SM. 2303-1) from June 2015 on WPT systems describes RF exposure assessment methodologies, yet no definitive assessment method was introduced. An exposure assessment method of WPT for EV was described in IEC 61980-3:2019, however, there is currently no other product standard related to WPT. As WPT systems will become ubiquitous in a multitude of applications in the near future, IEC and IEEE established a joint working group to address WPT assessment methods related to human exposures to electric, magnetic and electromagnetic fields.

In this document, IEC TC 106 describes the basic methods to assess the direct and indirect effects of exposure to WPT systems, case studies, and relevant research. These methods mainly focus on frequency up to 30 MHz to consider both stimulation and thermal effects. The document specifies:

- assessment procedures (Clause 5);
- measurement methods (Clause 6);
- numerical assessment methods (Clause 7);
- assessment combining measurement and numerical methods (Clause 8).

ASSESSMENT METHODS OF THE HUMAN EXPOSURE TO ELECTRIC AND MAGNETIC FIELDS FROM WIRELESS POWER TRANSFER SYSTEMS – MODELS, INSTRUMENTATION, MEASUREMENT AND NUMERICAL METHODS AND PROCEDURES (FREQUENCY RANGE OF 1 kHz TO 30 MHz)

1 Scope

The objective of this document is to specify the assessment methods to evaluate compliance of stationary and dynamic wireless power transfer (WPT) systems with electromagnetic human exposure guidelines (external electric and magnetic fields, specific absorption rate (SAR), internal electric fields or current density including contact currents). The frequency range of this document is from 1 kHz to 30 MHz.

2 Normative references

The following documents are referred to in the text in such a way that some or all of their content constitutes requirements of this document. For dated references, only the edition cited applies. For undated references, the latest edition of the referenced document (including any amendments) applies.

IEC 60050 (all parts), *International Electrotechnical Vocabulary* (available at http://www.electropedia.org)

ISO/IEC Guide 98-1:2009, *Uncertainty of measurement – Part 1: Introduction to the expression of uncertainty in measurement*

ISO/IEC Guide 98-3:2008, *Uncertainty of measurement – Part 3: Guide to the expression of uncertainty in measurement (GUM:1995)*

IEC 61786-1:2013, *Measurement of DC magnetic, AC magnetic and AC electric fields from 1 Hz to 100 kHz with regard to exposure of human beings – Part 1: Requirements for measuring instruments*

IEC 61786-2:2014, *Measurement of DC magnetic, AC magnetic and AC electric fields from 1 Hz to 100 kHz with regard to exposure of human beings – Part 2: Basic standard for measurements*

3 Terms and definitions

For the purposes of this document, the following terms and definitions apply.

ISO and IEC maintain terminological databases for use in standardization at the following addresses:

- IEC Electropedia: available at http://www.electropedia.org/
- ISO Online browsing platform: available at http://www.iso.org/obp

3.1
basic restriction
BR
restriction on exposure to time-varying electric, magnetic and electromagnetic fields that is based directly on established health effects.

Note 1 to entry: Examples of basic restrictions can be found in Annex II of the Council Recommendation 1999/519/EC [1], ICNIRP Guidelines [2], [3], [4], IEEE Std C95.6 [5] and IEEE Std C95.1 [6], [7], [8].

[SOURCE: IEC 62311:2019 [12], 3.1.2]

3.2
complex relative permittivity
under sinusoidal conditions in a medium where the phasors $\underline{\boldsymbol{D}}$ and $\underline{\boldsymbol{E}}$ representing respectively the electric flux density and the electric field strength are linearly related, complex quantity $\underline{\varepsilon}_r$ defined by the relation

$$\underline{\boldsymbol{D}} = \varepsilon_0 \underline{\varepsilon}_r \underline{\boldsymbol{E}}$$

where ε_0 is the electric constant

Note 1 to entry: The complex relative permittivity is generally frequency dependent. For an isotropic medium the complex relative permittivity is a scalar; for an anisotropic medium it is a tensor.

Note 2 to entry: Generally $\underline{\varepsilon}_r$ is expressed as $\underline{\varepsilon}_r = \varepsilon_r' - j\varepsilon_r''$ where ε_r' is the real relative permittivity and ε_r'' is the dielectric loss index which represents dielectric losses.

[SOURCE: IEC 60050-121:2019, 121-12-14]

3.3
contact current
<for human body> current flowing into the body resulting from contact with a conductive object in an electromagnetic field.

Note 1 to entry: This is the localized current flow into the body (usually the hand, for a light brushing contact).

3.4
coupling factor
factor which correlates the measured incident field to the induced field in the human body

3.5
current density
<in a body> current density induced inside the body as a result of exposure to electromagnetic fields.

3.6
device under test
DUT
device that is tested according to the procedures specified in this document.

3.7
direct effect
biological effect resulting from direct interaction of electromagnetic field with biological structures.

[SOURCE: ICNIRP Guidelines:2010 [3]]

3.8
dynamic wireless power transfer
DWPT
transmission of electrical energy by electromagnetic fields, in which the secondary device (connected to the electrical load) is intentionally moving with respect to the primary device (connected to the power source) or along a track of multiple power sources acting as the primary device.

3.9
electric field strength
vector field quantity $\boldsymbol{E}$ which exerts on any charged particle at rest a force $\boldsymbol{F}$ equal to the product of $\boldsymbol{E}$ and the electric charge Q of the particle:

$$\boldsymbol{F} = Q\,\boldsymbol{E}$$

[SOURCE: IEC 60050-121:1998, 121-11-18]

3.10
exposure
<of a body> situation that occurs wherever a person is subjected to electric, magnetic or electromagnetic fields

3.11
incident field
field that would exist in the absence of a person at a point where a person could be located

Note 1 to entry: In some documents, the incident field is called an unperturbed field or environmental field.

3.12
indirect effect
biological effect resulting from indirect interactions of electromagnetic fields with biological structures such as contact currents

3.13
internal electric field
<in a body> electric field induced inside the body as a result of exposure to electromagnetic fields

3.14
magnetic field gradient
variation of the magnetic field with respect to the position

3.15
magnetic field strength
magnitude of the vector quantity obtained at a given point by subtracting the magnetization M from the magnetic flux density B divided by the magnetic constant μ_0

[SOURCE: IEC 60050-121:1998, 121-11-56, modified – "magnitude of the" has been added at the start of the definition.]

3.16
peak spatial-average SAR
psSAR
maximum average SAR within a local region based on a specific averaging volume or mass, e.g. any 1 g or 10 g of tissue in the shape of a cube

3.17
phantom
physical model with an equivalent human anatomy and comprised of a tissue-equivalent medium with dielectric properties specified in this document

[SOURCE: IEC/IEEE 62209-1528 [15]]

3.18
reference level
<of a field> field level derived from the basic restrictions under worst-case assumptions (e.g. exposure to a homogeneous field) used for the assessment of incident fields

Note 1 to entry: Examples of reference level can be found in Annex II of the Council Recommendation 1999/519/EC [1], ICNIRP Guidelines [2], [3], [4], IEEE Std C95.6 [5] and IEEE Std C95.1 [6], [7], [8].

3.19
specific absorption rate
SAR
measure of the rate at which energy is absorbed by the human body when exposed to a radio frequency electromagnetic field

Note 1 to entry: The SAR in the tissue-equivalent medium can be determined by the rate of temperature increase or by E-field measurements, according to the following formulas:

$$SAR = \frac{\sigma E^2}{\rho}$$

$$SAR = c_h \left.\frac{\partial T}{\partial t}\right|_{t=0}$$

where

SAR is the specific absorption rate in W/kg;

E is the RMS value of the electric field strength in the tissue medium in V/m;

σ is the electrical conductivity of the tissue medium in S/m;

ρ is the mass density of the tissue medium in kg/m^3;

c_h is the specific heat capacity of the tissue medium in J/(kg K);

$\left.\frac{\partial T}{\partial t}\right|_{t=0}$ is the initial time derivative of temperature in the tissue medium in K/s.

[SOURCE: IEC/IEEE 62209-1528 [15]]

3.20
stationary wireless power transfer
SWPT
transmission of electrical energy by electromagnetic fields, in which the primary device (connected to the power source) and the secondary device (connected to the electrical load) do not intentionally change their relative position and orientation, throughout the duration of the power transfer

3.21
wireless power transfer
WPT
transmission of electrical energy by electromagnetic fields

Note 1 to entry: SWPT and DWPT are WPT systems.

4 Symbols and abbreviated terms

4.1 Physical quantities

The internationally accepted SI units are used throughout this document.

Symbol	Quantity	Unit	Dimensions
B	Magnetic flux density	tesla	T
C_h	Specific heat capacity	joule per kilogram per kelvin	J/(kg K)
E	Electric field strength	volt per metre	V/m
f	Frequency	hertz	Hz
H	Magnetic field strength	ampere per metre	A/m
J	Current density	ampere per square metre	A/m^2
P	Average (temporal) absorbed power	watt	W
T	Temperature	kelvin	K
ε	Permittivity	farad per metre	F/m
λ	Wavelength	metre	m
σ	Electric conductivity	siemens per metre	S/m

NOTE In this document temperature is quantified in degrees Celsius, as defined by: T (°C) = T (K) − 273,15.

4.2 Constants

Symbol	Physical constant	Magnitude
η_0	Intrinsic impedance of free space	$120\pi\ \Omega$ or $377\ \Omega$
ε_0	Permittivity of free space	$8{,}854 \times 10^{-12}$ F/m
μ_0	Permeability of free space	$4\pi \times 10^{-7}$ H/m

4.3 Abbreviated terms

BEM boundary element method
BR basic restriction
DUT device under test
EV electric vehicle
FDFD finite difference frequency domain
FDTD finite difference time domain
FEM finite element method
FIT finite integration technique
GGSM generic gradient source model
IM impedance method
MoM method of moments
RF radio frequency
RL reference level
RMS root mean square
RSS root sum square
SAR specific absorption rate

psSAR peak spatial-average SAR
SPFD scalar potential finite difference
WPT wireless power transfer

5 Assessment procedures

5.1 General

Figure 1 presents a flowchart for the assessment procedure for evaluating both the direct effects (internal electric field, current density, and/or SAR) and indirect effects (contact current) of electromagnetic fields generated by WPT systems. The assessment methods for these quantities are different.

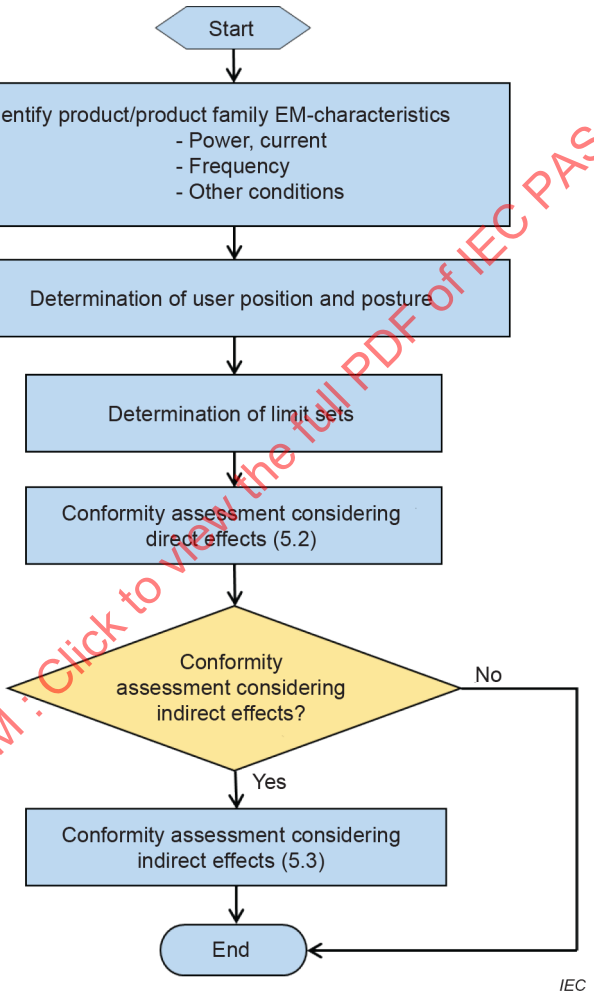

Figure 1 – Flowchart for the assessment procedure

5.2 Conformity assessment considering direct effects

5.2.1 General

This clause provides basic assessment methods considering the direct effects of electromagnetic fields [2], [3], [4], [5], [6], [7], [8]. Evaluations are made either against basic restrictions or against derived reference levels. In the international guidelines, different limits on basic restrictions and reference levels are defined for thermal and stimulation effects. Figure 2 describes four steps to assess exposure from WPT and demonstrate conformity with the basic restrictions or reference levels. Any of the four steps can be selected, depending on which is the most practicable for the exposure scenario. While the evaluation based on coil current (5.2.2) is the easiest method, followed by the evaluation of incident fields against reference levels (5.2.3), those methods are more conservative than the conformity assessment considering basic restrictions. The evaluation of internal E-field, current density and/or SAR against basic restrictions (5.2.5) represents practical exposure conditions without additional assumptions. The evaluation of incident fields against basic restrictions (5.2.4) is another method to evaluate incident fields and to assess the in-body quantities from the incident fields.

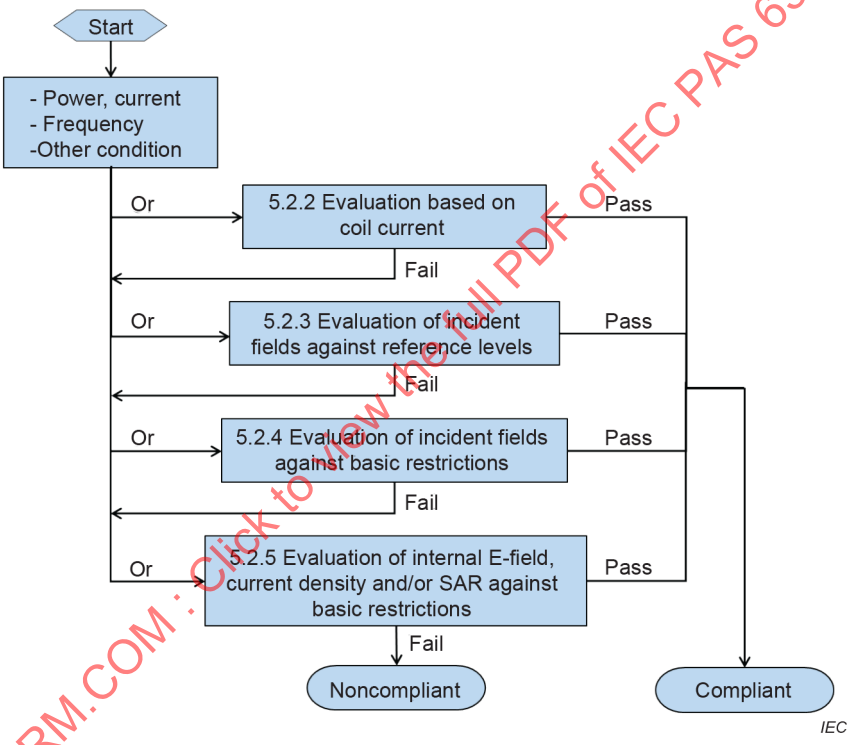

Figure 2 – Flowchart for the assessment procedure considering the direct effect

5.2.2 Evaluation based on coil current

The maximum permissible coil current I_{lim} can be assessed by evaluating the magnetic flux density of a circular coil at a fixed distance of 1 cm and comparing it against the reference level B_{lim}. For a circular coil with radius r, I_{lim} can be calculated using Formula (1):

$$I_{\text{lim}}(r) = \frac{2\pi d_0 B_{\text{lim}}}{\mu_0 n} \mathrm{e}^{\frac{r_0}{r}} \tag{1}$$

where

r is the coil radius (> 50 mm);

d_0 is the fixed distance of 10 mm at which the magnetic flux density is compared to B_{lim};

B_{lim} is the reference level of magnetic flux density;

μ_0 is the free space permeability;

n is the number of turns of the coil;

r_0 is a constant of 21,5 mm.

Formula (1) is based on an approximation of the Biot-Savart integral for a circular loop. The accuracy of this approximation is better than 0,25 dB for coil radii within the limits given above. It is conservative for any coil shape if r is set to infinity.

Annex A provides additional information regarding exposure evaluations using approximations.

5.2.3 Evaluation of incident fields against reference levels

Both incident electric and magnetic field strengths are measured or calculated at different distances including the closest distance and in all directions where the DUT can operate near people. When the field is uniform over the area of interest, the measured or calculated values of electric and magnetic fields are compared to the reference level. In the case of non-uniform fields, the measured or calculated field values may be spatially averaged over the exposed regions of the body.

5.2.4 Evaluation of incident fields against basic restrictions

5.2.4.1 General

The reference levels of electromagnetic fields are derived from the maximum coupling conditions between the fields and the human body, i.e. the maximum induced quantities in the human body exposed to the uniform electromagnetic fields. In many situations of localized exposure, such as in the vicinity of WPT systems, the evaluations are too conservative when the maximum or spatial average value is compared to the reference levels of EMF.

Coupling factors can be applied for the incident field to mitigate the over-estimation and still warrant conservativeness with respect to the basic restrictions.

$$\text{QoI} = k \times F \tag{2}$$

where QoI is the quantity of interest to be compared to the limits, k is a generic coupling factor that shall be derived according to 5.2.4.2 for specific coil configurations and evaluation distances or according to 5.2.4.3 for the generic gradient source model (GGSM), and F is the measured incident field at the location of the evaluation.

Two methods are defined: the coupling factor k_{L} is estimated from localized exposure scenarios based on the concept described in the IEC 62233 [9], and the generally applicable coupling factor k_{G} is characterized with respect to the incident field gradient at the location of the exposure evaluation by applying the GGSM method [10].

5.2.4.2 Coupling factor k_{L} based on the analysis of localized exposure scenarios

The coupling factor was originally introduced for exposure assessments in low frequencies in IEC 62226-2-1 [11] and IEC 62311 [12], then amended in IEC 62233 [9]. The coupling factor for the current density $k_{\text{L},J}$ is defined by Formula (3).

$$k_{\mathrm{L},J} = \frac{J_{\max} / B_{\max}}{J_{\lim} / B_{\lim}} \tag{3}$$

where

$J_{\max}$ is the maximum current density induced in the human body;

$B_{\max}$ is the maximum magnetic flux density in the absence of a person at a point where a person could be located;

$J_{\lim}$ is the basic restriction of current density;

$B_{\lim}$ is the reference level of magnetic flux density.

Using this coupling factor, the measured magnetic field strength, multiplied by the coupling factor, can be compared to the reference level directly.

Instead of estimating the coupling factor by the measured gradient of the magnetic field, the coupling factor can be numerically derived by the incident magnetic field and the current density from Formula (3). If the typical value of the coupling factor is defined for a particular type of WPT product, the compliance assessment can be performed by comparing the multiplied value of the measured magnetic field strength and the coupling factor to the reference level of the magnetic field strength.

The concept of compliance using coupling factor is expanded to the internal electric field and local SAR [13], [14].

$$k_{\mathrm{L},E} = \frac{E_{\max} / B_{\max}}{E_{\lim} / B_{\lim}} \tag{4}$$

$$k_{\mathrm{L},SAR} = \frac{\sqrt{SAR_{\max}} / B_{\max}}{\sqrt{SAR_{\lim}} / B_{\lim}} \tag{5}$$

where

$E_{\max}$ is the maximum internal electric field induced in human body;

$E_{\lim}$ is the basic restriction of internal electric field strength;

$SAR_{\max}$ is the maximum SAR induced in human body;

$SAR_{\lim}$ is the basic limit for local SAR.

Conservative coupling factors k_{L} are typically determined by numerical simulation with the ratio of the induced quantities to the incident magnetic field [13], [14], e.g. for a specific frequency, field distribution, distance to human body and for different anatomies. Based on such an evaluation, conservative values of the coupling factors can be derived.

$E_{\lim}$ and $B_{\lim}$ depend on frequency. The coupling factor k_{L} is multiplied by the measured magnetic fields to consider the effects of field non-uniformity. Compliance with basic restrictions (internal electric field strength, current density or local SAR) is then assessed by comparing the multiplied value to the reference level of the magnetic fields only.

The method may be applied only if the following are true.

a) The induced quantities such as internal electric field, current density or SAR caused by incident electric fields are negligible compared to those induced by the incident magnetic fields.

b) The whole-body average SAR is negligible compared to respective limits and the contribution of the localized average SAR (psSAR) or the internal electric field is dominant.

c) Evaluation conditions such as frequency, field distribution, distance to human body, etc., are identical to those used in the derivation of the coupling factor. Otherwise the uncertainty due to the deviation must be determined.

5.2.4.3 Coupling factor k_G based on the GGSM method

A generally applicable coupling factor $k_G(G_n)$ was proposed using a GGSM in [10] to mitigate over-estimation by incident magnetic field assessment in strong field gradients that are common in the vicinity of WPT systems. The method is conservative for real sources, as the coupling factors are derived from a 2D gradient model, whereas real sources have gradient in 3D. However, it requires measuring both the local field amplitude and the local gradient.

The method is based on the following quantities of the incident magnetic field:

– frequency;

– B-field amplitude (B_{xyz});

– local B-field gradient G_n (T/m/T) at any point in free space.

A GGSM source consists of a two-line magnetic field source. The induced fields are normalized to the maximum B-field amplitude and gradient at the skin. Based on a large-scale numerical study including human body models of different ages, heights, and weights [10], worst-case exposure conditions were determined for each gradient and frequency analysed. Coupling factors $k_G(G_n)$ are determined per Formula (6):

$$k_{G,QoI} = \frac{QoI_{max}(G_n)/B_{max}(G_n)}{QoI_{BR}/B_{RL}} \tag{6}$$

where $QoI_{max}(G_n)$ represents the maximum of the induced metric of interest (electric field, current density or SAR) in the body when the field gradient is G_n, $B_{max}(G_n)$ is the maximum measured B-field at the human body surface, QoI_{BR} is the basic restriction of the induced metric QoI and B_{RL} is the reference level of the magnetic flux density B.

The coupling factors related to each specific induced metric defined by the guidelines are then expressed by physics-based approximation – Formula (7) through Formula (10) – as a function of the gradient:

$$k_{G,E;ICNIRP\,2010}(G_n) = \frac{1}{\left[1+6{,}5\times10^{-6}\times(G_n/c_3)^{5,8}\right]^{(1/5,8)}} \tag{7}$$

$$k_{G,E;IEEE\,2005}(G_n) = \frac{1}{\left[1+4\times10^{-11}\times(G_n/c_3)^{6,6}\right]^{(1/6,6)}} \tag{8}$$

$$k_{G,J;ICNIRP\,1998}(G_n) = \frac{1}{\left[1+4\times10^{-3}\times(G_n/c_3)^{2,9}\right]^{(1/2,9)}} \tag{9}$$

$$k_{\mathrm{G},psSAR\,10\,\mathrm{g}}\left(G_n\right)=\frac{1}{\left[1+2\times10^{-1}\times\left(G_n/c_3\right)^{1,2}\right]^{(1/1,2)}} \tag{10}$$

where c_3 = 1 m^{-1}.The trend of the approximation formulas as a function of the gradient is shown in Figure 3. The method has been analytically verified (see Appendix of [10]).

To test compliance with basic restrictions, the WPT system is evaluated by measuring the magnetic field amplitude (B_{meas}) and the field gradient ($G_{n,\mathrm{meas}}$) at any closest accessible location from the source using equipment that provides both values or measures the field using a field meter at different locations and derives the gradient. The internal electric field, current density and SAR can then be predicted by Formula (11), Formula (12), and Formula (13):

$$E=k_{\mathrm{G},E}\left(G_{n,\mathrm{meas}}\right)\times E_{\mathrm{BR}}\times\frac{B_{\mathrm{inc,meas}}}{B_{\mathrm{RL}}} \tag{11}$$

$$J=k_{\mathrm{G},J}\left(G_{n,\mathrm{meas}}\right)\times J_{\mathrm{BR}}\times\frac{B_{\mathrm{inc,meas}}}{B_0} \tag{12}$$

$$SAR=k_{\mathrm{G},SAR}\left(G_{n,\mathrm{meas}}\right)\times SAR_{\mathrm{BR}}\times\left(\frac{B_{\mathrm{inc,meas}}}{B_0}\right)^2\times\left(\frac{f}{f_0}\right)^2\times2\times10^{-4} \tag{13}$$

where:

$k(G_{n,\mathrm{meas}})$ is the value of the coupling factor calculated for the specific measured gradient $G_{n,\mathrm{meas}}$;

$B_{\mathrm{inc,meas}}$ is the local magnetic field measured by the field gradient probe;

B_0 is the magnetic flux density, which corresponds to the B_{RL} of 6,25 µT for frequencies from 3 kHz to 150 kHz. For higher frequencies, the reference level needs be appropriately adjusted;

f_0 is a constant normalization frequency of 100 kHz.

The method may be applied only if the following are true.

a) The induced quantities caused by incident electric fields are negligible compared to those by incident magnetic fields.

b) The incident magnetic field is dominated by a single source.

d) The whole-body average SAR is negligible compared to the respective limits and the contribution of the localized average SAR or the internal electric field is dominant.

e) Quasi-static conditions (7.2) apply for the incident magnetic field.

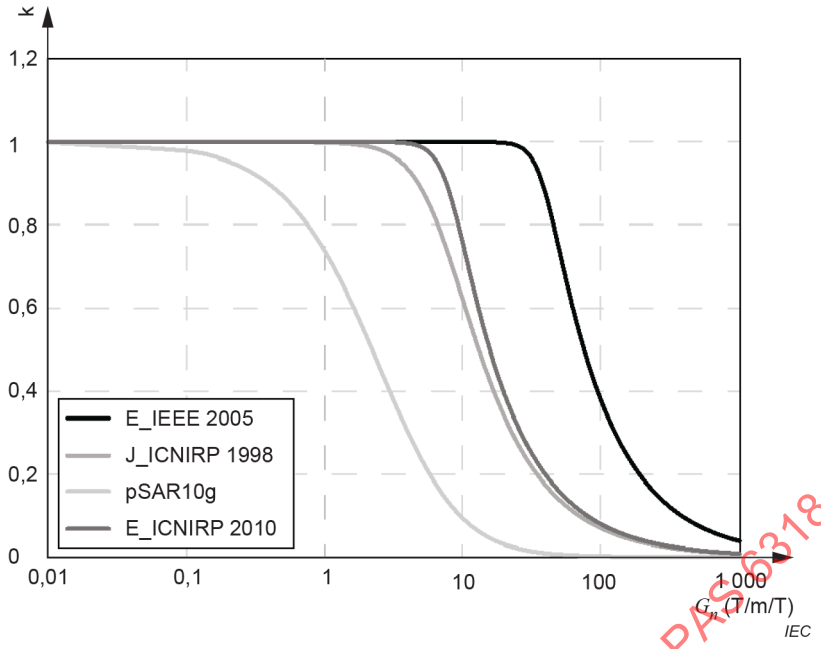

Figure 3 – Trend of the approximation formulas as a function of the gradient [10]

5.2.5 Evaluation of internal E-field, current density and/or SAR against basic restrictions

SAR can be measured using a small probe in a liquid-filled phantom model of the human body, which is exposed to electromagnetic fields created by the DUT. Measured values can be directly compared with basic restrictions. The evaluation and validation procedure are described in IEC/IEEE 62209-1528 [15], whose frequency range is 4 MHz to 10 GHz. The assessment method is described in detail in 6.2.

Internal electric field, current density or SAR can be calculated by numerical simulation using anatomical human models, analytical methods, etc. for comparison with basic restrictions. The simulation model and methodology need to be validated prior to evaluation. The assessment method based on numerical simulation is described in detail in Clause 7.

5.3 Conformity assessment considering indirect effect

This subclause describes the basic assessment methods considering the indirect effect of electromagnetic fields. Contact currents are the only indirect effects considered in this document. Contact currents flow into a biological body via a contacting electrode or other source of current.

Contact currents can be assessed either by incident electromagnetic fields or direct measurement.

The following two considerations must be applied to ensure compliance by incident electromagnetic fields.

– Incident electric field levels to prevent adverse indirect effects of contact current (shocks and burns) are shown in the guidelines [2], [3], [4].

– Incident magnetic field levels to prevent adverse indirect effects of contact currents can be calculated by the current induced in the loop formed with the grounded metal and the human body with Formula (14).

$$H = \frac{Z}{2\pi f \mu_0 S} I_c \tag{14}$$

where

I_c is contact current (A);

Z is the impedance of the human body (Ω) (see 6.3);

S is the area of the loop such as 1,5 m × 0,5 m.

Contact currents can also be directly measured by a contact current meter with an ungrounded or grounded metal object placed in the vicinity of the WPT systems. Figure 4 shows exposure situations for ungrounded and grounded metal objects.

Figure 5 presents a flowchart for the assessment procedure. Details of measurement conditions, measurement setup, etc., are summarized in IEC TR 63167 [16]. The assessment method is described in detail in 6.3.

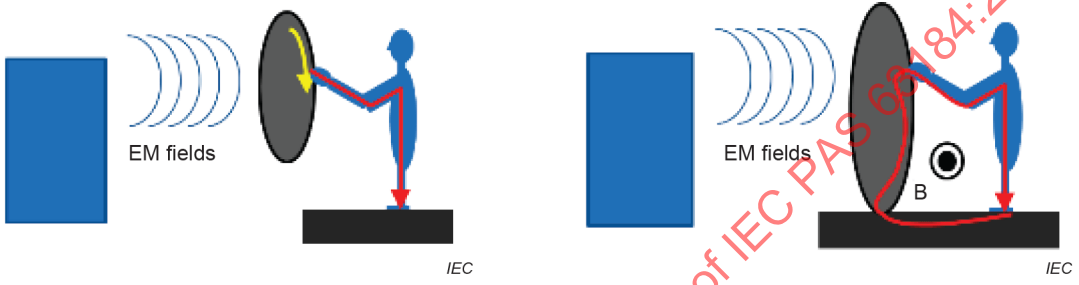

a) Currents when touching ungrounded metal

b) Currents when touching grounded metal

Figure 4 – Two exposure situations for ungrounded and grounded metal objects

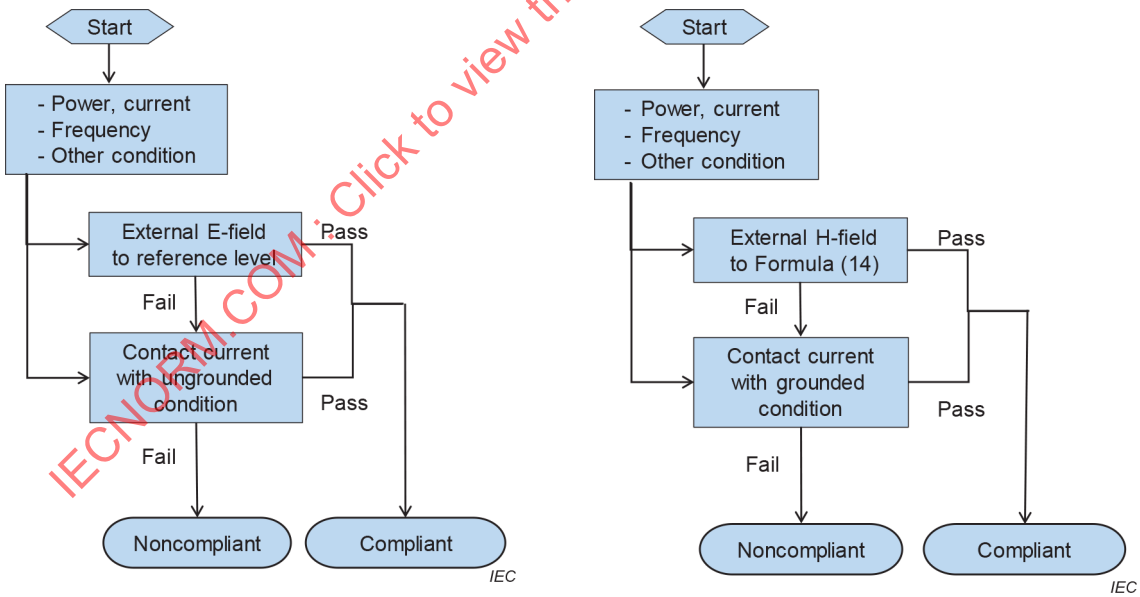

a) ungrounded condition (incident E)

b) grounded condition (incident H)

Figure 5 – Flowchart for assessment procedures for indirect effects

6 Measurement methods

6.1 Incident fields

6.1.1 General procedure

IEC 61786-1:2013 [17] and IEC 61786-2:2014 [18] describe electromagnetic field basics, measurement methods, and requirements of the measurement equipment at frequencies below 100 kHz. In addition, IEC 62233 [9] and IEC 62311 [12], [19] describe electromagnetic field measurements based on guidelines conformity assessment.

a) Equipment for measuring electric fields, magnetic fields, and magnetic field gradient is described in 6.1.2.1, 6.1.2.2, and 6.1.2.3, respectively. The calibration methods are described in Annex B.

b) The validation method is described in Annex C.

c) Both incident electric and magnetic field strengths are measured at a specific distance including the closest distance and in all directions where the DUT may operate near people. These International Standards specify measurement positions based on the size and regular usage of equipment. IEC 62311 [12], [19] specifies it as a "user's usual position". IEC 62233 [9] specifies the measurement position in detail for household appliances and similar apparatuses, including inductive battery chargers.

d) The measured value is based on the time average or maximum instantaneous value of the target electromagnetic field.

e) In principle, the measurement is performed in the space without the human body. In general, the existing position of the human body against the WPT cannot be determined completely. Therefore, typical measurement positions that are conservative with respect to human exposure shall be selected.

f) When the measurement probe comes close to the source and metallic and/or highly insulated objects, electromagnetic coupling may occur and the probe sensor impedance changes. In addition, large probes may cause electromagnetic field disturbances and averaging of the field over the antenna area. These measurement errors cannot be ignored. The measured value and its uncertainty need to be properly evaluated.

g) In the case of non-uniform fields, the measured field values may be spatially averaged over the exposed regions of the body, with the important proviso that the basic restrictions for local SAR and internal electric fields are not exceeded. In some cases, the concept of spatial averaging may be applicable. Whether or not averaging is applicable highly depends on the spatial field characteristics caused by the source and the distance of the exposed person to the source. If averaging is applied in the case where one or more of the measured values is above the reference levels or action levels, it is necessary to provide sound evidence that the assessment based on the averaged values does not lead to exceeding the underlying basic restrictions or exposure limit values, respectively.

h) The concept of spatially averaged exposure levels is applicable when the distance between the source and the body is greater than 20 cm, depending on the characteristics of the field source. The evidence and rationale, usage of the spatial averaging, and its precise method must be provided. Either the peak or spatially averaged field strength is compared to the applicable reference levels to determine compliance.

Assessment procedures for SWPT, heavy duty EVs, and drones are described in I.1, I.2, and I.3, respectively. Examples of assessment results are introduced in Annex J.

If the incident field consists of non-negligible multiple frequency components based on the guidelines, these contributions must be considered in the assessment. Summation regimes in Annex B of IEC 62311:2019 [19] can be applied to consider spectral contributions.

6.1.2 Equipment

6.1.2.1 Equipment for electric field measurement

Electric field strength can be measured by a calibrated antenna that is sensitive to electric fields exclusively (e.g. small dipoles) and connected to the calibrated measurement equipment.

Electric field measurement equipment is divided into two classes: one-axis-sensor types, and three-axis-sensor types in which three sensors are set perpendicular to one another. IEC 61786-2 [18] recommends using the three-axis type. Using single-axis instruments is possible in some cases, e.g. when the direction of the field is already known [17]. The electric field of the three-axis component readings given in Formula (15) applies.

$$E_{\mathrm{R}} = \sqrt{E_x^2 + E_y^2 + E_z^2} \tag{15}$$

where

E_x, E_y, and E_z are effective electric field strengths for the three orthogonal axes.

Three-axis electric field measurement equipment has the advantage of measuring the net field E_{R} irrespective of the probe orientation.

In general, there are two classes of measurement equipment for the electric field: broadband and narrowband. For both measurement systems, the equipment consists of an antenna (including power feeding section), measurement part, and data recording and processing unit. The following describes the system characteristics and selection method.

a) The broadband system uses dipole antennas. It is small enough to ensure uniform sensitivity at each frequency. To ensure isotropy, three antennas are generally placed orthogonal to one another and each signal or the combined signal is extracted. This type of antenna is suitable for near-field electromagnetic fields of complicated distributions. A broadband isotropic electric field strength meter designed for radio wave protection is typically used for measurement. Other systems may include waveform observation equipment, such as diode detectors and oscilloscopes.

b) The narrowband system is tuned to each target frequency. The measurement system generally has broad measurement frequencies, high receiving sensitivity and short responses. It is thus also suitable for pulsed waves or multiple sources. However, for the pulsed wave measurement, it is acceptable to measure in the frequency domain where the target frequency range is broader than the passband width of the measurement system. A biconical antenna with broadband characteristics is often used for far-field region because the size of the antenna is not electrically small. A three-axis orthogonal small dipole is suitable for near-field measurements.

c) For an electromagnetic environmental assessment, a broadband isotropic electric field strength meter is preferred unless the equipment cannot be measured properly with such a device, in which case it must be replaced by another measurement system.

When selecting a measurement system, the required performance, frequency response, and electromagnetic field strength range must be considered.

6.1.2.2 Equipment for magnetic field measurements

Search coil sensors are often used for a low frequency range of several hundred kilohertz and less. In general, the search coil probe is used for measuring environmental magnetic fields. The coil probe measures the induced voltage associated with the time-varying magnetic flux normal to the plane of the coil, averaged over the coil area. In a field that is uniform over the area of the coil, the induced voltage at the coil terminals is calculated according to Formula (16). All the quantities are in phasor forms.

$$V = -\mathrm{j}\omega NBS \tag{16}$$

where

V is the induced voltage;

ω is the angular frequency (= $2\pi f$);

N is the number of turns;

B is the magnetic flux density (normal to the plane of the coil);

S is the cross-sectional area of the coil.

To gain sufficient sensitivity, the area and winding number are increased, and the magnetic flux density is enhanced by using ferromagnetic material to the core of the coil. The signal is processed to gain flat frequency characteristics by an integrator in subsequent stages as the output is proportional to the frequency. The uncertainty for the measured field at the centre of the sensor caused by the extent of S has to be assessed for the maximum gradient field and shall be considered.

Magnetic field measurement equipment is divided into two classes: one-axis-sensor type and three-axis-sensor type in which three sensors are set perpendicular to one another. IEC 61786-2 [18] recommends using the three-axis type. The magnetic field of the three-axis component given in Formula (17) applies.

$$B_{\mathrm{R}} = \sqrt{B_x^2 + B_y^2 + B_z^2} \tag{17}$$

where

B_x, B_y, and B_z are effective magnetic flux densities for the three orthogonal axes.

Three-axis magnetic field measurement equipment has the advantage of measuring the net field B_{R} irrespective of the probe orientation.

6.1.2.3 Equipment for magnetic field gradient

The evaluation method based on the coupling factor as a function of the magnetic field gradient requires knowledge about the local B-field amplitude and gradient.

The magnetic field amplitude and gradient can be measured by sampling the field spatially in 3D around the location of exposure. The measurement can be performed by one field sensor or multiple isotropic magnetic field sensors. A probe with one sensor can be moved to measure the field at different locations of known spatial replacement, e.g. by a robot system if the test signal is repetitive and phase relation can be established. A probe with multiple sensors can be used to measure the gradient directly, e.g. an axial or planar gradiometer [9], [20], [21].

6.2 SAR

SAR can be measured experimentally and directly compared with the basic restrictions. The evaluation and validation procedures of SAR measurement for wireless communication devices are described in IEC/IEEE 62209-1528 [15], whose frequency range is 4 MHz to 10 GHz. Similar measurement procedures can be used for the WPT system. In this document, only the deviations required to assess the spatial peak SAR values of WPT systems are described. Clause B.2 describes the procedure for the measurement of the peak spatial-average SAR in a phantom model that simulates a human body exposed to electromagnetic fields generated by the WPT systems. Using an isotropic electric field probe, the local SAR inside an irradiated body model can be determined. A SAR measurement system consists of a suitable phantom, an electric field probe and a probe scanning system.

The physical characteristics of the phantom model (size, shape, electrical properties, etc.) must simulate the human exposure condition by the WPT system. Phantom models such as the elliptic phantom defined in IEC/IEEE 62209-1528 [15] may be used. The phantom model must consist of materials with dielectric properties similar to humans. At a frequency lower than 30 MHz, the electrical properties of the material are dominantly affected by the conductivity of the material. The liquid defined in IEC/IEEE 62209-1528 [15] may be used (Table 1) at frequencies between 4 MHz and 30 MHz. NaCl solution with an appropriate conductivity may also be used (Table 2). The relationship between conductivity and NaCl concentration is described in reference [22]. The dependency of SAR on phantom properties and size are shown in Annex D.

Table 1 – Dielectric properties of the tissue equivalent liquid as specified in IEC/IEEE 62209-1528

Frequency (MHz)	Real part of the complex relative permittivity, ε'_r	Conductivity, σ (S/m)
4	55	0,75
6	55	0,75
30	55	0,75

Table 2 – Dielectric properties of the tissue equivalent NaCl solution of 0,074 mol/L

Frequency (MHz)	Real part of the complex relative permittivity, ε'_r	Conductivity, σ (S/m)
4	77	0,75
6	77	0,75
30	77	0,75

The WPT system shall be operated at the closest compliance distance to the elliptical phantom. Due to the high SAR gradients of the induced field, measurements closer than 2 mm from the phantom surface shall be performed. If the boundary effect, which is caused by mutual interaction between the probe and the phantom surface, causes a large uncertainty in the measurement, the measurement may be performed at a distance of up to 2,5 cm from the phantom surface as long as it can provide a sufficient signal-to-noise ratio for the results. An extrapolation method (see Annex E) of the induced field may then be used to determine the SAR peak at the phantom surface. In that case, uncertainty due to the interpolation method with respect to SAR values shall be included in the uncertainty budget. The extension of the Area Scan or Fast Volume Scan (preferred) is used to determine the location of maximum SAR. It shall be 20 % larger than the source or as large as the phantom, whichever is smaller. The grid for the zoom scan to be performed around the locations of the SAR maxima (all peak SAR values within 2 dB of the global maximum) shall be in compliance with the requirements set forth in Table 4 of IEC/IEEE 62209-1528 [15].

6.3 Contact currents

6.3.1 General

IEC TR 63167 [16] introduces general information on the assessment of contact current related to human exposure to electric, magnetic, and electromagnetic fields including assumed situations and a proposed method for measuring contact currents.

6.3.2 Equipment

An electrical equivalent circuit human body impedance model, which is frequency dependent, is used to measure contact currents. Figure 6 shows an equivalent circuit, as depicted in IEC 60990 [23], that simulates a human body. Recently, several studies have evaluated human body impedance and proposed more precise equivalent circuits with a series of resistors and capacitors [24], [25], [26], [27]. The frequency characteristics of human body impedance with grasping conditions are compared in Figure 7. The impedance depends on area of contact and usually the impedance for grasping contact is lower than that for point contact. The assumed conditions of contact are "point contact" (area not specified) in ICNIRP guidelines [2], [3], and "touch contact" with a contact area of 1 cm^2 and "grasping contact" (applicable only for a controlled environment) with a contact area of 15 cm^2 for IEEE safety standards [5], [6], [7], [8].

Figure 8 shows the configuration of a contact current meter. The contact terminal is made of metal. If the target point of the contact part is painted, a 10 cm × 20 cm metal foil should be attached to it to simulate a hand palm contact, according to IEC 60990 [23]. A metal board equivalent to the size of a foot is used as the ground electrode. The contact current is measured from the current flowing through the equivalent circuit of the human inside the meter.

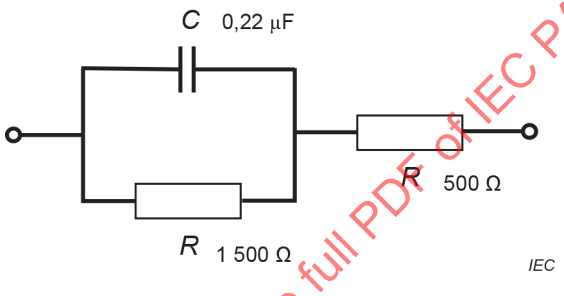

Figure 6 – Human body equivalent circuit proposed in IEC 60990 [23]

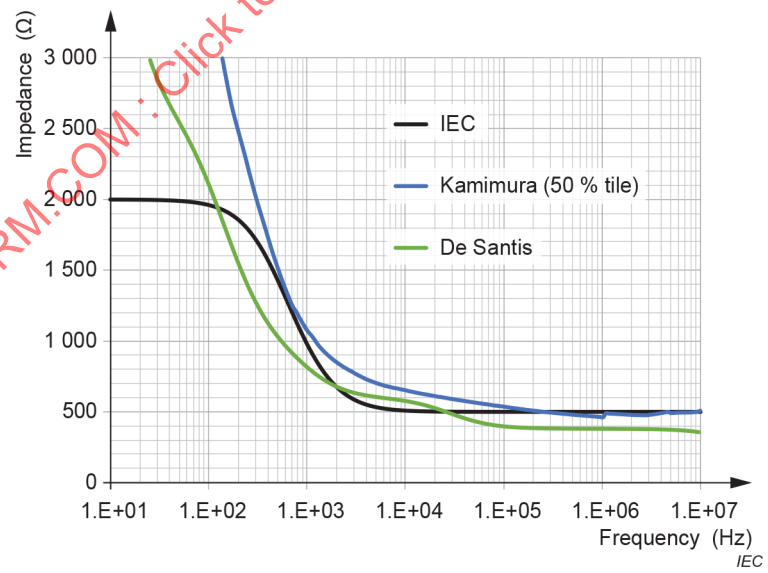

Figure 7 – Impedance frequency characteristics of adult male and equivalent circuits proposed in IEC 60990 [23] and evaluated values [24], [25], [26], [27]

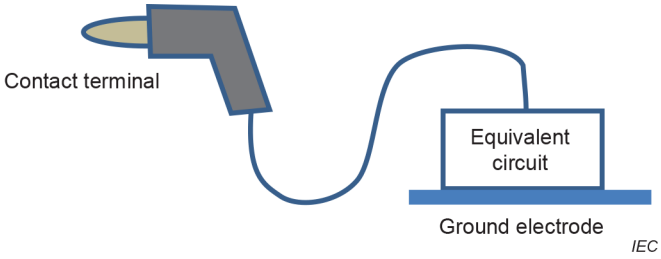

Figure 8 – Example of contact current measurement equipment

6.3.3 Measurements

The following issues must be considered for the measurement of contact currents.

- Select measurement system properly.
- Avoid electromagnetic field disturbances caused by the measurer and measurement systems as much as possible.
- Environmental conditions (temperature, humidity, vibration, electromagnetic field etc.) may affect the measurement equipment.
- Use a calibrated measurement system.

There are two types of measurements, depending on the expected exposure scenario.

a) Measurement methods using an ungrounded metal board
   1) Place a ground electrode where the human may stand.
   2) Place an ungrounded metal board large enough at the location where metal objects may exist in the actual usage condition. For an EV, a metal board larger than 1,2 m × 1,2 m may be used. Choose the closest position in the actual usage, as the contact current tends to become higher as metal objects come closer to the WPT system. Find the maximum condition of the contact current, as the metal board position (height) and direction may change the contact current strength.
   3) Touch the contact terminal to the metal board where the human may touch. Find a stable indicated value. Find the maximum value if there is a dependency on the touch position.

b) Measurement methods using a grounded metal board
   1) Place a ground electrode where the human may stand.
   2) Place a grounded metal board at the location where metal objects may exist in the actual usage condition. Choose the closest position in the actual usage, as the contact current tends to become higher as metal objects come closer to the WPT system. Find the maximum position of the contact current, as the metal board position (height) and direction may change the contact current strength.
   3) Touch the contact terminal to the metal board where the human may touch. The contact current becomes larger according to the magnitude of the interlinkage magnetic flux to a loop created by grounded metal board and human body. The size of the rectangular loop approximately 1,5 m (height) × 0,5 m (width) can be used to evaluate the contact current. Find the loop arrangement which gives the maximum contact current value.

7 Computational assessment methods

7.1 General

The internal electric field, psSAR or whole-body SAR for comparison with basic restrictions shall be calculated by numerical simulation using a representative set of anatomical human models. Calculations may be carried out using full wave methods or quasi-static methods depending on the electrical size of the problem. For quasi-static problems, the effect of the induced fields in the human body on the incident field source is assumed to be negligible. The incident fields and the induced fields can be evaluated in separate simulations using separate computational methods. For the calculation of the incident fields, analytical or quasi-analytical methods may be applicable. Table 3 summarizes the computational methods for exposure evaluation. A brief description of computational methods is also given in Annex F. Annex H describes averaging algorithms and code verification and model validation, respectively. Currently, there is no available body phantom to conservatively test for compliance of WPT systems with safety limits. Hence, the relevant induced fields need to be evaluated in a representative set of anatomical body models. These models shall include the following:

- availability of larger bodies, which have higher absorption rates of low frequency magnetic fields and smaller bodies (children), which can be closer to the field source;
- individual segmentation of the tissues of the central and peripheral nervous systems for evaluation with the respective basic restrictions;
- posable or movable limbs for the modelling of realistic exposure scenarios.

NOTE Numerical simulations can be also applied to assess the incident fields with respect to the reference levels.

All computational algorithms should be verified for technically correct implementation. Guidance is provided in Annex H.

Table 3 – Computational methods

Calculation method	Note
BEM (boundary element method)	Full-wave computation
FDFD (finite difference frequency domain)	Full-wave computation
FDTD (finite difference time domain)	Full-wave computation
FEM (finite element method)	Full-wave or quasi-static approximation computation
QS-FDTD	Quasi-static approximation computation
FIT (finite integration technique)	Full-wave computation
MoM (method of moments)	Full-wave computation
Hybrid method (e.g. MoM + FDTD)	Full-wave computation
SPFD (scalar potential finite difference)	Quasi-static approximation computation
IM (impedance method)	Quasi-static approximation computation

7.2 Quasi-static approximation

For the applicability of a computational method based on the quasi-static approximation, the upper frequency limit is defined considering the dimensions of the exposed body region or person, the size of the field source and the distance between them. The field source dimensions are referred to as feature size D hereinafter. The frequency limit is then given by the quasi-static approximation:

$$\left|\omega^2 \varepsilon \mu D^2\right| < x \ll 1 \Leftrightarrow \left(\frac{D}{\lambda}\right)^2 < x \ll 1 \tag{18}$$

or

$$\omega^2 \Re\{\varepsilon\} \mu D^2 < x \ll 1 \tag{19}$$

and

$$\omega \sigma \mu D^2 < x \ll 1 \tag{20}$$

where

ω is the angular frequency;

ε is the complex permittivity with the maximum absolute value within the exposed region;

μ is the permeability;

λ is the minimum wavelength within the exposed region;

x is a real number which shall be much smaller than 1;

σ is the conductivity.

For the calculation of the upper frequency limit for the application of quasi-static methods without considering an additional uncertainty, a value of x = 0,005 shall be applied.

NOTE If $x \geq 0{,}005$, the uncertainty posed by the quasi-static approximation is determined and considered.

7.3 Computational assessment against the basic restrictions

7.3.1 General

Depending on the applicable safety guidelines and on the frequency range, the basic restrictions on human exposure are defined in terms of:

- peak spatial average SAR [2], [4], [6], [7], [8] (7.3.2);
- whole-body average SAR [2], [4], [6], [7], [8] (7.3.3);
- averaged current density on a surface [2] (G.1);
- averaged E-field in a cubical volume [3] (G.2);
- averaged E-field along a line [5], [6], [7], [8] (G.3).

Different limits may apply for these quantities depending on the exposed body region. The numerical code or the applied post-processing techniques shall implement the required averaging methods. As the descriptions of the averaging algorithms in the exposure guidelines that define them are generally not sufficiently detailed for an implementation as a computational algorithm, this document refers to the respective numerical International Standards that define them or specifies its own algorithms if an appropriate definition is not available elsewhere. Details are given in 7.3.2, 7.3.3, and Annex G. The implementation of these algorithms should be validated according to the methods described in Annex H.

7.3.2 Peak spatial-average SAR

The peak spatial average SAR shall be evaluated according to IEC 62704-1 [28] for Cartesian meshes and according to IEC 62704-4 [29] for unstructured meshes.

7.3.3 Whole-body average SAR

The whole-body average SAR shall be evaluated according to IEC 62704-1 [28] for Cartesian meshes and according to IEC 62704-4 [29] for unstructured meshes.

8 Combination of measurement and computational assessment methods

8.1 General

As internal electric field, current density, or SAR are difficult to measure directly, the evaluation is often performed using computational approaches. However, it is difficult to accurately model an actual exposure situation in numerical simulations including an electric vehicle body, ground planes, etc. In addition, it is sometimes difficult to retrieve information about the size, shape, and design of the WPT systems. It is possible to evaluate internal electric field or SAR by an approach combining both the measurement of electromagnetic fields around the system and numerical analyses of induced quantities. The magnetic near-field data are first measured in the area occupied by the human body. Then, the measured magnetic fields are used as incident fields in the IM or SPFD to derive the internal electric field strength inside the human-body model.

8.2 Measurement of magnetic field

For the measurement of the magnetic field distribution in a frequency range below 10 MHz, search coil sensors are often used. Both amplitude and phase of the magnetic near-field shall be measured in the area occupied by the human body. To measure the phase of magnetic field, one magnetic sensor should be fixed at a specific position to retrieve the reference phase and the other sensor is moved over the area occupied by the human body.

8.3 Computational analyses of induced quantities

A realistic human model is used to calculate induced quantities. Numerical methods for the calculation of induced quantities are summarized in Annex F. For a low frequency region, measured magnetic field data is applied as the incident field in the numerical method such as IM or SPFD. Measured magnetic field data may be directly applied as a source in IM. However, since SPFD uses vector potentials as a source to calculate the internal electric field, the reconstruction of vector potentials from the measured magnetic field (H) or the magnetic flux density (B) is required. A finite number of samples of B from numerical simulations could be used for field reconstruction. Otherwise a finite number of sample measurements could be collected through ad-hoc field meters (monitor points). In this case the spatial coordinate of the collected measurement samples is also needed.

The procedure to reconstruct the B-field distribution *in silico* is described in [30]. The magnetic flux density is assumed to be $\boldsymbol{B} = u_x B_x + u_y B_y + u_z B_z$, which satisfies $\nabla \cdot \boldsymbol{B} = 0$, where $u_{x,y,z}$ are unit vectors. Hence it can be represented using a vector potential A, so that $\nabla \cdot \boldsymbol{A} = \boldsymbol{B}$. A vector potential is given by Formula (21), Formula (22), and Formula (23):

$$A_x = -\int_0^y \left[\frac{1}{3}B_z(x,y',z) + \frac{1}{6}B_z(x,y',0)\right] \mathrm{d}y' + \int_0^z \left[\frac{1}{3}B_y(x,y,z') + \frac{1}{6}B_y(x,0,z')\right] \mathrm{d}z' \quad (21)$$

$$A_y = -\int_0^z \left[\frac{1}{3}B_x(x,y,z') + \frac{1}{6}B_z(0,y,z')\right] \mathrm{d}z' + \int_0^x \left[\frac{1}{3}B_z(x',y,z) + \frac{1}{6}B_z(x',y,0)\right] \mathrm{d}x' \quad (22)$$

$$A_z = -\int_0^x \left[\frac{1}{3}B_y(x',y,z) + \frac{1}{6}B_y(x',0,z)\right] \mathrm{d}x' + \int_0^y \left[\frac{1}{3}B_x(x,y',z) + \frac{1}{6}B_x(0,y',z)\right] \mathrm{d}y' \quad (23)$$

Formula (21), Formula (22), and Formula (23) do not depend on electric or magnetic properties, therefore they are valid for any arbitrary inhomogeneous, anisotropic or nonlinear media.

8.4 Computational assessment against the basic restrictions

Details of the averaging algorithms are given in 7.3.

9 Uncertainty assessments

9.1 Measurement methods

In the following subclauses, the uncertainty sources that need to be assessed for estimating the total evaluation uncertainty are listed. The budget is based on the concept of ISO/IEC Guide 98-1, ISO/IEC Guide 98-3, [31], and [32]. For most methods described in this document, each source of uncertainty can be considered independent, and can therefore be assessed separately. Table 4 summarizes the main parameters related to H-field measurements.

Table 4 – Example of uncertainty evaluation of the exposure assessment using measurement methods

Item	Uncertainty source	Tolerance (dB)	Distr.	Div.	c_i	Std. unc. (dB)
Probe uncertainty						
1	Amplitude calibration uncertainty		norm	1	1	
2	Gradient calibration uncertainty		norm	1	1	
3	Probe anisotropy		rect	√3	1	
4	Probe dynamic linearity		rect	√3	1	
5	Probe frequency domain response		rect	√3	1	
6	Modulation response		rect	√3	1	
7	Spatial averaging (maximum gradient)		rect	√3	1	
8	Gradient uncertainty		rect	√3	1	
9	Gradient detection uncertainty		rect	√3	1	
10	Parasitic E-field sensitivity		rect	√3	1	
11	Detection limit		rect	√3	1	
12	Readout electronics		norm	1	1	
13	Response time		norm	1	1	
14	Probe positioning		norm	1	1	
15	Shaping, filtering, signal conditioning		norm	1	1	
16	Nominal position		rect	√3	1	
17	Repeatability		norm	1	1	
	Combined uncertainty (k = 1)					
	Expanded uncertainty (k = 2)	RSS				

Descriptions per item number of the uncertainty sources in Table 4:

1 Uncertainty of the probe calibration system with respect to field amplitude.

2 Uncertainty of the probe calibration with respect to field gradient.

3 Probe anisotropy shall be tested in the incident field condition representative for WPT systems, covering normalized gradients from 0 T/m/T to > 200 T/m/T.

4 Probe dynamic range shall be evaluated covering the dynamic range from 1 % of the general public exposure limits to > 4 × the occupational exposure limit within the probe's specified operating range.

5 Probe frequency domain response is evaluated for a homogenous incident field over specified operational frequency range.

6 Probe modulation response shall be evaluated for modulated carriers in the specified frequency range with rectangular pulse modulation, 10 % duty cycle, 10 Hz, 100 Hz, 1 000 Hz pulse repetition rate (whatever is applicable at the carrier frequency).

7 Spatial averaging shall be tested in the incident field condition representative for WPT systems, covering normalized gradients from 0 T/m/T to ≥ 200 T/m/T.

8 Gradient uncertainty shall be tested in the incident field condition representative for WPT systems, covering normalized gradients from 0 T/m/T to ≥ 200 T/m/T with the probe oriented through all spherical gradient directions.

9 Uncertainty in the accuracy of field gradient measurements.

10 Parasitic E-field sensitivity is tested with the probe in maximum hold swept through all possible spherical E-field incidences with the E-field at the occupational exposure limit.

11 Detection limit is the contribution of the readout electronic noise at 1 % of the general public exposure limits.

12 Readout electronics is the uncertainty contribution by analogue-to-digital conversion.

13 If the probe is operated in swept mode, response time is the sampling response error for the probe swept through a gradient field of ≥ 200 T/m/T.

14 If the probe is operated in spatial sampling mode, probe positioning is the error in a gradient field of ≥ 200 T/m/T.

15 Shaping, filtering, and signal conditioning are the uncertainty contributions by analogue or digital signal conditioning.

16 Nominal position: positioning uncertainty with respect to assessing the worst-case exposure.

17 Repeatability is relative to the measurements performed at a specific point at the closest accessible distance to the source. It is estimated by performing 10 repeated measurements.

For incident E-field measurements the same components as in Table 4 apply. Parasitic H-field sensitivity shall be evaluated instead of parasitic E-field sensitivity in element 10.

The possible variations caused by the exposure systems are:

a) incident field distribution (i.e. gradient);
b) frequency;
c) geometry of WPT source (size of the coils, shape, alignment);
d) system setup (closest accessible point, possible objects around the source not removable);
e) calibration differences.

9.2 Numerical methods

Table 5 summarizes the sources of uncertainty for numerical methods.

Table 5 – Example of uncertainty evaluation of numerical methods

Item	Uncertainty source	Tolerance (dB)	Distr.	Div.	c_i	Std. unc. (dB)
1	Numerical method		rect	√3	1	
2	Grid resolution		rect	√3	1	
3	Tissue parameters		rect	√3	1	
4	Averaging method		rect	√3	1	
5	Model and exposure location		rect	√3	1	
6	Source representation		norm	1	1	
7	Convergence		rect	√3	1	
8	Boundary conditions		rect	√3	1	
9	Post-processing, interpolation		rect	√3	1	
	Combined uncertainty (k = 1)					
	Expanded uncertainty (k = 2)	RSS				

Descriptions per item number of the uncertainty sources in Table 5:

1 The intrinsic uncertainty of the applied numerical method, e.g. uncertainty of the quasi-static approximation, too weak field coupling in case of FDTD.

2 Grid resolution uncertainty is tested by increasing and decreasing the grid resolution by a factor of 2 from its nominal state.

3 Tissue parameter uncertainty is tested by varying the nominal tissue dielectric parameter by ±10 %.

4 The averaging method depends on the analysed metric (i.e. induced E-field, current density or SAR) and is tested analytically and numerically as a function of tissue composition and grid resolution (1).

5 Placement uncertainty of the source with respect to the human model.

6 Validation uncertainty of the source. If the source is validated in absence of the human body the loading effect of the body should be considered.

7 Convergence of the numerical simulation, e.g. test by time-variant stability criteria or law of energy conservation.

8 Boundary condition uncertainty can be tested by modification of the boundary condition representation.

9 Numerical uncertainties in the post-processing, e.g. interpolation and extrapolation.

9.3 Assessment of combining measurement and numerical methods

Since in practical exposure scenarios the magnetic flux density B is known in a finite number of points, the described approach is approximate. Once the induced exposure in the human body due to the field reconstructed *in silico* is assessed, an uncertainty budget needs to be carried out. According to [33] an example of an uncertainty analysis is shown in Table 6.

Table 6 – Example of uncertainty evaluation of the exposure assessment combining measurements and numerical methods

Item	Uncertainty source	Tolerance (dB)	Distr.	Div.	c_i	Std. unc. (dB)
Probe uncertainty						
1	Probe uncertainty of Table 6		norm	1	1	
Numerical simulations						
2	Numerical method					
3	Grid resolution		rect	√3	1	
4	Tissue parameters		rect	√3	1	
5	Averaging method		rect	√3	1	
6	Model and exposure location		rect	√3	1	
7	Convergence		rect	√3	1	
8	Boundary conditions		rect	√3	1	
9	Post-processing, interpolation		rect	√3	1	
Field reconstruction						
10	Reconstruction algorithm; i.e. calculation of vector potential from measured magnetic flux density		rect	√3	1	
	Combined uncertainty (k = 1)					
	Expanded uncertainty (k = 2)	RSS				

Descriptions per item number of the uncertainty sources in Table 6:

1 Uncertainty determined according to Table 6.

2 The intrinsic uncertainty of the applied numerical method, e.g. uncertainty of the quasi-static approximation, too weak field coupling in case of FDTD.

3 Grid resolution uncertainty is tested by increasing and decreasing the grid resolution by a factor of 2 from its nominal state.

4 Tissue parameter uncertainty is tested by varying the nominal tissue dielectric parameter by ±10 %.

5 The averaging method depends on the analysed metric (i.e. induced E-field, current density or SAR) and is tested analytically and numerically as a function of tissue composition and grid resolution (1).

6 Placement uncertainty of the source with respect to the human model.

7 Convergence of the numerical simulation, e.g. test by time-variant stability criteria or law of energy conservation.

8 Boundary condition uncertainty can be tested by modification of the boundary condition representation.

9 Numerical uncertainties in the post-processing, e.g. interpolation and extrapolation.

10 Uncertainty for reconstruction algorithm when using SPFD method. In case of IM, this uncertainty is not required.

Annex A
(informative)

Exposure evaluations using approximations

Above 10 MHz, the upper limit of the peak spatial exposure of a device can be characterized by the maximum transmit power P_{max} provided that it can be shown that the coupling to the body is not better than with the receiving coil, per Formula (A.1).

$$P_{max} = SAR_{max} \times m \tag{A.1}$$

where:

SAR_{max} is the basic restriction of local SAR;

m is the averaging mass.

For frequencies from 3 kHz to 10 MHz and for inductive WPT, the induced field levels and SAR can be calculated analytically for known geometry and loop currents ([34], [35]) using Formula (A.2), Formula (A.3), and Formula (A.4):

$$E = \left(\frac{NM\omega I}{2\pi R} \right) \tag{A.2}$$

$$J = \sigma \left(\frac{NM\omega I}{2\pi R} \right) \tag{A.3}$$

$$SAR = \frac{J^2}{\rho\sigma} = \frac{\sigma}{\rho} \left(\frac{NM\omega I}{2\pi R} \right)^2 \tag{A.4}$$

where

N is the number of turns in the transmitter coil;

I is the RMS current in the coil;

ω is the angular frequency;

M is the mutual inductance between the coil and induced current path of hypothetical radius R inside the body or phantom;

ρ is the mass density of the tissue medium in kg/m^3.

The mutual inductance can be calculated using Formula (A.5):

$$M = \mu_0 \sqrt{Rr} \left[\left(\frac{2}{\kappa} \right) - \kappa \right] F(\kappa) - \frac{2}{\kappa} E(\kappa) \tag{A.5}$$

with

$$\kappa = \frac{2\sqrt{Rr}}{\sqrt{(R+r)^2 + d^2}} \tag{A.6}$$

where

r is the radius of the coil in m;

d is the distance between the coil and the body in m.

where $F(\kappa)$ and $E(\kappa)$ are the complete elliptic integrals of the first and second kinds [34], [35], [36]. For a specific configuration R shall be determined over an interval from zero to the body (or phantom) size to maximize M. The induced metric can be compared to the corresponding basic restriction limits to determine compliance.

For the application of Formula (A.2), Formula (A.3), and Formula (A.4), quasi-static conditions (7.2) must apply. Additional limitations and considerations are specified in the following paragraphs.

According to comparisons with numerical solutions, Formula (A.2), Formula (A.3), and Formula (A.4) can be assumed to be valid for coil radii less than half the width of the exposed body phantom [36]. A validation for radii up to 75 mm has been carried out in [35]. It should be noted that numerical results reported in [34] show a steady increase of the induced J and 10 g psSAR with respect to Formula (A.3) and Formula (A.4), which can reach the order of magnitude 3 dB at a distance 200 mm. The application of the approach given here should therefore be limited to this distance.

Because Formula (A.2), Formula (A.3), and Formula (A.4) were derived for homogeneous body phantoms, an additional correction factor should be applied to take into account enhancements of the induced E and psSAR due to the dielectric contrasts of the tissues in the inhomogeneous body models [35]. From 100 kHz to 10 MHz, these factors can be assumed to be largely independent of frequency as the dielectric contrast between tissues with high and low water content does not change greatly [35]. For the induced E-field and psSAR, the appropriate correction factors should be applied. If this is not known a factor of 20 dB is considered too conservative.

Formula (A.2), Formula (A.3), and Formula (A.4) do not consider coupling via strong local incident E-fields that may be caused, e.g. by tuning capacitors, voltage drops between coils and may lead to exposures above those induced by the magnetic fields.

Annex B
(normative)

Calibration methods

B.1 General

In this Annex B, methods for calibrating E-field and H-field probes as well as dosimetric probes, separately, are described. The proposed calibration method for E-field and H-field probes can be referred to as Method B (IEEE Std 1309-2005 [37]), which is based on a calibration using calculated field strengths, i.e. the probe under calibration is placed in a reference field, which is calculated based on the geometry of the field generator and the measured input parameters of the field generator. For the dosimetric probes the calibration procedures described in IEC/IEEE 62209-1528 [15] can be used. In the following, the probe under calibration is the device under test (DUT).

B.2 E-field and H-field calibration

B.2.1 Standard field generation methods

Table B.1 lists the devices and setups that are used in the proposed calibration method to generate standard electric field (E-field) and magnetic field (H-field) for calibrations. The field generation devices are classified with respect to the usage, i.e. in frequency, time-domain calibration, or both and the frequency range of applicability. Related standards shall be consulted for details not included in this document.

Table B.1 – EM field generation setups for probe and sensor calibrations

Field type	Usage [a]	Field generation	Related standard cross-reference	Procedure
H, E	F, T	TEM cell	IEEE Std C95.3-2002, 5.5.1.3, IEEE Std 1309-2005	B.2.3.1
H	F, gradient verification	Helmholtz coil	IEEE Std C95.3-2002, 5.5.1.4, IEEE Std 1309-2005 IEC 61786-1	B.2.3.2
E	F, T	Parallel plate	IEEE Std 1309-2005 IEC 61786-1	B.2.4.1
[a] T = time, F = frequency				

B.2.2 Characteristics to be measured

B.2.2.1 Frequency domain calibration parameters

B.2.2.1.1 General

In the frequency domain the parameters to be calibrated for both E- and H-fields are described below.

B.2.2.1.2 Frequency response

Calibration may be performed at one or more frequencies, depending on the application (see Annex A of IEEE Std 1309-2005 [37]).

B.2.2.1.3 Dynamic range

Calibration may be performed at one or more field strengths depending on the intended application (see Annex A of IEEE Std 1309-2005 [37] for example of applications).

B.2.2.1.4 Isotropy

The isotropic response is usually measured in terms of anisotropy (A). According to IEEE Std 1309-2005 [37] this is defined as the maximum deviation from the geometric mean of the maximum response and minimum response. The anisotropy is therefore defined as:

$$A = 20\lg\left(\frac{S_{\max}}{\sqrt{S_{\max}S_{\min}}}\right)\text{dB} \quad \text{(B.1)}$$

In Formula (B.1), S is expressed in field strength units.

B.2.2.2 Time domain calibration parameters

B.2.2.2.1 General

In the time domain the parameters to be calibrated for both E-field and H-field are described in the following subclauses.

B.2.2.2.2 Amplitude

Amplitude calibration is the calibration of the sensitivity of the sensor or probe, which represents the transfer function of the sensor for converting an EM field component into an electrical signal. The sensitivity for a sensor is normally specified, and the deviation of the actual sensor response from its specified value must be calibrated.

B.2.2.2.3 Dynamic range

Calibration may be performed on one or more field strengths, depending on the application. Annex A of IEEE Std 1309-2005 [37] provides requirements for specifying grades of calibration and selection of calibration amplitudes.

B.2.2.2.4 Rise time

Rise time is defined as the duration of the first transition in a pulsed waveform. Rise time shall be measured with an instrumentation system that has a rise time at least five time faster than the response time of the sensor being calibrated. If this setup is not possible, then the response time of the instrumentation system shall be at least as fast as the sensor response time, and deconvolution techniques shall be used to determine the sensor rise time.

B.2.3 Frequency domain calibration

B.2.3.1 Frequency response

B.2.3.1.1 General

The H-field and E-field generation setup for frequency response calibration is shown in Figure B.1. The devices used in the setup are described in Table B.2. Prior to calibration, the cross coupling between E- and H-fields is characterized.

In order to electrically characterize the TEM cell the suggestions provided in Annex B of IEEE Std 1309-2015 [37] can be followed. Besides the orientation with respect to the field, the DUT should be placed within the TEM cell in the area of highest field homogeneity.

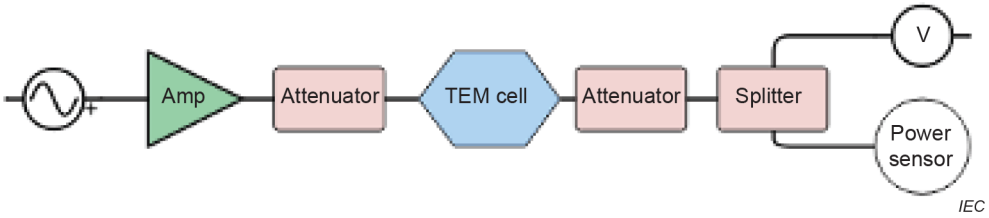

Figure B.1 – H-field and E-field generation setup for probe calibration

Table B.2 – Main components of H-field and E-field generation setup for frequency response calibration

Item	Description
Voltage source	Chosen according to the target voltage
Amplification	Chosen with respect to the target maximum H-field and/or E-field
Power sensor	Chosen according to the target power

B.2.3.1.2 Procedure

a) Place probe inside the TEM cell with one sensor axis aligned to the H-field or E-field.

b) Verify that the probe does not distort the incident calibration field.

c) Set the generator to frequency f_k.

d) Set the generator amplitude to reach the desired target field strength.

e) Record the exact power from the power sensor and relay it to the actual reference field strength in the TEM cell (H_{TEM}, E_{TEM}).

f) Collect the measured H-field and E-field from the DUT (H_{DUT} and E_{DUT}, respectively).

g) Compare the sensor output H_{DUT} to the reference field H_{TEM} or sensor output E_{DUT} to the reference field E_{TEM}.

h) Logarithmically sweep in frequency.

i) Repeat the procedure for the other two axes.

j) In case of multiple sensors repeat the procedure for each sensor in the DUT.

k) Report the maximum deviation $H_{\text{DUT}}/H_{\text{TEM}}$ and $E_{\text{DUT}}/E_{\text{TEM}}$ as a function of frequency.

B.2.3.1.3 Uncertainty for frequency response calibration

Table B.3 shows a template for the uncertainty of frequency response calibration.

Table B.3 – Template for uncertainty in frequency response calibration

Item	Uncertainty source	Tolerance (dB)	Distr.	Div	c_i	Std. unc. (dB)
Frequency response system						
1	TEM cell field variation		rect	√3	1	
2	TEM cell attenuation		rect	√3	1	
3	Field homogeneity		rect	√3	1	
4	H-field pre-calculation		norm	1	1	
Probe						
5	Probe anisotropy		rect	√3	1	
6	Probe dynamic linearity		rect	√3	1	
7	Parasitic E-field sensitivity (for H-field calibration) or H-field (for E-field calibration)		rect	√3	1	
8	Spatial averaging		rect	√3	1	
9	Gradient detection		rect	√3	1	
10	Detection limit		rect	√3	1	
11	Readout electronics		norm	1	1	
12	Response time		norm	1	1	
13	Shaping, filtering, signal conditioning		norm	1	1	
14	Probe position		norm	1	1	
Procedure						
15	Nominal position		rect	√3	1	
16	Repeatability		norm	1	1	
17	Post-processing		rect	√3	1	
Instrumentation						
18	Power sensor calibration		norm	1	1	
19	Power sensor linearity		rect	√3	1	
20	Power sensor SNR		rect	√3	1	
21	Attenuator/splitter uncertainty		rect	√3	1	
22	Mismatch uncertainty		rect	√3	1	
23	Broadband harmonic distortion		rect	√3	1	
Combined uncertainty						

B.2.3.2 H-field dynamic range

B.2.3.2.1 General

The linearity of the H-field probe sensors over the whole dynamic range is checked. The dynamic range test is repeated for all sensors in the DUT. Figure B.2 shows the setup for the generation of H-field for dynamic range calibration, whose main components are described in Table B.4.

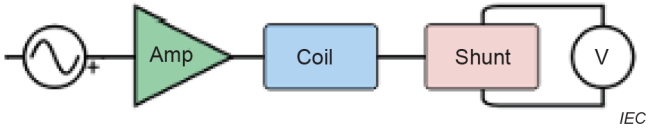

Figure B.2 – H-field generation setup for dynamic range calibration

Table B.4 – Main components of H-field generation setup for dynamic range calibration

Item	Description
Voltage source	Chosen according to the target voltage
H-field source	Magnetic field source (MFS), e.g. Helmholtz coil
Calibrated shunt resistance	Calibrated shunt resistance chosen to reach the maximum target H-field

B.2.3.2.2 Procedure

a) Place the DUT in the centre of the MFS with one sensor axis aligned to the MFS axis.
b) Set the generator at the chosen frequency.
c) Logarithmically sweep the H-field amplitude over the dynamic range to be calibrated.
d) Collect H_{DUT} and E_{DUT} from each sensor axis.
e) Determine the maximum deviation from linearity of H_{DUT}/MFS for each sensor axis.
f) Repeat the procedure for each sensor in the DUT.
g) E/H crosstalk: maximum ratio between sensitivity of H_{DUT} and E_{DUT} from all collected measurements at step d).

B.2.3.2.3 Uncertainty for H-field dynamic range calibration

Table B.5 shows a template for the uncertainty of H-field dynamic range calibration.

Table B.5 – Template for uncertainty in H-field dynamic range calibration

Item	Uncertainty source	Tolerance (dB)	Distr.	Div	c_i	Std. unc. (dB)
Dynamic range system						
1	Resonant Helmholtz coil field variation		rect	√3	1	
2	Resonant Helmholtz coil cell attenuation		rect	√3	1	
3	Field homogeneity		rect	√3	1	
4	H-field pre-calculation		norm	1	1	
Probe						
5	Probe anisotropy		rect	√3	1	
6	Probe dynamic linearity		rect	√3	1	
7	Parasitic E-field sensitivity		rect	√3	1	
8	Spatial averaging		rect	√3	1	
9	Gradient detection		rect	√3	1	
10	Detection limit		rect	√3	1	
11	Readout electronics		norm	1	1	
12	Response time		norm	1	1	
13	Shaping, filtering, signal conditioning		norm	1	1	
14	Probe position		norm	1	1	
Procedure						
15	Nominal position		rect	√3	1	
16	Repeatability		norm	1	1	
17	Post-processing		rect	√3	1	
Combined uncertainty						

B.2.3.3 H-field measurement isotropy

B.2.3.3.1 General

The DUT isotropy is estimated in a homogeneous field for the calibrated range and in a gradient field (> 5 T/m/T), separately. Isotropy is determined by measuring the deviation of the DUT sensor output from target, under rotation of the DUT around its main axis from 0° to 360° with 15° steps.

B.2.3.3.2 Procedure

a) Place the probe with the main symmetry axis aligned to the field, i.e. polar angle 0°.

b) Set the frequency and amplitude of the generator.

c) Sweep the azimuthal angle between 0° and 360° with 15° steps.

d) Isotropy is the maximum deviation of H_{DUT} from the target, compared to the target value over all angles.

B.2.4 E-field calibration

B.2.4.1 Frequency response (alternative approach)

B.2.4.1.1 General

An alternative to the TEM cell for calibration of the frequency response of the E-field sensor is shown in Figure B.3. The devices used in the setup are described in Table B.6.

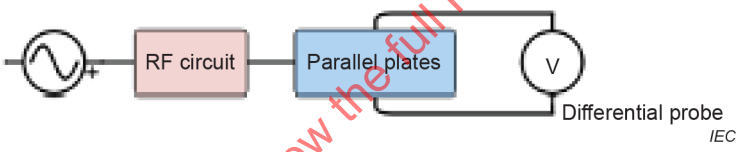

Figure B.3 – E-field generation setup for frequency response calibration

Table B.6 – Main components of E-field generation setup for frequency response calibration

Item	Description
Voltage source	Selected according to the target voltage
RF circuit	Generation of a fully differential voltage
E-field source	Parallel plates
Voltage sensor	Differential voltage probe

B.2.4.1.2 Procedure

a) Place the DUT in the centre of the parallel plates with one axis aligned to the reference E-field (E_{PP}) direction.

b) Set the frequency in the generator.

c) Measure the voltage across the parallel plates.

d) Logarithmically sweep in frequency.

e) Collect E_{DUT} and H_{DUT}.

f) Determine frequency response parameters: E_{DUT}/E_{PP}.

g) Repeat the procedure for the other two axes.

h) Repeat the procedure for each E-field sensor in the DUT.

i) E/H crosstalk: maximum ratio between sensitivity to E_{DUT} and H_{DUT} from all the frequency points tested across all sensors.

B.2.4.1.3 Uncertainty for E-field frequency response

Table B.7 shows a template for the uncertainty of the E-field frequency response calibration.

Table B.7 – Template for uncertainty in E-field frequency response calibration

Item	Uncertainty source	Tolerance (dB)	Distr.	Div	c_i	Std. unc. (dB)
Frequency response system						
1	Parallel plates field variation		rect	√3	1	
2	Parallel plates field attenuation		rect	√3	1	
3	Field homogeneity		rect	√3	1	
4	E-field pre-calculation		norm	1	1	
Probe						
5	Probe anisotropy		rect	√3	1	
6	Probe dynamic linearity		rect	√3	1	
7	Parasitic H-field sensitivity		rect	√3	1	
8	Spatial averaging		rect	√3	1	
9	Gradient detection		rect	√3	1	
10	Detection limit		rect	√3	1	
11	Readout electronics		norm	1	1	
12	Response time		norm	1	1	
13	Shaping, filtering, signal conditioning		norm	1	1	
14	Probe position		norm	1	1	
Procedure						
15	Nominal position		rect	√3	1	
16	Repeatability		norm	1	1	
17	Post-processing		rect	√3	1	
Instrumentation						
18	Voltage sensor calibration		norm	1	1	
19	Voltage sensor dynamic		rect	√3	1	
20	Voltage sensor frequency response		rect	√3	1	
Combined uncertainty						

B.2.4.2 Dynamic range

B.2.4.2.1 General

The E-field generation setup for the dynamic range calibration is shown in Figure B.4. The devices used in the setup are described in Table B.8.

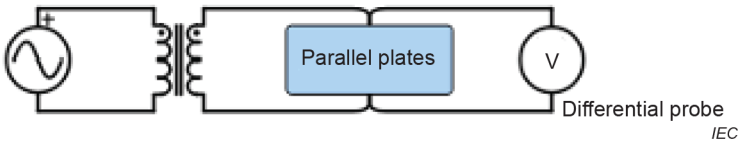

Figure B.4 – E-field generation setup for dynamic range calibration

Table B.8 – Main components of E-field generation setup for dynamic range calibration

Item	Description
Voltage source	Selected according to the target voltage
Transformer	Amplification of voltage
E-field source	Parallel plates
Voltage sensor	Differential voltage probe

B.2.4.2.2 Procedure

a) Place the DUT in the centre of the parallel plates with one sensor axis aligned to the reference E-field (E_{PP}) direction.

b) Set the generator at the chosen frequency.

c) Logarithmically sweep the reference E_{PP} amplitude over the dynamic range to be calibrated.

d) Collect H_{DUT} and E_{DUT}.

e) Determine the deviation from the linearity of E_{DUT}/E_{PP}.

f) Repeat the procedure for the other two axes.

g) Repeat the procedure for each E-field sensor in the DUT.

h) E/H crosstalk: maximum ratio between the sensitivity of E_{DUT} and H_{DUT} from all points.

B.2.4.2.3 Uncertainty for E-field dynamic range

Table B.9 shows a template for the uncertainty of the E-field frequency response calibration.

Table B.9 – Template for uncertainty in E-field frequency response calibration

Item	Uncertainty source	Tolerance (dB)	Distr.	Div	c_i	Std. unc. (dB)
Dynamic range system						
1	Parallel plates field variation		rect	√3	1	
2	Parallel plates field attenuation		rect	√3	1	
3	Field homogeneity		rect	√3	1	
4	E-field pre-calculation		norm	1	1	
Probe						
5	Probe anisotropy		rect	√3	1	
6	Probe dynamic linearity		rect	√3	1	
7	Parasitic H-field sensitivity		rect	√3	1	
8	Spatial averaging		rect	√3	1	
9	Gradient detection		rect	√3	1	
10	Detection limit		rect	√3	1	
11	Readout electronics		norm	1	1	
12	Response time		norm	1	1	
13	Shaping, filtering, signal conditioning		norm	1	1	
14	Probe position		norm	1	1	
Procedure						
15	Nominal position		Rect	√3	1	
16	Repeatability		norm	1	1	
17	Post-processing		rect	√3	1	
Combined uncertainty						

B.2.4.3 E-field measurement isotropy

B.2.4.3.1 General

The DUT isotropy is estimated in a homogeneous field. Isotropy is determined by measuring the deviation of the DUT sensor output from the target, under rotation of the DUT around its main axis from 0° to 360° with 15° steps. The setup for dynamic range calibration is used.

B.2.4.3.2 Procedure

a) Place the DUT with the main symmetry axis aligned to the field, i.e. polar angle 0°.

b) Set the generator at the desired frequency and amplitude.

c) Sweep an azimuthal angle between 0° and 360° with 15° steps.

Isotropy is the maximum deviation of E_{DUT} from the target E_{PP}, compared to the mean over all angles.

B.3 Gradient response verification

B.3.1 General

The gradient estimated by the DUT will be verified by comparison to the one analytically calculated in numerical simulations. The gradient is verified by means of a well-defined magnetic gradient field source.

B.3.2 H-field gradient verification: Main steps

a) a numerical model of the reference coil is developed, and the H-field is registered with a constant step dx, starting at 5 mm from the coil wire and moving in horizontal and vertical directions.

b) The gradient (G_{REF}) at each step is analytically estimated as:

$G_{REF} = (B_{max} - B_{min})/dr/0{,}5 \times (B_{max} + B_{min})$.

c) Measurements of the H-field generated by the reference coil with the DUT are collected at the same distances used in the simulation. The DUT estimates the gradient (G_{DUT}) at each step.

d) G_{DUT} is compared to G_{REF} for < 1 T/m/T to > 80 T/m/T.

B.3.3 Uncertainty for H-field gradient verification

Table B.10 shows a template for the uncertainty of the H-field gradient verification.

Table B.10 – Template for uncertainty in H-field dynamic range calibration

Item	Uncertainty source	Tolerance (dB)	Distr.	Div	c_i	Std. unc. (dB)
Gradient verification system						
1	Coil field variation		rect	√3	1	
2	Coil cell attenuation		rect	√3	1	
3	Field homogeneity		rect	√3	1	
4	H-field pre-calculation		norm	1	1	
Probe						
5	Probe anisotropy		rect	√3	1	
6	Probe dynamic linearity		rect	√3	1	
7	Parasitic E-field sensitivity		rect	√3	1	
8	Spatial averaging		rect	√3	1	
9	Gradient detection		rect	√3	1	
10	Detection limit		rect	√3	1	
11	Readout electronics		norm	1	1	
12	Response time		norm	1	1	
13	Shaping, filtering, signal conditioning		norm	1	1	
14	Probe position		norm	1	1	
Procedure						
15	Nominal position		rect	√3	1	
16	Repeatability		norm	1	1	
17	Post-processing		rect	√3	1	
Numerical simulation						
18	Grid resolution		rect	√3	1	
19	Model and exposure location		rect	√3	1	
20	Source representation		norm	1	1	
21	Convergence		rect	√3	1	
22	Boundary conditions		rect	√3	1	
23	Post-processing		rect	√3	1	
Combined uncertainty						

B.4 Dosimetric probe calibration

B.4.1 General

The calibration method for the dosimetric (SAR) probe is defined in IEC/IEEE 62209-1528 [15]. A two-step procedure and a one-step procedure are described. Recently, a one-step calibration method using a short dipole antenna was proposed [38].

B.4.2 Calibration with short dipole antennas via transmit antenna factor

The reference antennas used here are short dipole antennas designed for operating within the appropriate tissue equivalent liquid.

a) The transmit antenna factor of the reference dipole antenna (see Figure B.5) is determined as a function of the distance by the two-antenna method according to the following protocol.

1) Position the antennas in the liquid such that their main-beam axes are aligned and at a specified distance d. The antennas shall be placed at least 10 cm away from the walls of the liquid container.

2) Measure the S parameters between the antennas as a function of the distance d.

3) Calculate the power transmission coefficient η by S parameter:

$$\eta(d) = \frac{|S_{21}(d)|^2}{\left(1-|S_{11}(d)|^2\right)\left(1-|S_{22}(d)|^2\right)} \tag{B.2}$$

where $|S_{21}(d)|$ is the transmission coefficient and $|S_{11}(d)|$ and $|S_{22}(d)|$ are the reflection coefficients of the transmit antenna and receive antenna, respectively.

4) The transmit antenna factor is given by Formula (B.3):

$$F(d) = \left[\frac{\sqrt{\eta(d)}}{K(d)}\right]^{1/2}. \tag{B.3}$$

$K(d)$ is given by Formula (B.4), assuming a current distribution of piecewise hyperbolic sinusoidal function on the dipole antenna:

$$K(d) = \frac{1}{16\pi}\left|\left(\frac{\sqrt{\mu_0/\varepsilon}}{\left[l^{\mathrm{e}}\sinh(\gamma l/2)\right]^2}\right)\int_{-l/2}^{l/2} \mathrm{e}_z(z,l)\sinh\left[\gamma\left(l/2-|z|\right)\right]\mathrm{d}z\right| \tag{B.4}$$

where

$$\mathrm{e}_z(z,l) = \frac{\mathrm{e}^{-\gamma R_1}}{R_1} + \frac{\mathrm{e}^{-\gamma R_2}}{R_2} - 2\cosh(\gamma l/2)\frac{\mathrm{e}^{-\gamma R_0}}{R_0} \tag{B.5}$$

$$l^{\mathrm{e}} = \frac{2}{\gamma}\frac{\cosh(\gamma l/2)-1}{\sinh(\gamma l/2)} \tag{B.6}$$

$$R_0 = \sqrt{d^2+z^2}, \quad R_1 = \sqrt{d^2+(z-l/2)^2}, \quad R_2 = \sqrt{d^2+(z+l/2)^2}$$

l is the length of the reference dipole antenna;

$\gamma = \alpha + \mathrm{j}\beta$ is propagation constant of the liquid.

b) The following protocol shall be used for evaluating the sensitivity coefficients of the probe (see Figure B.6):

1) Position one antenna in the tissue-equivalent liquid. The antenna shall be positioned at a minimum distance of 10 cm away from the walls of the liquid container.

2) Connect a power source to the input port of the reference antenna. The average electric field produced by the short dipole antenna $E_{\mathrm{th}}^{\mathrm{av}}(d)$ in the near-field region is given by Formula (B.7):

$$E_{\mathrm{th}}^{\mathrm{av}}(d) = \left[8P_{\mathrm{inc}}\left(1-|\Gamma|^2\right)\right]^{1/2} F(d)K(d) = \left[8P_{\mathrm{inc}}\left(1-|\Gamma|^2\right)\sqrt{\eta(d)}K(d)\right]^{1/2} \tag{B.7}$$

where

P_{inc} is the incident power;

Γ is the reflection coefficient of the short dipole antenna.

It is recommended to connect a bi-directional coupler to control the input power. Tune the input power so that $E_{th}^{av}(d)$ ~ 30 V/m.

3) Position the probe in the liquid so that the centre of the detectors is at a distance d from the antenna.
4) Orient the probe to align the direction of the sensor with the polarization of the reference antenna.
5) Measure the voltage $V_{1,meas}$ at the transmitting antenna port.
6) The sensitivity coefficient K_1 for this antenna is $K_1 = V_{1,meas} / E_{th}^{av}(d)$.
7) Repeat Steps 4) to 6) for the other two sensors to evaluate K_2 and K_3.

c) Using the sensitivity coefficients of the probe, SAR is determined by the Formula (B.8):

$$SAR = \left(\frac{V_{1,meas}}{K_1} + \frac{V_{2,meas}}{K_2} + \frac{V_{3,meas}}{K_3} \right). \quad \text{(B.8)}$$

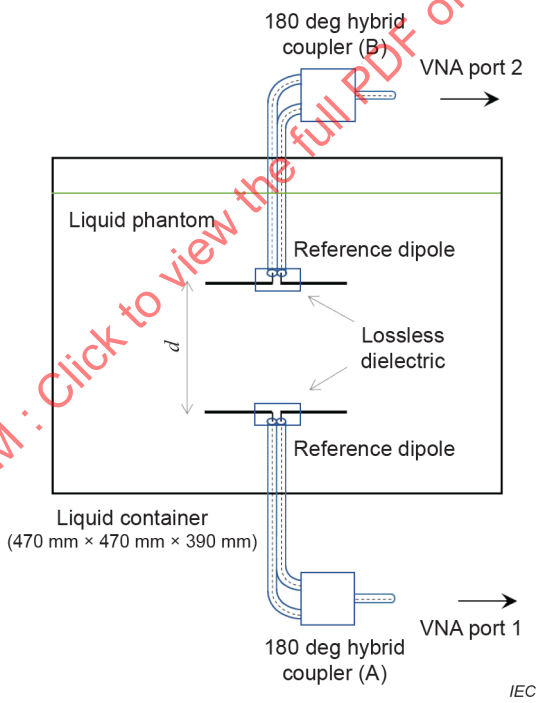

Figure B.5 – Illustration of the transmit antenna factor evaluation setup [38]

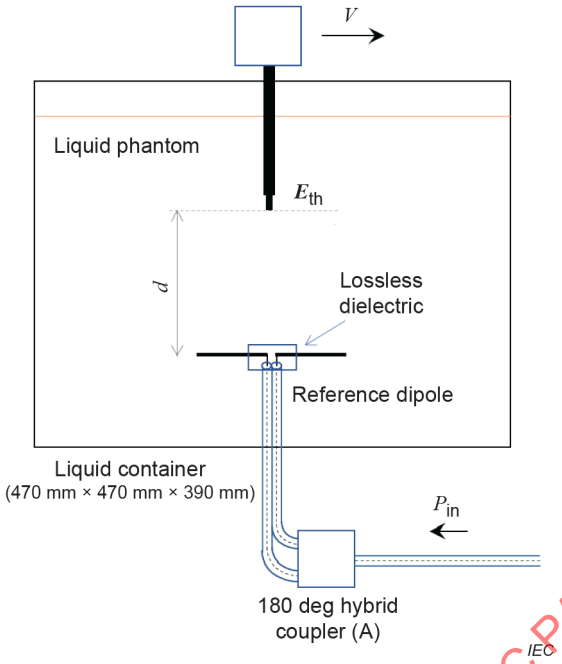

Figure B.6 – Illustration of the sensitivity coefficients evaluation setup [38]

B.4.3 Uncertainty

When performing an uncertainty analysis of the calibration with reference antennas, at least the parameters included in Table B.11 shall be considered.

Table B.11 – Uncertainty template for evaluation of average electric field produced by short dipole antenna via transmit antenna factor

Source of uncertainty	Uncertainty value ± %	Probability distribution	Divisor	c_i	Standard uncertainty u_i ± %	v_i or v_{eff}
Probe position		rect	1,73			
Antenna length		rect	1,73			
Liquid conductivity		norm	2			
Liquid permittivity		norm	2			
Transmission coefficients		rect	1,73	1		
Reflection coefficient for Tx		rect	1,73			
Reflection coefficient for Rx		rect	1,73			
Input power		rect	1,73	1		
Combined standard uncertainty		RSS				

Annex C
(normative)

Verification and validation methods for measurement

C.1 General

In this Annex C the system verification and system validation procedures are described to enable users and third parties to verify the performance of the measurement system and procedure by applying well-established protocols.

- Measurement system verification: procedure that uses specific reference sources to verify that the measurement system is operational and repeatable for the intended measurements.
- Measurement system validation: procedure that uses specific reference sources to validate that a measurement system meets the accuracy, performance and uncertainty specifications required before it is deployed and also after hardware or relevant software changes are performed.

C.2 Objective

The measurement system verification provides a fast and reliable method to routinely verify that the measurement system is operational with no system component failures, including probe defects, drifts or deviation from target performance requirements. The system verification also verifies the repeatability of the measurement system before compliance testing.

The system verification consists of a complete measurement using simple well-defined reference sources. The system verification is successful if the measured results are within established tolerances. The instrumentation and procedures used for system verification should ensure the system is ready for performing compliance tests.

The measurement system validation provides a means to independently evaluate the system against its specifications and its specified uncertainties. The system validation assures that the measurement system provides accurate results.

The validation tests should cover the frequencies and field amplitude and gradient levels supported by an individual measurement system.

C.3 Measurement setup and procedure for system verification and system validation

In Clause C.3 the measurement setups for magnetic and electric fields measurements are described. Recommended test setups for magnetic and electric field measurements are shown in Figure C.1.

The requirements of the components used in the setup shown in Figure C.1 are described as follows.

- The signal generator and the amplifier should be stable (after warm-up). The signal to the reference source should be high enough to avoid the influence of measurement noise.
- For frequencies up to 150 kHz, the coil could be connected to a shunt resistance.

To avoid unacceptable field level drifts during system validation and system verification, the equipment should be allowed to warm-up for the duration recommended by the manufacturer(s) before any measurement.

For both system verification and validation, target values from the reference sources are previously characterized. The measurements are normalized with respect to the input current or voltage used for the characterization of the validated sources.

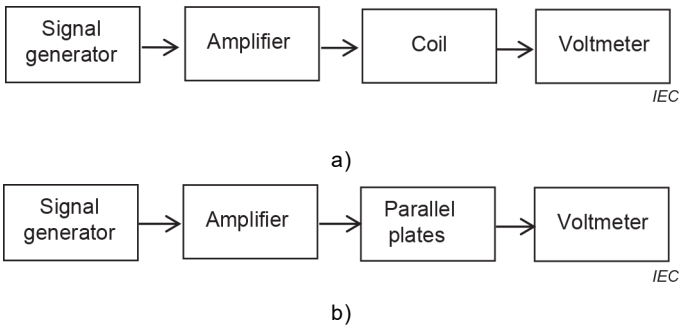

Figure C.1 – A recommended magnetic and electric field setup for measurement system verification and validation

C.4 Measurement system verification: test procedure

The system verification is a magnetic and electric field measurement at a specific position. The results are normalized and compared to the validated target values.

The system verification is successful if both of the following conditions are satisfied:

- the difference between the normalized measured field level and the numerically validated target value is within the combined uncertainty of the reported expanded uncertainty of the measurement system and that of the target values (< 10 %);
- for gradient probes, the difference between the target gradient and the determined gradient is not larger than its uncertainty.

The measured reference value is determined for the individual measurement system after calibration using the same source.

C.5 Measurement system validation: test procedure

The validated source used for system validation might be different than the ones used for system verification.

System validation should cover the range of frequencies applicable to the system. If the measurement system covers the entire frequency range of this document, the validation should be performed at 3 kHz, 85 kHz, 6,78 MHz, and 30 MHz and gradients from 10 T/m/T, 25 T/m/T, and 50 T/m/T. If the measurement system does not cover the entire frequency range, the validation should be performed up to the above-mentioned frequencies that fall within the frequency range used by the system. The reference sources should be calibrated in amplitude at the defined reference distances.

System validation is a magnetic and electric field measurement. Magnetic field measurements are performed with respect to the calibrated plane at a specific distance from the source, while electric field measurements are performed within a cube of side 5 cm centred in the parallel plates. Results are normalized to input current/voltage at the reference source and compared with the numerically validated target values. A comparison of the target values and the field distribution is performed.

The system validation is successful if the following condition is satisfied: the difference between the normalized measured field level and the numerically validated target value is within the reported expanded uncertainty of the measurement system.

Annex D
(informative)

Dependency of SAR on phantom property and size

D.1 Phantom property

The SAR dependence on the phantom material properties for the WPT exposure assessment is considered in Clause D.1. The results of SAR calculations for the WPT systems operating close to the elliptical phantom and the heterogeneous human body model are compared for the different coil orientations with respect to phantom and human body surfaces. For the elliptical phantom, tissue material properties have been used in the EM simulations, as shown in Table 2. Simulation models are depicted in Figure D.1 and Figure D.2. Three different exposure conditions (A, B, C) for the various orientations of inductive coils with respect to the human body are considered as shown in Figure D.2. Similar cases A, B, and C have been used with the elliptical phantom. In the calculation, two types of WPT coils are considered. The first is the relatively large circular spirals with an outer diameter of 50 cm and small squared spirals sized as $L \times L$ = 10 cm × 10 cm.

SARs are calculated for the input power of 1 W with the hybrid MoM/FDTD method. In this study, 10 g-averaged SAR values are obtained and compared at two frequencies where the S_{21} parameter of WPT system without human body is at the maximum. The analysis frequencies are 6,75 MHz to 7,54 MHz for the cases A, B, and C.

Figure D.3 compares the obtained SARs between the elliptical phantom and the human body model. For both the elliptical phantom and human model, relatively higher SAR value is found for case C, in which the vector of the incident magnetic field is normal to the flat surface of the phantoms. In some cases, the results produced with the elliptical phantom substantially underestimate the SAR values obtained with the high-resolution heterogeneous body model.

Similar calculations and comparisons were carried out for the WPT system utilizing small-sized coils (see Figure D.4). Squared spirals with the dimensions 10 cm × 10 cm were used in the simulations. Resonant frequency of WPT system is 6,59 MHz. Similar to previous WPT model, two exposure conditions (cases A and C) were considered here since Case B can be considered the same as Case A. The comparison results obtained for the elliptical phantom and heterogeneous human body model are shown in Figure D.5. The elliptical phantom now provides the conservative SAR values for WPT exposure assessment unlike the case of the large size coils.

As compared to the case of the elliptical phantom exposure, heterogeneity introduces a twofold increase in SAR values for some exposure conditions for relatively large WPT systems. However, for small WPT systems, SAR obtained with the elliptical phantom are conservative compared to those obtained with the human body model. Therefore, in order to provide conservative results with the phantoms having uniform dielectric properties, as shown in Table 2, the phantom dimensions must be chosen with respect to that of the WPT systems under test.

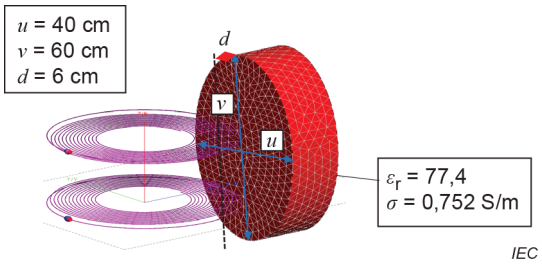

a) Elliptical phantom

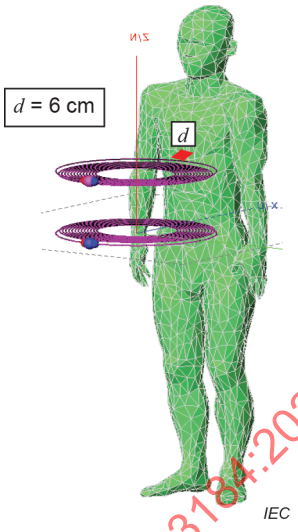

b) Human body model

Figure D.1 – Simulation model of large WPT system operating close to a) elliptical phantom and b) human body model

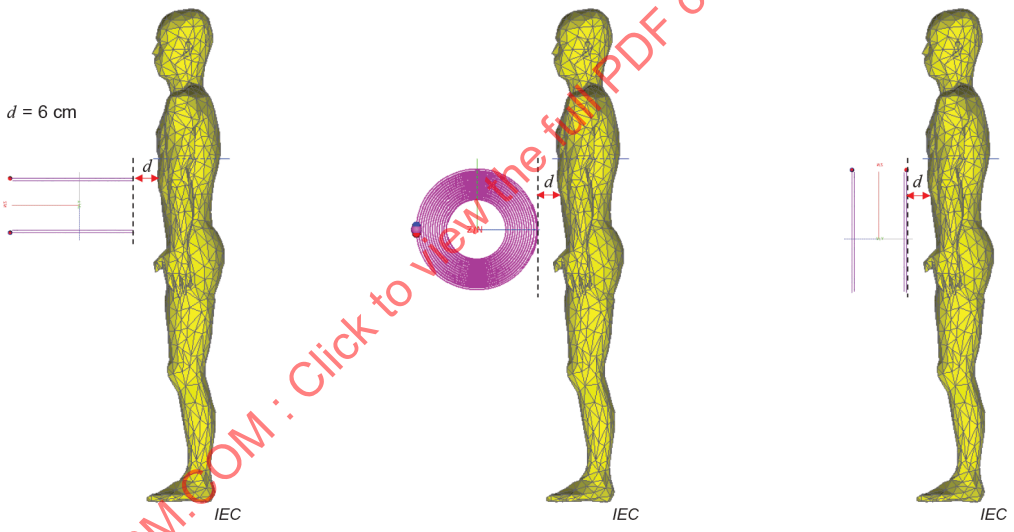

Case A **Case B** **Case C**

Figure D.2 – Different exposure conditions for human body model

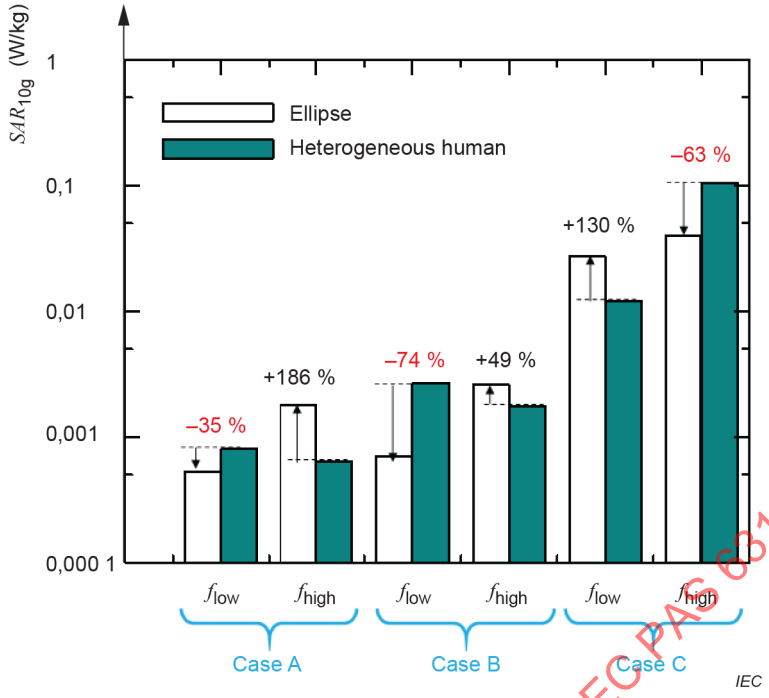

Figure D.3 – Calculated SAR for circular coils with a 50 cm diameter operating at 6 cm from the elliptical phantom and heterogeneous human model

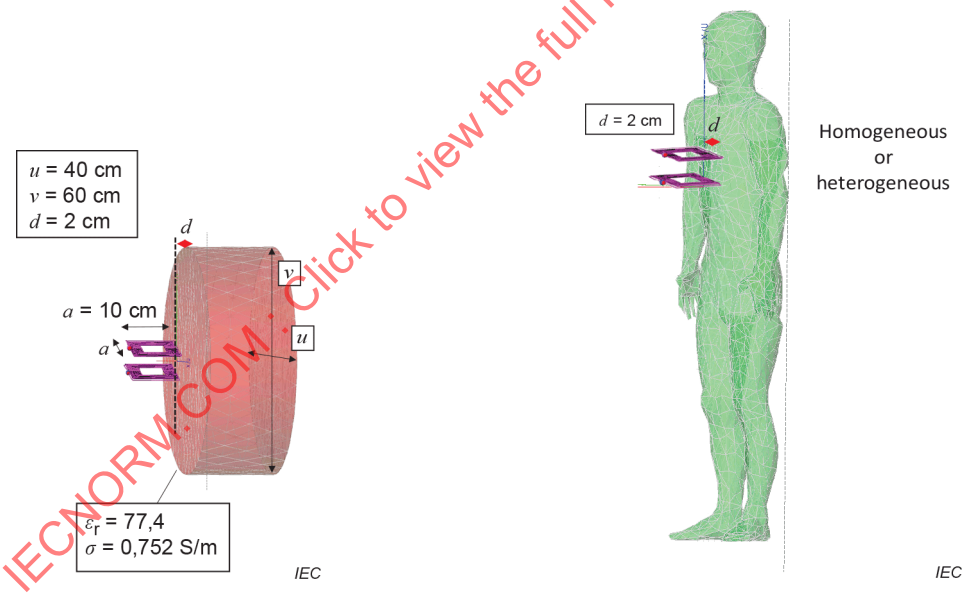

a) Elliptical phantom **b) Human body model**

Figure D.4 – Simulation model of small WPT system operating close to a) elliptical phantom and b) human body model

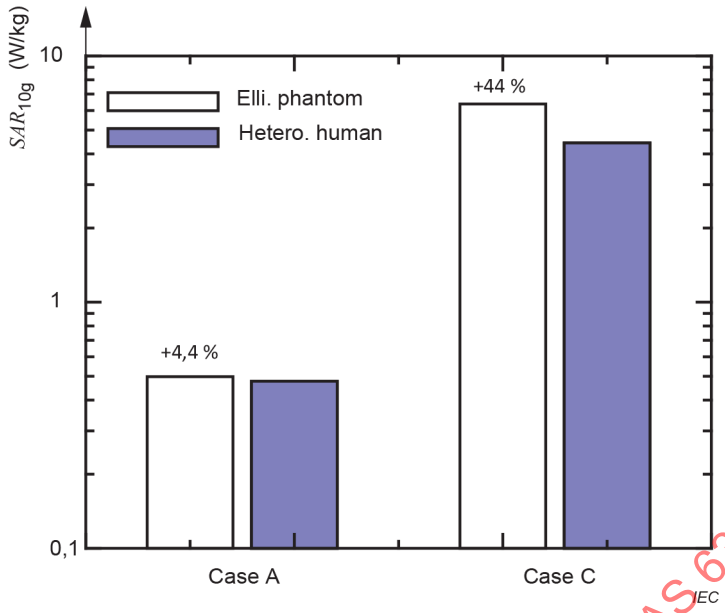

Figure D.5 – Calculated SAR for the small squared coils with dimensions 10 cm × 10 cm operating at 2 cm from the elliptical phantom and heterogeneous human model

D.2 Phantom size

For the human exposure assessment of WPT systems, phantoms of different shapes and dimensions can be used. The effect of phantom size variation on the SAR values obtained in the assessment of WPT systems should be considered. In Clause D.2, the results of the EM simulation of simple WPT coils operating close to the elliptical and rectangular phantoms are presented. The following application scenarios of WPT systems operating near the phantoms are considered as shown in Figure D.6: large circular coils are placed normal to the elliptical phantom (case A) and parallel to the elliptical phantom (case C). Here, the exposure conditions are similar to those described in Clause D.1.

In cases A and C, the distance from the circular coil to the elliptical phantom is fixed at 2 cm while the distance between the coils is 20 cm. Under these conditions, the dimensions of the phantom are changed by varying the ellipse axes u and v and keeping the phantom height fixed (15 cm). The shape of the elliptical phantom is maintained by the unchanged ratio u/v = 1,5, i.e. for each next value of u the value of v is changed accordingly. 10 g-average SAR has been calculated for each set of u and v at two frequencies where the S_{21} parameter of WPT system is at the maximum. These frequencies have been obtained by the EM simulations and are as follows: f_{low} = 6,64 MHz and f_{high} = 7,54 MHz for case A, f_{low} = 6,14 MHz and f_{high} = 7,18 MHz for case C.

The calculated SAR values versus the smaller ellipse axis v normalized by the outer diameter of the circular coils D are presented in Figure D.7. The results are normalized with the input power of 1 W. For case C (Figure D.7 b)) when the coils are parallel to the phantom, SAR remains almost unchanged for the larger dimensions of the phantom. However, there is a substantial increase of the SAR values when the phantom size decreases and becomes comparable to the coil dimension. Such an effect is not observed in case A (Figure D.7 a)) when the coils are normal to the phantom. SAR experiences a small decrease when the phantom size becomes comparable to the coil dimension.

Similar calculations and comparisons have been carried out for the WPT system utilizing small-sized coils (see Figure D.8). In this calculation, only case C was examined. The calculated SAR values versus the smaller ellipse axis v normalized by the small square coil diagonal K (as the largest dimension of the coil) are presented in Figure D.9 a). The frequencies of maximum S_{21} parameter for the case C of small-sized coils are f_{low} = 6,6 MHz and f_{high} = 7,64 MHz. Similar to the large WPT system, the SAR values increase when the elliptical phantom dimension decreases though the increase factor is somewhat smaller. For the larger phantom sizes, the SAR remains practically unchanged. Similarly, the SAR values versus the width of rectangular phantom W normalized by the square coil diagonal K are presented in Figure D.9 b). Again, the SAR values increase significantly when the phantom width decreases and becomes equal to the coil dimension.

SAR increases substantially (by a factor of 2) with a decrease in the phantom dimensions for the case C of coils placed parallel to the phantom. 10 g-SAR reaches the maximum when the coil size is comparable to the size of the phantoms. Such an effect is not observed when coils are placed normal to the phantom. It is recommended that the dimension of the phantoms used should be at least two times larger than the size of the WPT coils to perform a correct SAR evaluation in the exposure assessment of WPT systems.

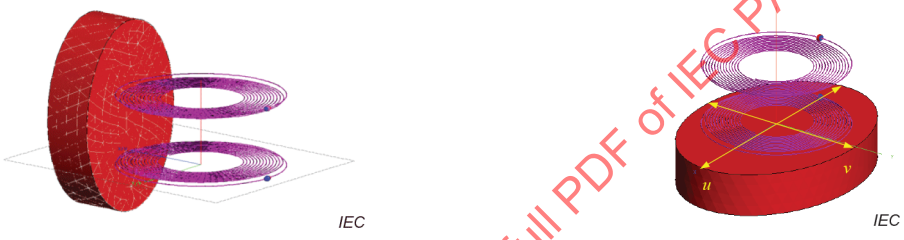

a) case A b) case C

Figure D.6 – Layout of large WPT system for exposure condition of a) case A and b) case C with respect to the elliptical phantom surface

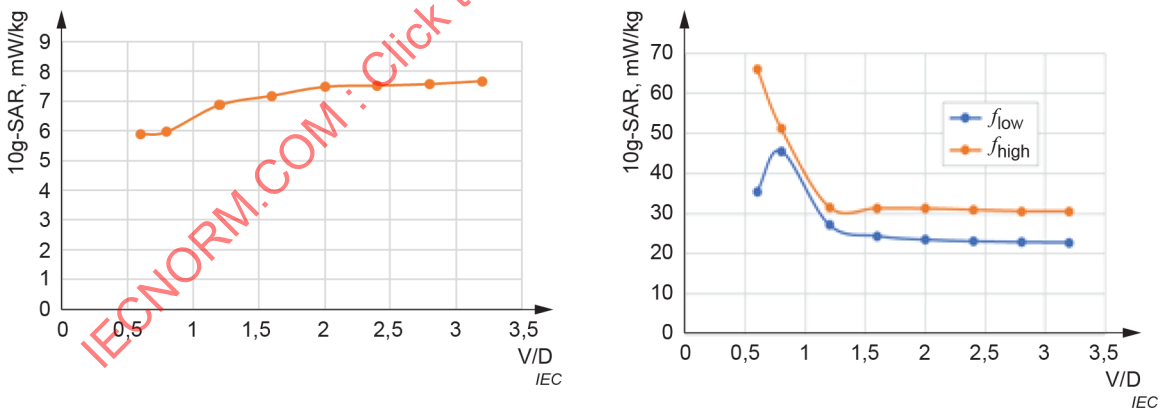

a) case A b) case C

Figure D.7 – Calculated 10 g-averaged SAR versus the smaller axis of elliptical phantom v normalized by coil outer diameter D for a) case A (f_{high} = 7,54 MHz) and b) case C (f_{low} = 6,14 MHz, f_{high} = 7,18 MHz)

a) elliptical phantom b) rectangular phantom

Figure D.8 – Layout of small WPT system for exposure conditions of case C with respect to a) elliptical phantom and b) rectangular phantom

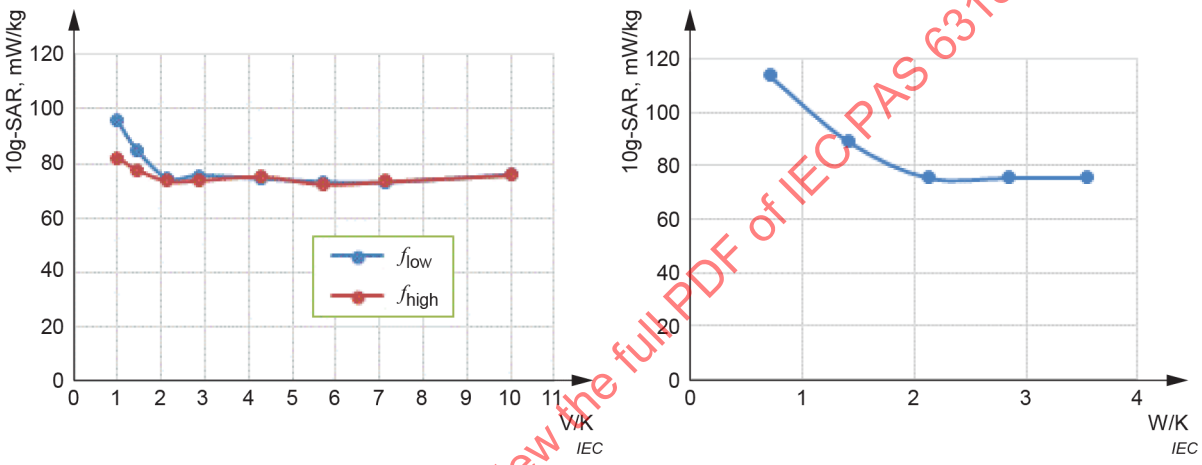

a) elliptical phantom b) rectangular phantom

Figure D.9 – Calculated 10 g-averaged SAR versus the smaller axis v or width W normalized by square coil diagonal K for a) elliptical phantom (f_{low} = 6,6 MHz, f_{high} = 7,64 MHz) and b) rectangular phantom (f_{low} = 6,59 MHz)

Annex E
(informative)

Extrapolation methods of SAR measurement

E.1 General

Measurements of SAR inside a human-equivalent liquid phantom are a practical method for exposure assessment. However, accurate measurements of SAR are sometimes difficult, especially at a location close to the phantom boundary, owing to the boundary effect; i.e. field disturbance due to the SAR probe itself. Hence, it is necessary to use an extrapolation method to determine the internal electric field or SAR.

E.2 Measurement and interpolation of electric field inside a phantom

E.2.1 General

Two steps to extrapolate the electric field strength inside a liquid phantom are described below. Note that the total electric field is used for all extrapolations performed in this study.

Step 1: Measure the electric field distribution inside a liquid phantom (denoted as $|E|$) in the depth direction with a regular interval of Δx. The closest distance to the phantom boundary for the measurements is set to d_{min}.

Step 2: Determine the fitting parameters for an extrapolation function using the measured electric field data. Then, calculate $|E|$ near the phantom boundary from the extrapolation function.

The parameter with the minimum distance from the phantom boundary d_{min} should be as far as possible to avoid the boundary effect, which is caused by the perturbation of the internal electric field by the measurement probe. However, d_{min} should also be as close as possible due to the rapid decay of the internal electric field and the limitation of sensitivity of the measurement probe. The parameter d_{min} may be determined experimentally to fulfil the above requirements. The parameter of the measurement interval Δx should also be determined as accurately as possible to maintain sufficient accuracy for the proposed extrapolation method.

E.2.2 Extrapolation functions

An extrapolation function for the internal electric field should include the effect caused by the decay of reactive near-fields, which depends on the distance from a source, and the medium loss in terms of an exponential decay [39]. Based on these considerations, the following extrapolation functions (indicated as Type-A and Type-B) may be used to determine the internal electric field close to the phantom boundary.

Type-A:

$$E_{\text{new}}(x) = \frac{A_1}{(x + A_2)^2} \mathrm{e}^{-\alpha_0 x} \tag{E.1}$$

where α_0 is an attenuation constant, A_1 and A_2 are fitting parameters, determined by a nonlinear regression method using the Levenberg–Marquardt algorithm [40]. The other type of extrapolation function is defined as a polynomial function as

Type-B:

$$E_{\text{poly}}(x) = D_1 x^2 + D_2 x + D_3 \tag{E.2}$$

The polynomial function in Formula (E.2) is actually applied to an extrapolation of the internal electric field strength inside a liquid phantom placed in the vicinity of a mobile phone, as described in IEC/IEEE 62209-1528 [15]. The fitting parameters D_1, D_2, and D_3 are determined by a linear regression method using the least-squares algorithm.

E.2.3 Three steps for determination of spatial-peak SAR

The extrapolation function in E.2.2 is utilized to evaluate the maximum local SAR averaged over a 10-g cube or 10 g averaged SAR, which is a basic restriction defined in the safety guidelines. The 10 g averaged SAR is calculated and compared with the exposure limit prescribed in the ICNIRP guideline. The calculation method for 10 g averaged SAR is described as follows.

- Step 1: Measure the SAR distribution with a coarse interval of 20 mm on a two-dimensional plane located 25 mm away from the phantom boundary to search for the peak of the measured SAR location. The measurement interval was set in accordance with the procedures prescribed in the IEC/IEEE 62209-1528 [15], which states that the maximum grid spacing should be 20 mm for frequencies below 3 GHz.
- Step 2: Measure the three-dimensional SAR distribution in a cube volume of 7 × 7 × 7 points at the local maxima locations identified in Step (1). Again, a fine interval of 4 mm is set in conformity with the measurement procedures prescribed in the IEC 62209-1528 [15].
- Step 3: By the proposed extrapolation method, estimate SAR in the region close to the phantom boundary. It should be noted that the 10 g averaged SAR was determined from the SAR averaged over 13,96 g and 8,08 g by using 73 and 63 extrapolated data with the 4-mm interval from the measurement, respectively. The measurement procedure proposed here is not versatile, but it conforms to the well-established IEC/IEEE 62209-1528 [15].

E.2.4 Validation of measurement methods using extrapolation

For SAR measurements, a measurement system is constructed and two types of WPT systems, i.e. solenoid and flat-spiral types, are fabricated. The schematic diagram and photograph of the constructed measurement system are shown in Figure E.1 and Figure E.2, respectively. The SAR probe was calibrated in-house by a calibration system for a SAR probe, which was fabricated by the National Physical Laboratory (NPL, United Kingdom) [41]. The input power was set as 30 W for the temperature measurement and 1 W for the voltage measurement of the probe. The calibration factor for the electric field probe was determined as 9,90 and 9,88 at 6 MHz and 13,56 MHz, respectively. The calibration factor at measurement frequencies was determined by a linear interpolation of the value at these two frequencies. The data readout unit (DAE4) was calibrated by the manufacturer.

The water tank is made of glass. The effect of the glass tank on the SAR inside the liquid phantom was investigated in advance by the method of moments (MoM). The difference in maximum SAR in the measurement plane located 2,5 cm away from the boundary of the glass tank is less than 0,8 % for the analysis model with and without the glass tank. Consequently, it was confirmed that the effect of the glass tank can be ignored.

Figure E.3 and Figure E.4 show the measured and simulated electric field distributions in the measurement plane located 2,5 cm away from the phantom boundary for the solenoid and flat-spiral-type WPT systems, respectively. Both experimental and simulation results show similar distributions with differences in maximum $|E|$ of 14 % and 6 % for the solenoid- and flat-spiral-type WPT systems, respectively. The difference in measured $|E|$ can be attributed to the uncertainty of the probe calibration (10,3 %) and the other sources of uncertainty such as probe position, WPT system position, variation in input power, linearity, etc.

Figure E.5 shows the results of 10 g averaged SAR estimated using the type-A extrapolation function when the input power is 10 W. The difference between the measured 10 g averaged SAR with the type-A extrapolation and the MoM-derived 10 g averaged SAR was found to be less than 29 % for the experiment in this example. It was confirmed that the type-A extrapolation function provides a smaller difference in 10 g averaged SAR than the type-B functions in this example.

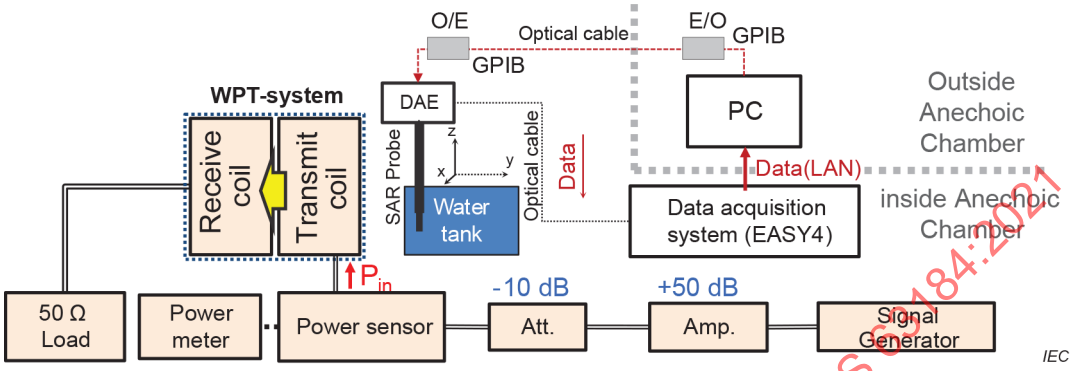

Key

O/E	optical/electrical converter	DAE	data acquisition electronics
E/O	electrical/optical converter	GPIB	general-purpose interface bus

Figure E.1 – Schematic diagram of measurement system

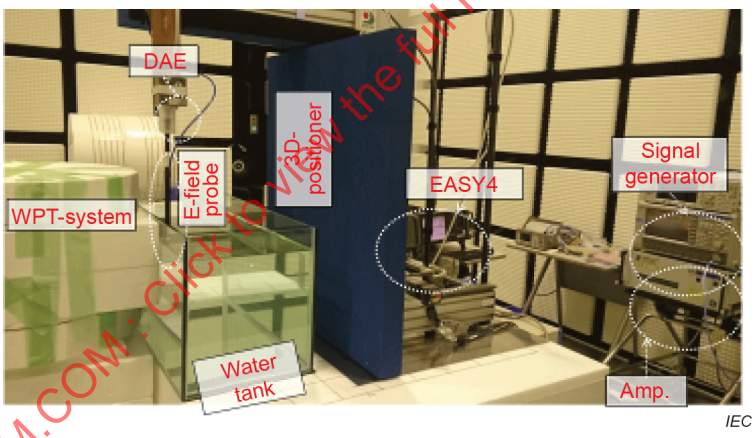

Figure E.2 – Measurement system

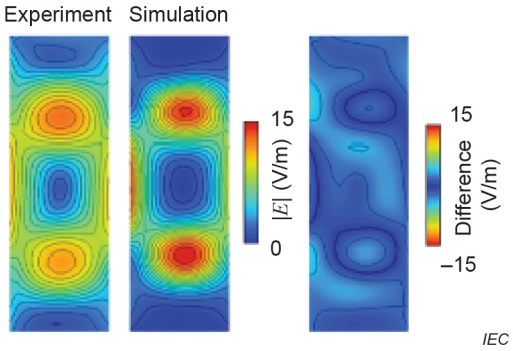

Figure E.3 – Measured and simulated electric field distributions in the measurement plane 2,5 cm away from the phantom boundary in the case of the solenoid-type WPT system

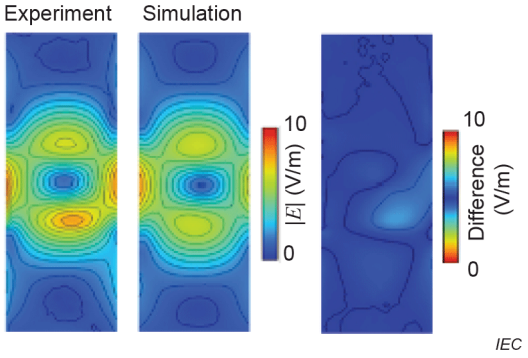

Figure E.4 – Measured and simulated electric field distributions in the measurement plane 2,5 cm away from the phantom boundary in the case of the flat-spiral-type WPT system

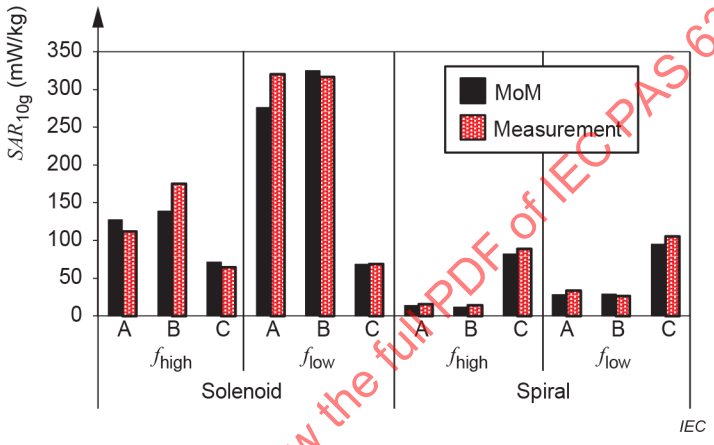

Figure E.5 – 10 g averaged SAR obtained by measurement with extrapolation and MoM-derived 10 g averaged SAR

E.2.5 Uncertainty

The measurement procedure for determining 10 g averaged SAR described in E.2.4 includes some uncertainty factor and it should be considered. Table E.1 shows the measurement uncertainty, which has been experimentally derived for the phantom conductivity and the probe calibration and numerically derived for the distance, density, and type-A extrapolation method. In this study, the uncertainty factors include the distance (2 % at 2,5 cm) from the vertical axis to the phantom boundary, conductivity and density of the liquid phantom, the uncertainty due to the probe calibration (5,15 %) and the type-A extrapolation method (8,11 %). Relative permittivity is not considered in this study because its influence is negligible to the total uncertainty of the 10 g averaged SAR. The total measurement uncertainty (k = 2) is equal to approximately 22 %.

The 10 g averaged SAR derived by MoM is determined exactly at its maximum position. The position of 10 g averaged SAR determined from the experimental data may have shifted away from the real maximum position since the measurements were conducted with a coarse interval of 2 cm.

Table E.1 – Measurement uncertainty of 10 g averaged SAR

	Tolerance [%]	Probability distribution	Sensitivity coefficient	Degrees of freedom	Standard uncertainty [%]
Distance	2,0	rect	4,56	11	5,26
Conductivity	1,21	norm	1,0	∞	0,61
Density	1,0	rect	1,0	∞	0,577
Probe calibration	5,15	norm	2,0	∞	5,15
Proposed extrapolation method	8,11	norm	2,0	11	8,11
Combined standard uncertainty					11,0
Extended standard uncertainty (k = 2)					22,0

Annex F
(informative)

Numerical calculation methods

F.1 General

Different calculation methods can be used for the determination of induced quantities in the human body by an external magnetic field emitted from WPT systems. This Annex F provides an overview of different calculation methods. As the information given in this Annex F is not sufficient for application, the source materials referred to should be reviewed.

All these methods are based on the resolution of the macroscopic Maxwell's equation. The choice of a precise method for the resolution is based on various criteria including calculation time.

F.2 Quasi-static finite element method

The finite element method (FEM) with cubic elements may be used to assess exposures from WPT systems. Under the quasi-static assumption and simply-connected domains, the electric field in the body can be represented as

$$\mathbf{E} = -\nabla\phi - \frac{\partial \mathbf{A}_0}{\partial t} \tag{F.1}$$

where ϕ is the electric scalar potential and $\mathbf{A}_0$ is the vector potential of the incident magnetic field. Due to the continuity condition, the electric scalar potential in the body satisfies the following elliptic partial differential equation

$$\nabla \cdot \sigma \nabla \phi = -\nabla \cdot \sigma \frac{\partial}{\partial t} \mathbf{A}_0 \tag{F.2}$$

with the boundary condition

$$\mathbf{n} \cdot \sigma (\nabla \phi + \frac{\partial}{\partial t} \mathbf{A}_0) = \frac{\partial}{\partial t} Q_s \tag{F.3}$$

where σ is the conductivity and Q_s is the surface charge induced by the incident electric field.

For modelling the exposure to a magnetic field, Q_s was set to zero and $\mathbf{A}_0$ was calculated analytically. The exposure to the external electric field was modelled in two steps. First, the external electric potential in air was determined assuming that the body is a perfect electric conductor by solving the following equation and boundary conditions:

$$\nabla \cdot \varepsilon_0 \nabla \phi_{ext} = 0 \tag{F.4}$$

$$\begin{cases} \mathbf{n} \cdot \nabla \phi_{ext} = -\mathbf{n} \cdot \mathbf{E_0}, & \text{on outer boundary} \\ \nabla \phi_{ext} = 0, & \text{on body surface} \end{cases} \tag{F.5}$$

where $\mathbf{E_0}$ is the incident electric field and ε_0 is the permittivity of air. In Formula (F.5), it is assumed that the outer boundary is at a sufficient distance so that the perturbation in the incident field due to the body is negligible at the boundary.

The induced charge Q_s in each voxel on the body surface was calculated from the normal component of the external electric flux density, and the internal potential was determined by solving Formula (F.2) and Formula (F.3).

The electric scalar potential equations – Formula (F.2) and Formula (F.4) – were discretized using Galerkin FEM with piecewise linear basis functions. The elements were cubical, and the degrees of freedom were the values of the electric potential at the corners of each cube. This resulted in a sparse matrix equation for the unknown scalar potential values. The matrix equation may be combined with the geometric multigrid method and solved iteratively.

F.3 Scalar potential finite difference method

The scalar potential finite difference (SPFD) method sets the branch current instead of the loop current. Defining scalar potentials (unknowns) at each node of a voxel, a branch current flowing from one node to a neighbouring one along the side of the voxels is derived, which includes a vector potential due to the applied magnetic fields and impedance between the nodes. By applying Kirchhoff's current law at all nodes, simultaneous equations are then set. The potential is then solved iteratively. The electric field along the side of the voxel is obtained by dividing the difference of the potentials between the nodes of the voxel by the distance across the nodes and adding the vector potential.

$$\sum_{n=1}^{6} S_n \phi_n - \left(\sum_{n=1}^{6} S_n \right) \phi_0 = j\omega \sum_{n=1}^{6} (-1)^n S_n l_n A_{0n} \tag{F.6}$$

where S_n, ϕ_n, l_n, ω, and A_{0n} denote the edge conductance derived from tissue conductivity, the scalar potential, the length between nodes, the angular frequency and the magnetic vector potential, respectively. The matrix equations for SPFD were solved iteratively by an iterative matrix solver. An algebraic or geometric multigrid method can be also combined into the method to accelerate the computation [42], [43].

F.4 Impedance method

The impedance method (IM) models an inhomogeneous human body as a three-dimensional impedance network [44], [45]. Each voxel is associated with dielectric constants corresponding to the location in the human body model. Since the impedance is assigned at each edge of the voxel, the impedances are determined by an average of the dielectric constants of four adjacent voxels, e.g. for an impedance along the x-direction:

$$z_x|_{i,j,k} = \frac{1}{j\omega\varepsilon_0 \dot{\varepsilon}_a|_{i,j,k}} \frac{l_x}{l_y l_z} \tag{F.7}$$

where ω and ε_0 are the angular frequency and free-space permittivity, respectively. l_x, l_y, and l_z are the edge lengths in the x-, y-, and z-directions, respectively. $\dot{\varepsilon}_a$ denotes the average complex relative permittivity, i.e. for the x-direction,

$$\dot{\varepsilon}_a|_{i,j,k} = \frac{\dot{\varepsilon}|_{i,j,k} + \dot{\varepsilon}|_{i,j+1,k} + \dot{\varepsilon}|_{i,j,k+1} + \dot{\varepsilon}|_{i,j+1,k+1}}{4}, \quad \dot{\varepsilon}|_{i,j,k} = \varepsilon_r|_{i,j,k} + \frac{\sigma|_{i,j,k}}{j\omega\varepsilon_0} \tag{F.8}$$

$\varepsilon_r|_{i,j,k}$ and $\sigma|_{i,j,k}$ are the relative permittivity and conductivity, respectively, associated with the voxel at the location indexes i, j, and k. Once the impedance network has been constructed, the induced loop currents at each voxel face are then determined by applying an electromotive force due to Faraday's law and solving the system of equations with the successive overrelaxation (SOR) method. After the loop currents are obtained, the line currents along the edges of each voxel can be calculated from four loop currents surrounding each edge and the current at the centre of each voxel is determined by averaging the four-line currents in each direction. Finally, the internal electric field is then computed using the following equation, e.g. for the z-component electric field,

$$E_z^{\text{in}}|_{i,j,k} = \frac{I_z^{\text{c}}|_{i,j,k}}{\sigma|_{i,j,k} + j\omega\varepsilon_0\varepsilon_r|_{i,j,k}} \frac{1}{l_x l_y} \tag{F.9}$$

where $I_z^{\text{c}}|_{i,j,k}$ is the z-component current at the centre of the voxel at the location indexes i, j, and k.

F.5 Finite-difference time-domain method

The finite-difference time-domain (FDTD) method, as first proposed by Yee in 1966, is a method for full-wave analysis [46]. It was first used to evaluate absorption in heterogeneous tissues in 1975 [47]. In this method, electric and magnetic fields are directly discretized in the time and space domain, respectively, and the central difference is used in the discretization process. The mesh is based on cubical cells. Mathematically speaking, the algorithm is called a leap-frog. The update equations are used in a leap-frog scheme to incrementally march the E and H fields forward in time. Since the method is an explicit time domain method, the matrix computation which is usually complicated is not needed. Also, the method is suitable for parallel computing [48], [49], [50]. The computational region must be truncated by a perfectly matched layer absorbing boundary [51], [52].

F.6 Hybrid technique of MoM and FDTD method

The concept of the hybrid MoM/FDTD method [53], [54] can be used. There are two analysis regions: the MoM, which includes metallic structures such as coils or loops of WPT systems, and the FDTD method, which includes biological bodies such as a human body. $\mathbf{J_a}$ and $\mathbf{J_h}$ are electric current densities residing on the WPT systems and displacement current densities inside a biological body, respectively. The displacement current densities $\mathbf{J_h}$ are determined as follows [68], [69]:

$$\mathbf{J_h}(\mathbf{r'}) = j\omega\frac{\hat{\varepsilon}_r - \varepsilon_0}{\hat{\varepsilon}_r}\mathbf{D}(\mathbf{r'}) = j\omega\left(\hat{\varepsilon}_r - \varepsilon_0\right)\mathbf{E}(\mathbf{r'}) = j\omega\varepsilon_0\left(\varepsilon_r - 1 - j\frac{\sigma}{\omega\varepsilon_0}\right)\mathbf{E}(\mathbf{r'}) \tag{F.10}$$

where ω, $\hat{\varepsilon}_r$, ε_0, ε_r, and σ are angular frequency, complex relative permittivity, free-space permittivity, relative permittivity and conductivity of biological tissues, respectively. $\mathbf{E}(\mathbf{r'})$ is the total electric field at a location $\mathbf{r'}$. Then, the displacement current over a volume cell having dimensions of $\Delta x \times \Delta y \times \Delta z$, where Δx, Δy, and Δz are the spatial intervals in the x-, y-, and z-axes, respectively, is determined as

$$\mathbf{I_h}(\mathbf{r'}) = \mathbf{J_h}(\mathbf{r'})\Delta x\Delta y\Delta z = j\omega\varepsilon_0\left(\varepsilon_r - 1 - j\frac{\sigma}{\omega\varepsilon_0}\right)\mathbf{E}(\mathbf{r'})\Delta x\Delta y\Delta z \tag{F.11}$$

This displacement current will be used in the calculation of the scattered field from biological bodies.

Calculation procedures of the MoM/FDTD method are as follows.

- Step 1: Apply an incident voltage at the antenna terminal and determine the current distribution $\mathbf{J_a}$ on the WPT system.
- Step 2: Radiated/scattered electric fields $\mathbf{E^{s1}}$ at an observation point in the FDTD region are calculated by using the following equation:

$$\mathbf{E^{s1}}(\mathbf{r}) = jk_0\eta_0 \int \left[\mathbf{J_a}(\mathbf{r'}) + \frac{1}{k_0^2} \nabla\nabla' \cdot \mathbf{J_a}(\mathbf{r'}) \right] G_0 d\mathbf{r'} \tag{F.12}$$

  where k_0 is the wavenumber, η_0 is the intrinsic wave impedance, G_0 represents the dyadic free-space Green's function, $\mathbf{R} = |\mathbf{r} - \mathbf{r'}|$, $\mathbf{r}$ is an observation point, $\mathbf{r'}$ is a source point. Calculated electric field $\mathbf{E^{s1}}$ is then transformed into the time-domain sinusoidal waveform to be used as an incident field in the FDTD method.
- Step 3: The total electric field, along with the SAR, inside biological bodies are calculated with the FDTD method. After the variation in the SAR or internal electric field at the consecutive time step is less than 10^{-5}, the FDTD calculation stops.
- Step 4: The displacement current inside biological bodies is calculated. Since the cell size in the FDTD method is small (on the order of one-tenth to one-twentieth of the wavelength at analysis frequency) the displacement current inside a cell can be considered infinitesimal. Consequently, the scattered electric fields at an arbitrary observation point outside the biological bodies can be calculated by using the following equations:

$$\mathbf{E}^{S_2}(\mathbf{r}) = -jk_0 \sum_{p=1}^{N_d} \frac{e^{-jk_0 R_p}}{4\pi R_p} \left\{ \eta_0 (\mathbf{j}_p - \mathbf{p}_p) + \frac{\eta_0 D}{jk_0} (\mathbf{j}_p - 3\mathbf{p}_p) \right\} \tag{F.13}$$

$$\mathbf{p}_p = \frac{(\mathbf{R}_p \cdot \mathbf{j}_p)\mathbf{R}_p}{R_p^2}, \quad D = \frac{1}{R_p}\left(1 + \frac{1}{jk_0 R_p}\right), \quad \mathbf{R}_p = \mathbf{r} - \mathbf{r}_p \tag{F.14}$$

  where N_d is the number of voxels comprising biological bodies and $\mathbf{j}_p = \mathbf{I_h}(\mathbf{r}_p)$, $\mathbf{r}_p$ is the centre coordinate of the pth voxel.
- Step 5: Induced voltages on metallic elements in the MoM region are calculated by the conventional MoM procedures using the scattered field in Step 4 as an incident field. Since they are treated as an additional source in the MoM. $\mathbf{J_a}$ obtained in this step must be added to those obtained in the previous iterations. Steps 2 to 5 are then repeated until the convergence of the antenna input impedance or input power is reached.

F.7 Hybrid technique of FEM and SPFD method

In this hybrid technique [55], the external magnetic induction field $\mathbf{B}$ is solved using any finite element method (FEM) approach [56], [57], while the internal electric field $\mathbf{E}$ is evaluated with the SPFD described in F.3. Specifically, the values of the current on the coils are needed to calculate the magnetic field behaviour while taking into account the ferromagnetic materials (e.g. shielding ferrite) and conductive materials (e.g. the car chassis). The resulting magnetic field is then exported with a fixed grid resolution and imported in any low-frequency (LF) magneto-quasi-static (MQS) solver based on the SPFD method, which has shown to work up to about 10 MHz [58]. In this method, the electric field is obtained starting from the knowledge of the magnetic vector potential $\mathbf{A}$.

Annex G
(informative)

Averaging algorithms

G.1 Current density averaging over an area

G.1.1 General

The averaged current density J_{av} according to [2] is calculated on a circular surface with an area A_0. The tissues of the anatomical models in which J_{av} is calculated should distinguish the following groups:

– central nervous tissue;
– peripheral nervous tissue;
– other tissues.

Depending on the numerical algorithm to calculate the induced fields, the anatomical models are meshed using either Cartesian voxels or tetrahedra. Each voxel or tetrahedron is assigned a single tissue which belongs to one of the three groups and which has one particular electric conductivity value. For the calculation of J_{av} in an anatomical model, its tissues should be selected from one or more of the groups listed above. Voxels or tetrahedra with unselected tissues should be disregarded by the averaging algorithm.

For the calculation of J_{av}, the current density vector should be determined for each voxel (G.1.2) or tetrahedron (G.1.3) and then averaged over one or more voxels or tetrahedra (G.1.3). The maximum J_{av} of all voxels or tetrahedra should be reported.

G.1.2 Calculation of the current density in a Cartesian voxel

For Cartesian computational meshes or voxel based meshes, a current density vector is calculated for each voxel. The twelve E-field components are calculated by linear interpolation of the vector components on the E-fields on the voxel edges (Figure G.1) into the voxel centre using Formula (G.1), Formula (G.2) and Formula (G.3).

$$E_x = \frac{1}{4}\left(E_{1x} + E_{2x} + E_{3x} + E_{4x}\right) \tag{G.1}$$

$$E_y = \frac{1}{4}\left(E_{1y} + E_{2y} + E_{3y} + E_{4y}\right) \tag{G.2}$$

$$E_z = \frac{1}{4}\left(E_{1z} + E_{2z} + E_{3z} + E_{4z}\right) \tag{G.3}$$

The current density vector is calculated by multiplying the interpolated E-field vector by the electrical conductivity assigned to the voxel.

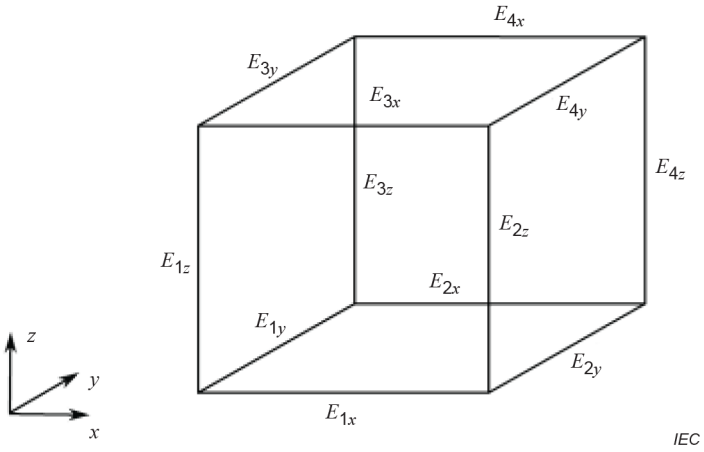

Figure G.1 – Field components on voxel edges

G.1.3 Calculation of the current density in a tetrahedron

For the calculation of the current density in the tetrahedra, the electric field vector should be calculated in the gravitational centre of each tetrahedron by evaluation of the respective finite elements. It should then be multiplied by the conductivity assigned to the respective tetrahedron.

G.1.4 Calculation of J_{av}

J_{av} should be evaluated for all points sampled on a rectilinear grid at a step width of sqrt(A_0)/10 or alternatively for each voxel or tetrahedron according to the following steps.

a) Determine the direction of the current density vector $\boldsymbol{j}_v$ at point v or in the centre of the current voxel v or tetrahedron v in terms of the normalized vector $\mathbf{n}_v$.

b) Determine a circle with the area A_0 and the direction of the current density of the normal vector.

c) Triangulate the circle with a maximum edge length of sqrt(A_0)/10.

d) Initialize two variables I_v and A_v to zero. These variables contain the current and the area contributing to J_{av} of the current voxel v or tetrahedron v.

e) Calculate the contribution of each triangle t in the circle to the averaged current density J_{av}:

1) Determine the current passing through each triangle I_t by multiplying the current density vector calculated in its centre by the normalized vector $\mathbf{n}_v$ and the dimensions of the respective triangle.

NOTE 1 The current through the triangle t may be very different from the current of the voxel v or tetrahedron v for which J_{av} is evaluated. Only the part of the current that is parallel to the current of the of the voxel v or tetrahedron v is considered.

2) If I_t is positive, add it to I_v and add the area of the current triangle t to A_v.

3) After iterating over all triangles of the circle, calculate J_{av} by dividing I_v by A_v.

NOTE 2 This algorithm automatically adapts the size of the averaging area to structures or current paths of the cross sections which are thinner than the area of the averaging circle (e.g. peripheral nerve cords) and reduces the dimensions of the averaging area at tissue-air interfaces. As a result, excessive overestimation due to a reduced averaging area is prevented.

G.2 E-field averaging in a cubical volume

The averaged E-field in a selected tissue group within cubical volumes should be evaluated using the following algorithm:

a) The magnitude of the local E-field should be sampled with a grid step of d_0 ≤ 0,7 mm at the centre points of virtual voxels with an edge length of d_0. For evaluation in anatomical voxel models, the virtual voxels should be aligned with the anatomical voxels such that the virtual voxels do not intersect with anatomical voxel surfaces, but are each fully contained in an anatomical voxel. For example, for a 2 × 2 × 2 mm^3 resolution anatomical voxel model, each anatomical voxel could contain 125 virtual voxels of 0,4 × 0,4 × 0,4 mm^3.

b) Each virtual voxel belongs to the tissue evaluated at its centre.

c) For each sample point, a cube C_{avg} with initial edge length d_1 = 2 mm should be constructed.

d) For each virtual voxel which belongs to the selected tissue group, its volume inside C_{avg} should be added up to V_{avg}.

e) While V_{avg} is smaller than 8 mm^3, the edge length d_1 should be increased to approximate V_{avg} = 8 mm^3, but only as long as $d_1 < d_{1,max}$ = 4 mm.

NOTE With this limitation, in the case of a voxel model with a thin nerve of 0,5 mm diameter, the E-field in this nerve would be averaged over a length of 4 mm, i.e. 8 voxels, instead of 32 mm with 64 voxels. A larger $d_{1,max}$ of e.g. 8 mm could also be used.

f) The final V_{avg} should not exceed 8 mm^3 by more than 0,1 %, the smallest V_{avg}, its d_1 and its centre point should be reported.

g) For the final V_{avg} all local E-field magnitudes should be multiplied by their virtual voxel's partial volume inside C_{avg} and summed up. The sum should be divided by V_{avg}. The resulting E_{avg} should be assigned to the virtual centre voxel.

G.3 E-field averaging along an averaging distance

G.3.1 General

The averaged E-field along an averaging distance should be evaluated by calculating the voltage difference ΔV on two points in a tissue or a group of tissues and dividing it by the averaging distance d_a. It is assumed that quasi-static conditions are met (G.1.3) such that the E-field integral over the distance d_a can be regarded as independent from the actual integration path. For exposure to E-fields at higher frequencies or to magnetic sources, the E-field integral can no longer be assumed to be independent of the integration path. The E-field averaging algorithm needs to consider this by finding a path that maximizes the integral of the E-field vector along this path. For typical mesh resolutions in anatomical models, the computational effort for rigorous search of the path that maximizes the E-field integral can be assumed to significantly exceed available resources.

Hence, the integration path of the E-field is constructed following the direction of the E-field vector through the tissue groups that are evaluated. For the quasi-static case, this method will identify the path that correctly calculates the voltage difference ΔV if the mesh resolution is sufficiently fine. For the general case, this method is expected to yield convergent results if the mesh resolution is refined.

If the E-field in the domain of interest is assumed to depend on the phase of the field source, the maximization should be carried out by integrating the real part of the E-field vector for seven different phase steps of 45° of the field source.

The tissues of the anatomical models in which E_{av} is calculated should distinguish the following groups:

- central nervous tissue;
- peripheral nervous tissue;
- other tissues.

Depending on the numerical algorithm to calculate the induced fields, the anatomical models are meshed using elements, i.e. either Cartesian voxels or tetrahedra. Each element is assigned a single tissue which belongs to one of the three groups. For the calculation of E_{av} in an anatomical model, its tissues should be selected from one or more of the groups listed above. Elements with unselected tissues should be disregarded by the averaging algorithm.

To improve the accuracy, e.g. in case of large tetrahedra of higher finite element order, virtual voxels can be used as elements in the following algorithm. These should be created by sampling the volume with a constant sampling step $d_0 < d_a/5$.

G.3.2 Algorithm to construct the integration path

The integration of the E-field vector along a path with the length of the averaging distance d_a should be carried out based on the following assumptions:

- Each element that belongs to the selected group of the three tissue groups listed in G.3 should be used as a starting point for the integration path.
- For each element, the E-field vector should be linearly interpolated into or evaluated in its gravitational centre. The reference location for each element should be assumed to be in the gravitational centre, as well.

The integration path should be determined in the following steps.

a) Define two variable arrays that store a) the dot product of the E-field vector and its direction and b) the location of the gravitational centre of the element.

b) At the starting element, determine the direction of the E-field vector and the dot product of the E-field vector and its direction. Store the result and the location of the vector in their respective variable arrays.

c) Identify the face of the voxel or tetrahedron through which the current direction vector passes. If the direction vector passes through an edge or vertex, all faces adjacent to this edge or vertex should be considered in the next steps.

d) For the faces identified in Step c), identify the elements that share these edges.

e) If no elements can be identified in Step d), disregard the current starting voxel and proceed to the next one.

f) For all elements identified in Step d), determine the one with the maximum $|E|$. Store this $|E|$ and its location as part of the path for the current starting element.

g) Calculate the distance covered by the path. If the distance is less than d_a, return to Step c) and add the next element.

h) Calculate the sum of the stored $|E|$ and scale it to the target distance d_a. Assign it to the current starting element.

i) Proceed to the next starting element and return to Step b).

Report the overall maximum of all elements. If no maximum could be determined (see Step e)) over the entire computational domain, report an error message.

Annex H
(informative)

Code verification and model validations

H.1 Code verification

H.1.1 Introduction

The implementation of a numerical code used in analyses should be verified for technical correctness by the manufacturer or the user according to the benchmarks defined in Annex H and in the referenced standards. The verification carried out by the manufacturer should be documented such that the user can reproduce it. Only a code which has been verified according to the methods described here can be used for determining the induced quantities in the human body for wireless power transfer systems. The following sections describe or reference benchmark tests for the verification of full-wave and quasi-static methods as well as the required averaging techniques listed in 7.1.

Full wave finite element and finite-difference time-domain codes should be verified according to the protocols specified in [28], [29].

NOTE Definition of verification benchmarks for other numerical full wave codes will be provided in a next revision, but [28], [29] can be consulted.

H.1.2 Quasi-static codes

H.1.2.1 Introduction

According to Table 3, different quasi-static algorithms can be applied to numerically quantify the exposure of the human body. Hence, no comprehensive methodology can be defined that would be appropriate for the verification of all applicable codes and their implementations. Therefore, to verify the implementation of a quasi-static algorithm, its numerical results should be compared to those given for the benchmark.

H.1.2.2 Homogeneous sphere exposed to magnetic field

The current density induced in a homogeneous sphere by a Helmholtz coil should be evaluated and compared to reference results. The sphere has a radius of 0,5 m and is positioned in the centre between two circular concentric loops. Its conductivity is σ = 0,2 S/m. The radii of the loops and their separation distance is 1 m. The current density should be evaluated within the sphere on the axis of the two circular loops starting in the centre of the loop and using a step size of 10 mm. The results should be compared to the analytical solution of [59], [60].

The B-field on the axis of the Helmholtz coil is given as

$$B_{\mathrm{Hz}} = \frac{I\mu_0}{\pi a\sqrt{(1+\alpha)^2+\beta^2}}\left[E(\kappa)\frac{1-\alpha^2-\beta^2}{(1+\alpha)^2+\beta^2-4\alpha}+F(\kappa)\right] \tag{H.1}$$

where I is the loop current, a is the radius of the loops, $\alpha = r/a$, $\beta = d/a$, r is the position on the axis, and $2d$ is the separation distance between the loops. $F(\kappa)$ and $E(\kappa)$ are the complete elliptical integrals of the first and second kinds.

The current density in the lossy sphere can then be calculated as

$$J(r) = \pi f \sigma B\, r \tag{H.2}$$

where f is the frequency.

H.1.3 Quasi-static codes for the calculation of the incident magnetic field

H.1.3.1 Introduction

Depending on the application, quasi-static codes for the calculation of the induced fields may merely calculate the fields in coils with known currents or may additionally calculate induced eddy currents in metallic conductors in the environment of the coil or the exposed body.

H.1.3.2 Loops with known currents by evaluation of Biot-Savart's law

The correct implementation of interpolation and superposition of vector field components should be verified by evaluating the fields from three loops L_1, L_2 and L_3 with DC currents of different amplitudes and phase offsets. The loops should have diameters of 200 mm. The normal axis of the first loop should be aligned with the z-axis of the coordinate system, the normal axis of the second loop should be aligned with the x-axis of the coordinate system centred with its feed point on the origin, and the normal axis of the third loop should be aligned with the y-axis of the coordinate system. The distances between the feed points should be 150 mm. The loops should be modelled as perfectly conducting filaments.

The amplitudes and phases of the loop currents are given in Table H.1. The x-, y- and z-vector components of the magnetic fields should be evaluated on two cubical surfaces with edge lengths of 300 mm and 175 mm centred about the origin. On the surfaces of the cube, evaluation points are defined on a rectilinear lattice with a spacing of 5 mm. All magnetic vector field components of the fields calculated with the software under test should be compared to reference results at those locations where the field components are ≥ 5 % of the maximum field amplitude on the six rectilinear lattices of the cube. The reference results are provided in a file according to the format defined in Annex B of IEC/IEEE 62704-4:2020 [29]. The maximum deviation of the H-fields should be reported in Table H.1. The maximum permissible deviation from the reference results is ±1,0 %.

Table H.1 – Interpolation and superposition of vector field components; maximum permissible deviation from the reference results is ±1,0 %

Excitation	Amplitudes and phases	Maximum deviation from reference on 175 mm cube	Maximum deviation from reference on 300 mm cube
consecutive	L_1: I = 1 A, ϕ = 0 L_2: I = 0,5 A, ϕ = 90° L_3: I = 2 A, ϕ = 180°		
	L_1: I = 2 A, ϕ = 0 L_2: I = 2 A, ϕ = 90° L_3: I = 2 A, ϕ = 0°		
	L_1: I = 1 A, ϕ = 180° L_2: I = 0,5 A, ϕ = 90° L_3: I = 2 A, ϕ = 180°		
simultaneous	L_1: I = 1 A, ϕ = 0 L_2: I = 0,5 A, ϕ = 90° L_3: I = 2 A, ϕ = 180°		
	L_1: I = 2 A, ϕ = 0 L_2: I = 2 A, ϕ = 90° L_3: I = 2 A, ϕ = 0		
	L_1: I = 1 A, ϕ = 180° L_2: I = 0,5 A, ϕ = 90° L_3: I = 2 A, ϕ = 180°		

H.1.4 Averaging algorithms

H.1.4.1 General

Currently code verification is only available for calculating the peak spatial average SAR. Subclause H.1.4 describes recommended procedures for other averaging algorithms.

H.1.4.2 Peak spatial-average SAR

For numerical algorithms operating on Cartesian meshes, such as FDTD or QS-FD, the verification of the calculation of the peak spatial average SAR should be carried out according to [28]. For numerical algorithms operating on other meshes, the verification should be carried out according to [29].

H.1.4.3 Whole-body average SAR

A constant electrical field vector with an amplitude of 1 V/m should be assumed inside the anatomical model. The anatomical model should be discretized with voxels or tetrahedra with edge lengths of up to 1,0 mm. The direction of the field vector should be varied over the solid angle in steps of 45° in theta-direction (five steps) and phi-direction (nine steps). For all combinations of phi and theta, the whole-body average SAR according to 7.3.3 should be calculated considering a) central nervous tissue, b) peripheral nervous tissue and c) all body tissues.

NOTE Anatomical model and results of the whole-body average SAR should be reported.

H.1.4.4 Averaged current density over an area

A constant electrical field vector with an amplitude of 1 V/m should be assumed inside the anatomical model. The anatomical model should be discretized with voxels or tetrahedral with edge lengths of up to 1,0 mm. The direction of the field vector should be varied over the solid angle in steps of 45° in theta-direction (five steps) and phi-direction (nine steps). For all combinations of phi and theta, the averaged current density should be calculated according to the algorithm of Clause G.1. It should be applied over a) central nervous tissue, b) peripheral nervous tissue and c) all body tissues. The area A_0 should be set to 1cm^2.

NOTE Anatomical model and results of the averaged current density should be reported.

H.1.4.5 Averaged E-field in a cubical volume

The SAR Star specified in [28] is exposed to a magnetic field with a constant amplitude of 1 A/m at a frequency of 100 kHz. Three averaged E-fields should be evaluated for orientation of the H-field vector along the x-, y-, and z-axes. The SAR Star should be centred about the origin of the coordinate system. The following conductivities should be assigned to the different regions of the SAR Star:

- outer layer: ε_r = 1; σ = 0,1 S/m;
- core and inner cube: ε_r = 1; σ = 0,02 S/m.

NOTE At a frequency of 100 kHz, the impact of the permittivity on the field distribution is negligible. It is specified here because it may be required, e.g. by full wave solvers, which can also operate in the quasi-static frequency range. The mass density of the layers of the SAR Star is not relevant.

The E-field should be averaged over a volume of 1 cm^3. Results should be reported using the table format specified in Annex C.3.2 of [28], where the column for the mass should be filled with zeros, and the columns for the local SAR and averaged SAR should be filled with the amplitude of the local E-field and of the averaged E-field. The result of the verification should be compared to reference results. The maximum permissible deviation of the averaging volume is ±0,000 2 % and the maximum permissible deviation of the local and averaged E-field is ±10 %.

H.1.4.6 Averaged E-field along a line

A constant electrical field vector with an amplitude of 1 V/m should be assumed inside the anatomical model. The anatomical model should be discretized with voxels or tetrahedra with edge lengths of up to 1,0 mm. The direction of the field vector should be varied over the solid angle in steps of 45° in theta-direction (five steps) and phi-direction (nine steps). For all combinations of phi and theta, the algorithm of Clause G.3 should be applied over a) central nervous tissue, b) peripheral nervous tissue and c) all body tissues.

The E-field should be averaged over a distance d_a of 10 mm. Results should be reported over the entire body.

H.2 Model validation

H.2.1 Introduction

Evaluation of the compliance with basic restrictions can be carried out in an entirely numerical approach or in a combined numerical and experimental approach. While the entirely numerical approach requires the development and validation of a numerical model of the field source (or the device under test) and the integration of both the model of the field source and the anatomical body model or phantom in the computational domain, a combined numerical and experimental approach may directly feed the incident field in the computational domain which then contains only the anatomical body model or the phantom. While the latter case is particularly suitable for exposure evaluation using the quasi-static evaluation, both approaches require the experimental assessment of the incident field at the location of the anatomical body model or phantom. In the frequency range where a full-wave evaluation is required, the impact

of the electrical load of the anatomical body model or phantom on the field source should be considered appropriately.

H.2.2 Recommendations for the development of the numerical model

The development of a numerical model of a field source for compliance testing requires the selection of the appropriate details to be represented in the computational domain. In many cases, not all required information may be available. Hence, only general recommendations for the development of the numerical model are provided here.

- The model of the field source should be based on its original CAD data.
- If possible, all conducting and magnetic parts of the field source should be integrated into the model.
- All parts of the environment that are relevant for the distribution and amplitude of the incident fields should be integrated in the model (body of a car, magnetic shielding, etc.).
- Depending on the frequency range, coil currents may be assumed to be constant over the entire extension of the coils.
- The real operation conditions of the field source should be considered to determine the current amplitudes in the coils. These include charging control circuits, charging status of the battery, etc. The inductances of the coils are generally not sufficient to determine the current amplitudes in the coils.

H.2.3 Determining the validity of the field source

The validation of the numerical model of the field source should be carried out according to the following steps.

a) Define a set of evaluation points encompassing the volume of the exposed anatomical body model or phantom.

b) In the frequency range where a full wave evaluation is required, i.e. when the conditions for the quasi static approximation do not hold, the coupling/back scattering caused by the dielectric load (human tissue) should be considered. The dielectric load can be a phantom that is equivalent to the exposed human body at the location where the exposure is evaluated.

c) If no dielectric load is present, measure the incident field (E-field or H-field amplitudes) distribution in the volume defined in Step a). The probe should be sufficiently small, i.e. the error due to the field gradient should be smaller than 1 dB. The measurements should include the entire exposed volume. If this is not possible, the distance to the exposure boundary shall not exceed 10 mm. If a dielectric load is present, measure the incident field on the surfaces both in front of and behind the dielectric load, or measure the induced field using a dosimetric probe.

d) Normalize the experimental field data, $v_{\mathrm{ref},n}$, to the measured output power or coil currents.

e) Determine the experimental uncertainty, U_{ref}, of the evaluation

f) Normalize the numerical near-field data $v_{\mathrm{sim},n}$, (simulated E-field or H-field amplitude) to the simulated output power or coil currents.

g) Determine the numerical uncertainty U_{sim} of the near-field evaluation according to Table 5.

h) At every point n for which $v_{\mathrm{ref},n}$ or $v_{\mathrm{sim},n}$ is larger than 5 % of the maximum measured or simulated value $\underset{n}{\mathrm{MAX}}\left(v_{\mathrm{sim},n} \mid v_{\mathrm{ref},n}\right)$ validate whether the deviation between the measured value at point n, $v_{\mathrm{ref},n}$ and the simulated value $v_{\mathrm{sim},n}$ are within the combined uncertainty of U_{ref} and U_{sim} by evaluating

$$E_n = \sqrt{\frac{(v_{\text{sim},n} - v_{\text{ref},n})^2}{(v_{\text{sim},n} \times U_{\text{sim}(k=2)})^2 + (v_{\text{ref},n} \times U_{\text{ref}(k=2)})^2}} \leq 1 \quad \text{(H.3)}$$

If the deviation is within the combined uncertainty, i.e. if E_n ≤ 1 for any considered point, the DUT model is valid. If $U_{\text{ref}} < U_{\text{sim}}$, U_{sim} is the uncertainty for the DUT model, otherwise U_{ref}. If E_n > 1, the DUT model is not valid and should be revised.

NOTE The subscript reference in the expressions above refers to the experimental reference results.

Annex I
(informative)

Use cases

I.1 EV (SWPT)

I.1.1 Determination of user position

Three physical regions are defined, to facilitate EMF safety management of the wireless charging system as shown in Figure I.1 and Figure I.2.

- Area 1 is the entire area underneath the vehicle, including and surrounding the wireless power assemblies. Area 1 should not extend beyond lower body structure edges (e.g. rocker panels or lower edge of bumpers).
- Area 2 is the region outside the periphery of the vehicle. The boundary between Region 1 and Region 2 extends downward from the lower periphery of the vehicle body sides.
- Area 3 is the vehicle interior (vehicle cabin).

It is not within the scope of this Annex I to define a procedure at Area 1 because Area 1 is not normally accessible to public and vehicle passengers. The procedure at Area 1 can be referenced from Annex K.

Areas 2 and 3 are both accessible to public and vehicle passengers. Therefore, this assessment procedure covers only Areas 2 and 3 to assess compliance to public exposure guidelines.

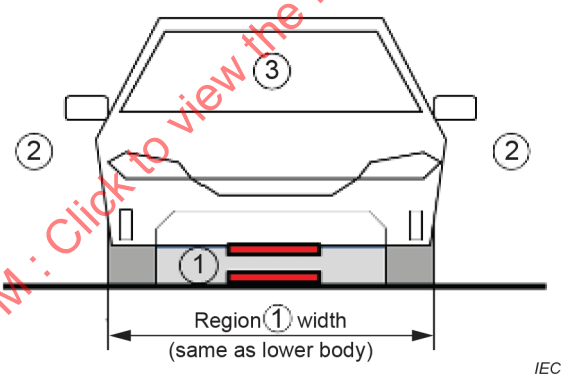

Key

Area 1: Area of operation

Area 2: Area surrounding the vehicle

Area 3: Vehicle interior

Figure I.1 – Example for areas of protection, for ground mounted systems (vehicle) [61]

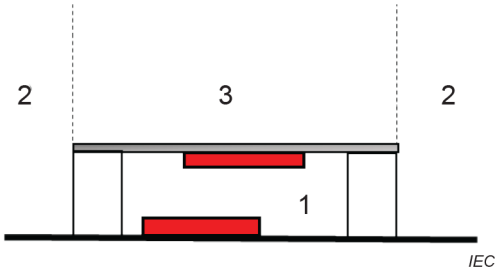

Key

1 Area of operation
2 Area surrounding the vehicle
3 Vehicle interior

Figure I.2 – Example for areas of protection, for ground mounted systems (using vehicle mimic plate)

I.1.2 Assessment procedures considering direct effects for WPT system for EV

I.1.2.1 General

There are four steps to assess the WPT exposure for EV use and demonstrate conformity with the basic restrictions and/or reference levels as described in Figure I.3 and based on Figure 2. Any of the four steps can be selected, depending on which is the most practicable for the exposure scenario.

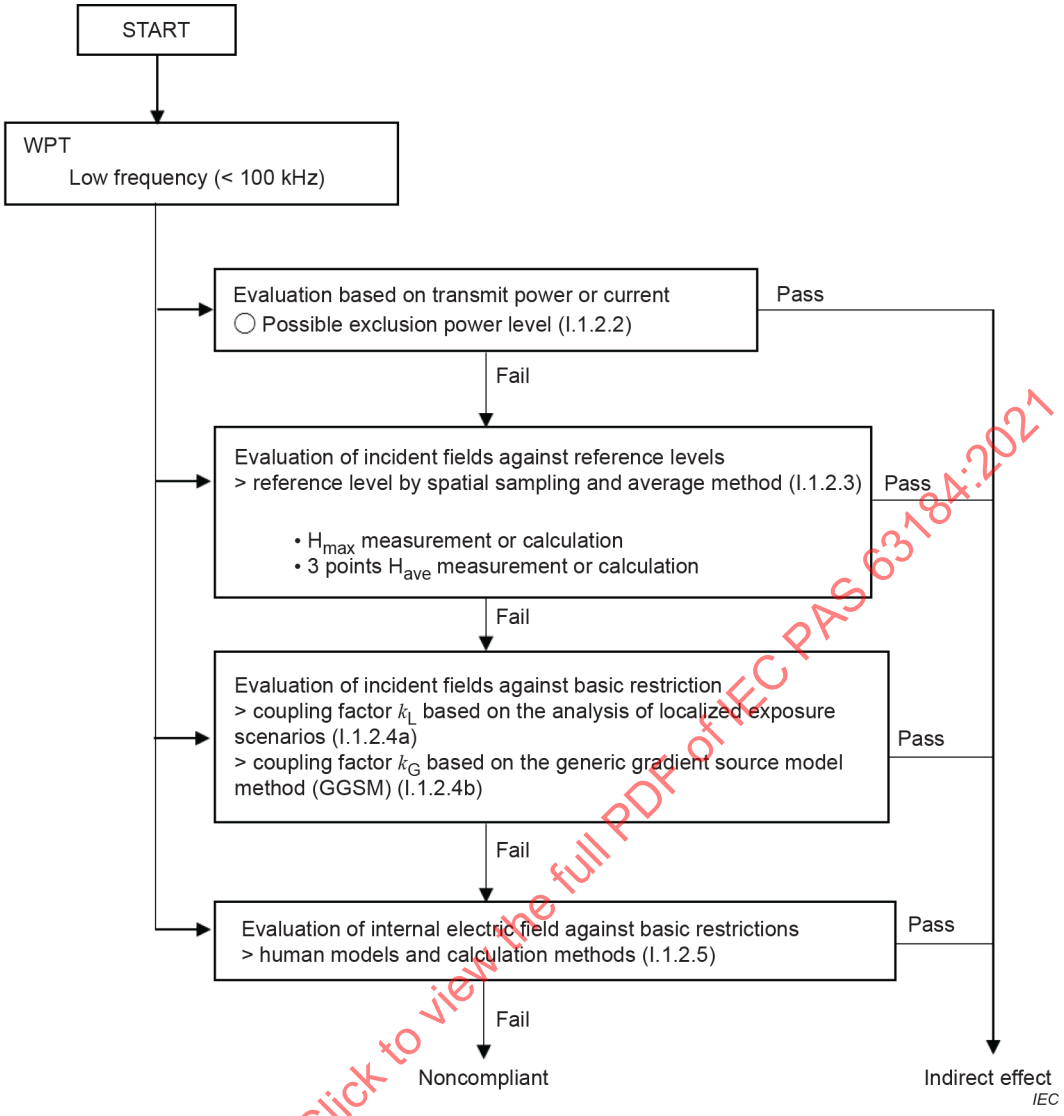

Figure I.3 – Flowchart for EV and vehicle mimic plate assessment (direct effect)

I.1.2.2 Evaluation based on coil current

The evaluation based on coil current for EV can be used. The procedure of the evaluation is defined in 5.2.2.

I.1.2.3 Evaluation of incident fields against reference levels

I.1.2.3.1 Vehicle

a) Assessment of incident H-fields of Area 2

1) The offset (x,y) in Figure I.4 should be determined experimentally or based on specifications provided by the device manufacturer because the maximum offset to allow energy transfer as well as the stray fields strongly depends on the design of the WPT coils.

2) Transmit efficiency should be kept at more than 80 % at the offset position.

3) The maximum magnetic field strength in Area 2 is measured at 0,2 m from the charging automobile using the WPT system and compared to the reference level as shown in Figure I.4.

4) If it exceeds the reference level, it is possible to use the spatially averaged value in the area occupied by human body. In that case, the averaged magnetic field strength which is measured on a plane at 20 cm from the closest accessible point and three points (0,5 m, 1 m, 1,5 m) in height, as shown in Figure I.4, can be used.

b) Assessment of incident H-fields of Area 3

1) The maximum magnetic field strength in Area 3 is measured during charging. The field at 0 cm or 10 cm surface for the driver's seat and the closest seat to the primary coil is measured and compared to the reference level of the magnetic field strength. The field at the surface for each seat can include the floor flat surface, as shown in Figure I.5.

2) It is possible to use the spatially averaged value. In that case, the spatial averaged magnetic field strength can be calculated based on the average of four values measured at a, b, c and d in Figure I.5.

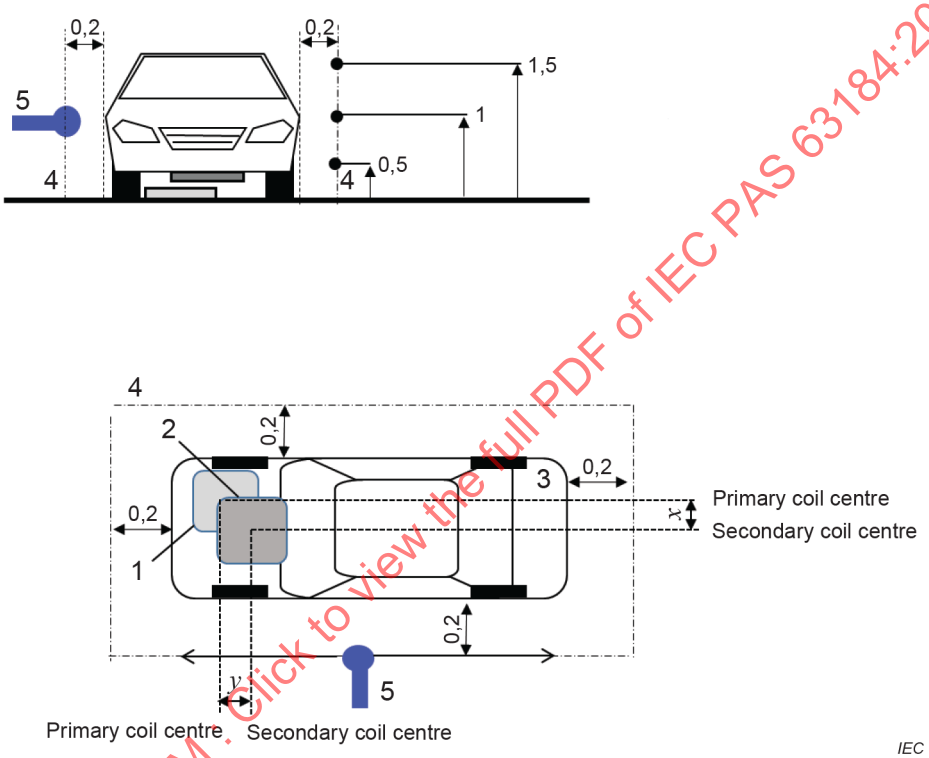

Key

1 Primary device
2 Secondary device
3 EV
4 Virtual area for scanning the worst-case position
5 Probe (P)

Figure I.4 – Area 2 measurement position (SWPT)

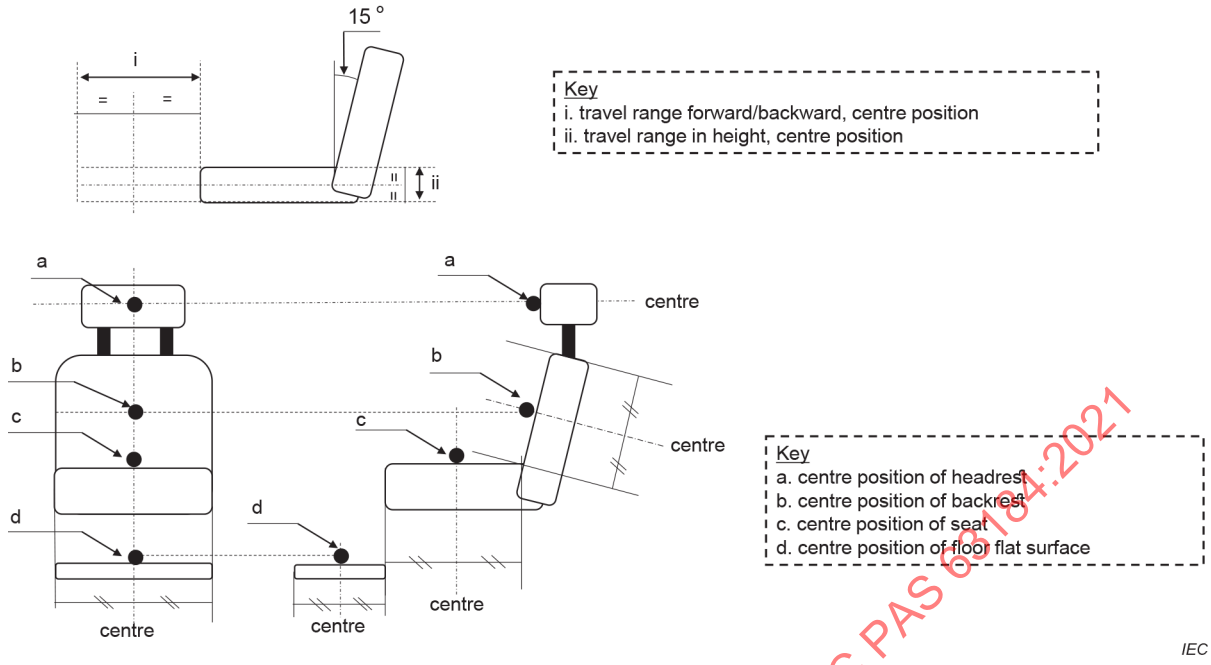

Key

i	travel range forward/backward, centre position
ii	travel range in height, centre position
a	centre position of headrest
b	centre position of backrest
c	centre position of seat
d	centre position of floor flat surface

Figure I.5 – Area 3 measurement position

I.1.2.3.2 Using vehicle mimic plate

a) Assessment of incident H-fields of Area 2

1) The offset (x,y) in Figure I.6 should be determined experimentally or based on specifications provided by the device manufacturer because the maximum offset to allow energy transfer as well as the stray fields strongly depends on the design of the WPT coils.

2) Unless stated otherwise in this Annex I, the setup should be performed according to IEC 61980-3.

3) Transmit efficiency should be maintained more than 80 % at the offset position.

4) The maximum magnetic field strength in Area 2 is measured at 0,2 m from the vehicle mimic plate using the WPT system and compared to the reference level as shown in Figure I.6.

5) If it exceeds the reference level, it is possible to use the spatially averaged value in the area occupied by the human body. In that case, the averaged magnetic field strength which is measured on a plane at 20 cm from the closest accessible point and 3 points (0,5 m, 1 m, 1,5 m) in height as shown in Figure I.6 can be used.

b) Assessment of incident H-fields of Area 3

1) The maximum magnetic field strength in Area 3 is measured during charging. The field at 0 cm or 10 cm surface on the vehicle mimic plate is measured and compared to the reference level of the magnetic field strength.

2) It is possible to use the spatially averaged value. In that case, the spatially averaged magnetic field strength can be calculated based on the average of four values measured at a, b, c and d in Figure I.7.

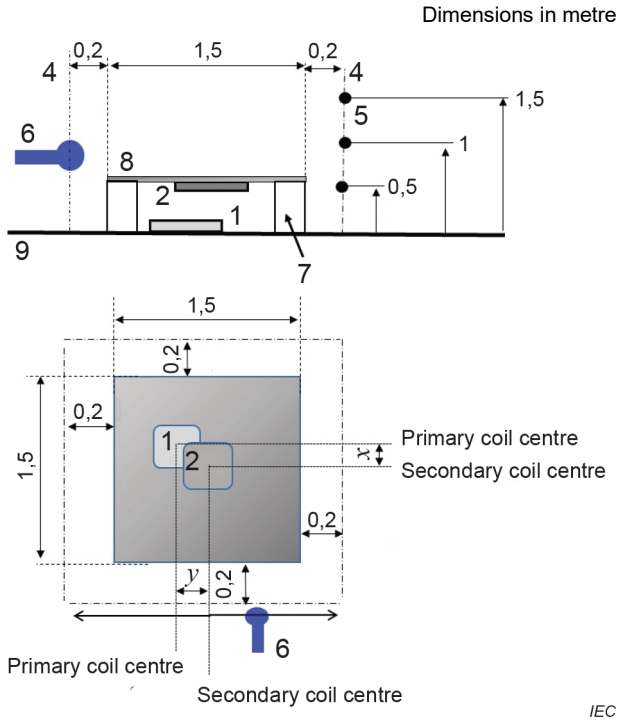

Key

1 Primary device
2 Secondary device
3 EV
4 Scanning area (-----)
5 Scanning point for spatially averaged value (•)
6 Probe (P)
7 Insulating support
8 Vehicle mimic plate
9 Ground plane

Figure I.6 – Area 2 measurement position of vehicle mimic plate (SWPT)

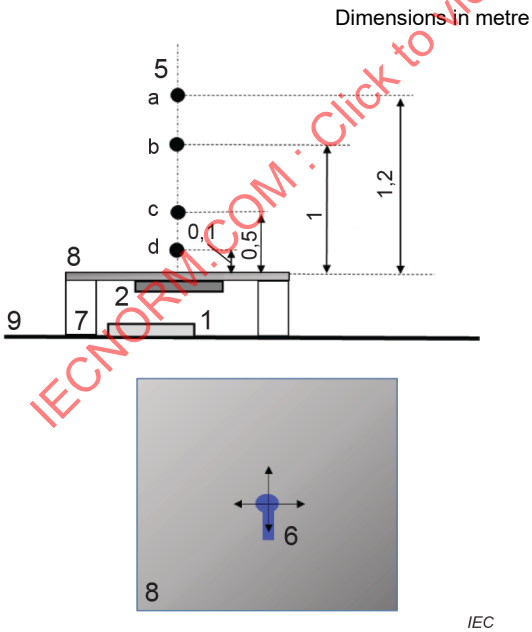

Key

1 Primary device
2 Secondary device
3 EV
4 Scanning area (-----)
5 Scanning point for spatially averaged value (•)
6 Probe (P)
7 Insulating support
8 Vehicle mimic plate
9 Ground plane

Figure I.7 – Area 2 measurement position of vehicle mimic plate (SWPT)

I.1.2.4 Evaluation of incident fields against basic restriction

a) Coupling factor k_L based on the analysis of localized exposure scenarios

   1) Vehicle – The coupling factor k_L 0,15 for ICNIRP 2010 [3] and 0,035 for ICNIRP 1998 [2] and ICNIRP 2020 [4] can be used for EV use case [62]. The conformity assessment procedure is defined in 5.2.4.2.

   2) Using vehicle mimic plate – The coupling factor k_L 0,15 for ICNIRP 2010 [3] and 0,035 for ICNIRP 1998 [2] and ICNIRP 2020 [4] can be used for EV use case [62]. The procedure of conformity is defined in 5.2.4.2.

b) Coupling factor k_G based on the generic gradient source model method (GGSM)

   1) Vehicle – Evaluation of the GGSM can be used. The compliance against the basic restrictions can be confirmed directly. The measurement procedure is defined in 5.2.4.3.

      The local peak magnetic field amplitude and the local gradient generated by the WPT system are measured at less than 0,2 m from the charging automobile using the WPT system.

   2) Using vehicle mimic plate – Evaluation of the GGSM can be used. The compliance against the basic restrictions can be confirmed directly. The measurement procedure is defined in 5.2.4.3.

      The local peak magnetic field amplitude and local gradient generated by the WPT system are measured at less than 0,2 m from the charging automobile using the WPT system.

I.1.2.5 Evaluation of internal electric field against basic restriction

Calculation methods are described in Clause 7.

I.1.3 Assessment procedures considering indirect effects for WPT system for EV

I.1.3.1 General

Figure I.8 presents a flowchart for the assessment procedure for EV use, which is based on Figure 5.

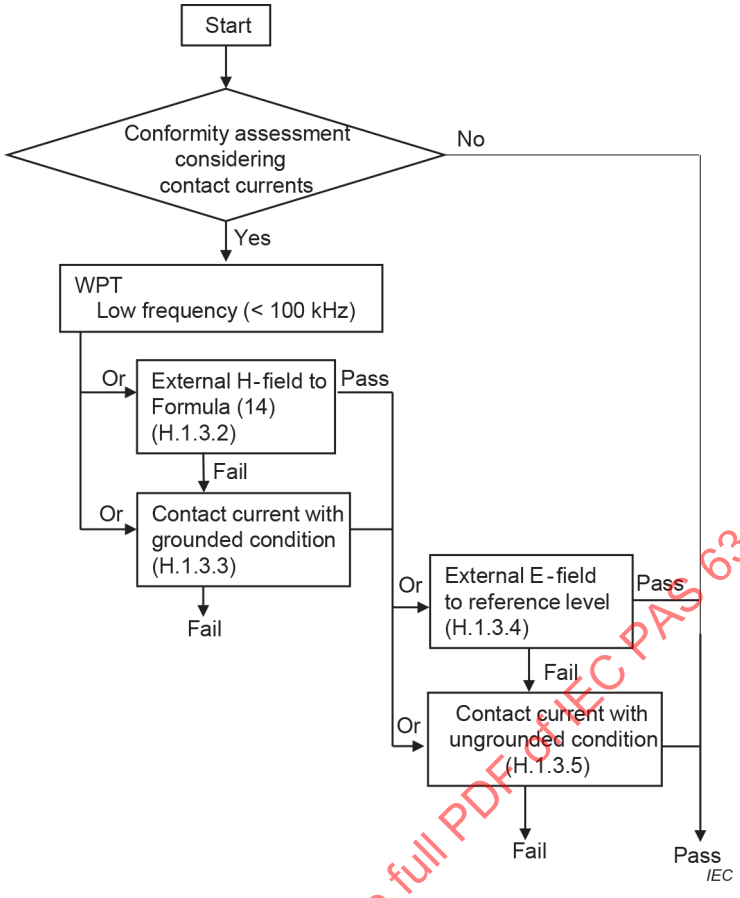

Figure I.8 – Flowchart for EV use and vehicle mimic plate assessment (indirect effect)

I.1.3.2 Assessment of external H-field to reference level

I.1.3.2.1 Vehicle

a) The maximum external H-field in Area 2 is measured at 0,2 m from the charging automobile using the WPT system and compared to the reference level as shown in Figure I.4.

b) If it exceeds the reference level, it is possible to use the spatially averaged value in the area occupied by the human body. In that case, the averaged magnetic field strength which is measured on a plane at 20 cm from the closest accessible point and 3 points (0,5 m, 1 m, 1,5 m) in height as shown in Figure I.4 can be used.

I.1.3.2.2 Using vehicle mimic plate

a) The maximum external H-field in Area 2 is measured at 0,2 m from the vehicle mimic plate using the WPT system and compared to the reference level as shown in Figure I.6.

b) If it exceeds the reference level, it is possible to use the spatially averaged value in the area occupied by the human body. In that case, the averaged magnetic field strength which is measured on a plane at 20 cm from the closest accessible point and 3 points (0,5 m, 1 m, 1,5 m) in height as shown in Figure I.4 can be used.

I.1.3.3 Assessment of contact current with grounded condition

I.1.3.3.1 Vehicle

a) The vehicle should be placed on the ground plane as shown in Figure I.9.

b) After conducting the assessment of I.1.3.2, the grounded metal plate should be placed at the maximum external H-field. The plane of the metal plate should be placed vertical to the vehicle body surface. The separation distance between the vehicle body and the grounded metal plate should be determined by the surface of body or body part edge. (e.g. side mirror for the body side or bumper for the front or rear) as shown in Figure I.9.

c) If the external H-field is not measured, the grounded metal plate is moved to obtain the maximum contact current.

I.1.3.3.2 Using vehicle mimic plate

a) The mimic vehicle should be placed on the ground plane.

b) After conducting the assessment of I.1.3.2, the grounded metal plate should be placed at the maximum external H-field. The plane of the metal plate should be placed vertical to the vehicle mimic plane surface. The separation distance between the vehicle mimic plate and the grounded metal plate should be determined by the surface of the body or body part edge as shown in Figure I.10.

c) If the external H-field is not measured, the grounded metal plate is moved to obtain the maximum contact current.

Dimensions in metre

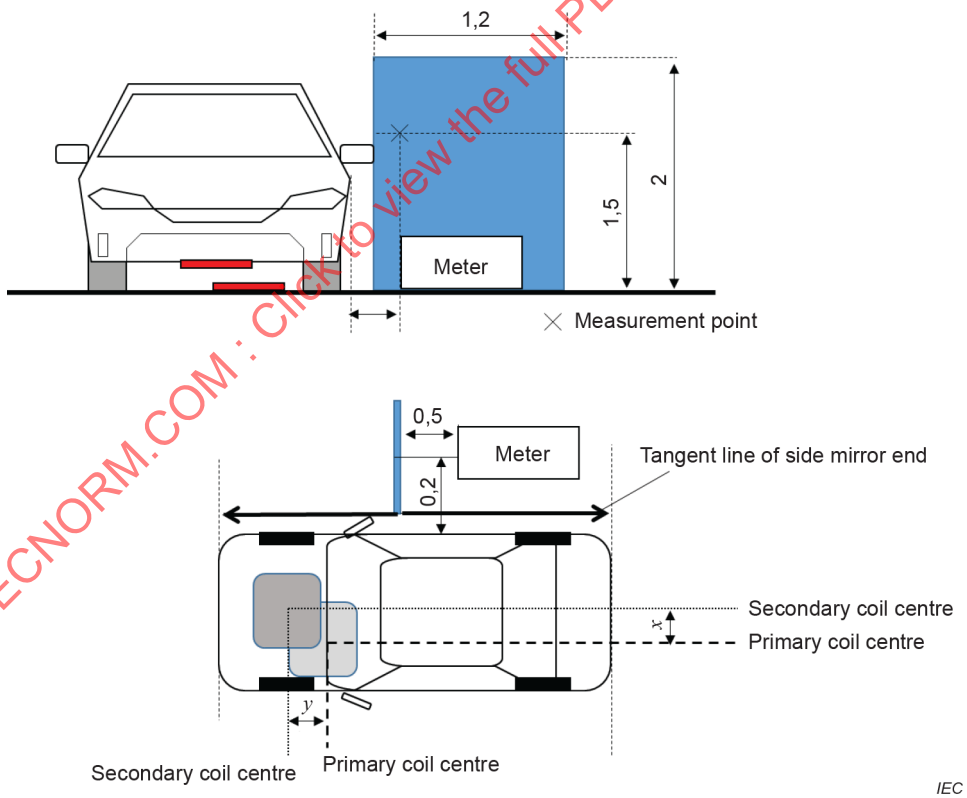

Figure I.9 – Configuration example of contact current with grounded condition: (1) with vehicle

Dimensions in metre

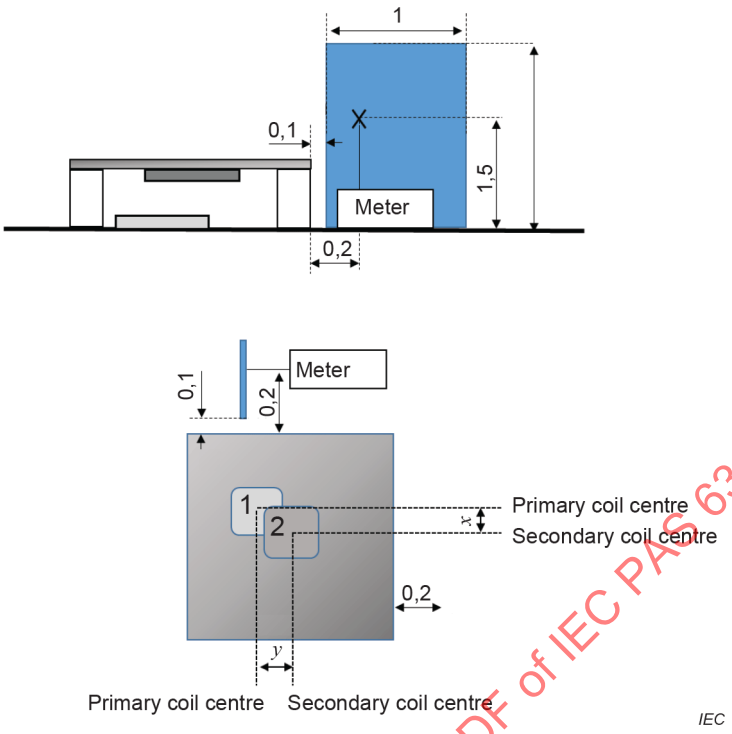

Figure I.10 – Configuration example of contact current with grounded condition: (2) with vehicle mimic plate

I.1.3.4 Assessment of external E to reference level

I.1.3.4.1 Vehicle

a) The maximum external E in Area 2 is measured at 0,2 m from the charging automobile using the WPT system and compared to the reference level.

b) If it exceeds the reference level, it is possible to use the spatially averaged value in the area occupied by the human body or the averaged electric field strength measured at the height of 0,5 m, 1 m and 1,5 m above the ground.

I.1.3.4.2 Using vehicle mimic plate

a) The maximum external E in Area 2 is measured at 0,2 m from vehicle mimic plate using the WPT system and compared to the reference level.

b) If it exceeds the reference level, it is possible to use the spatially averaged value in the area occupied by the human body or the averaged electric field strength measured at the height of 0,5 m, 1 m and 1,5 m above the ground.

I.1.3.5 Assessment of contact current with ungrounded condition

I.1.3.5.1 Vehicle

a) The vehicle should be placed on the ground plane as shown in Figure I.11.

b) The ungrounded metal plate should be larger than 1,2 m × 1,2 m, as defined in 6.3.3 and as shown in Figure I.11.

c) The ungrounded metal plate should be placed on a non-conductive, low relative permittivity (dielectric-constant) material ($\varepsilon_r \leq 1{,}4$), at 100 mm (+0 mm, −25 mm) above the ground.

d) After conducting the assessment of I.1.3.4, the ungrounded metal plate should be placed at the maximum external E. The plane of the metal plate should be placed parallel to the vehicle body surface. The separation distance between vehicle body and the grounded metal plate should be determined by surface of the body or body part edge (e.g. side mirror for the body side or bumper for the front or rear) as shown in Figure I.11.

e) If the external E is not measured, the ungrounded metal plate is moved to obtain the maximum contact current.

I.1.3.5.2 Using vehicle mimic plate

a) The mimic vehicle should be placed on the ground plane as shown in Figure I.12.

b) The ungrounded metal plate should be larger than 1,2 m × 1,2 m defined in 6.3.3.

c) The ungrounded metal plate should be placed on a non-conductive, low relative permittivity (dielectric-constant) material ($\varepsilon_r \leq 1{,}4$), at 100 mm (+0 mm, -25 mm) above the ground.

d) After conducting the assessment of I.1.3.4, the ungrounded metal plate should be placed at the maximum external E. The plane of the metal plate should be placed parallel to vehicle mimic plate. The separation distance between the vehicle mimic plate and the ungrounded metal plate should be determined by the surface of the body or body part edge. (e.g. side mirror for the body side or bumper for the front or rear) as shown in Figure I.12.

e) If the external E is not measured, the ungrounded metal plate is moved to obtain the maximum contact current.

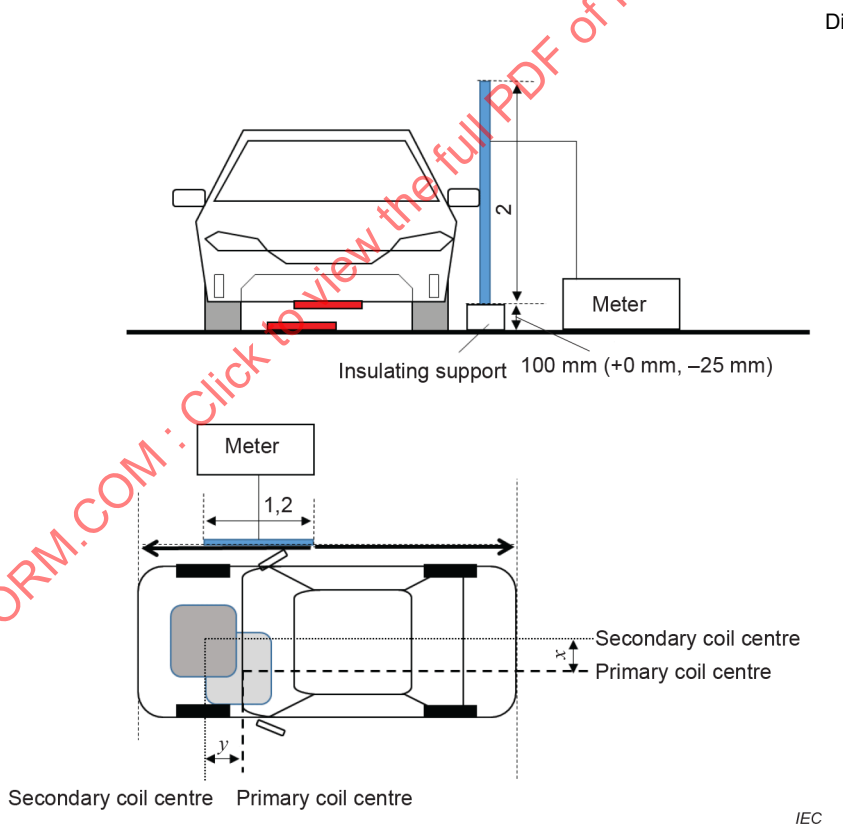

Figure I.11 – Configuration example of contact current with ungrounded condition: (1) with vehicle

Dimensions in metre

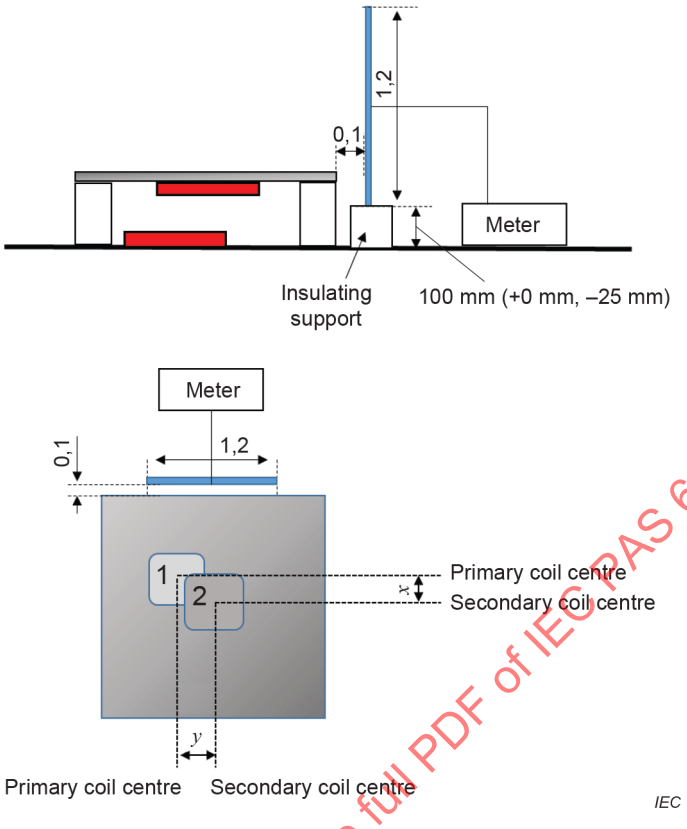

Figure I.12 – Configuration example of contact current with ungrounded condition: (2) with vehicle mimic plate

I.2 Heavy duty vehicle EMF measurement procedure

I.2.1 General

The WPT should operate within 50 % and 100 % of the rated transmission power (RESS [Rechargeable Energy Storage System] in charging mode) during the test. For determining the position of the worst-case for testing the following procedure should be applied.

I.2.2 Step 1

a) Scan with the field-probe according to IEC 62233 (100 cm^2 coil area) over the complete surface of an imaginary vertical plane which is located at 20 cm distance (centre) and parallel to each of the four sides of the vehicle, see Figure I.13 and Figure I.14.

b) The 20 cm should be measured from the most outstanding point of the vehicle surface. The plane should be limited by the size of the vehicle (sides, top) and the ground floor. The centre of the probe should be in the imaginary surface. At least one point should be measured and recorded in the test report for each of the four sides of the vehicle.

c) The centre of the measurement probe should at least be positioned in the middle of the distance between the ground floor and the vehicle under the body during this scan measurement.

d) No measurement is necessary at 50 cm above the height of the vehicle.

Dimensions in metres

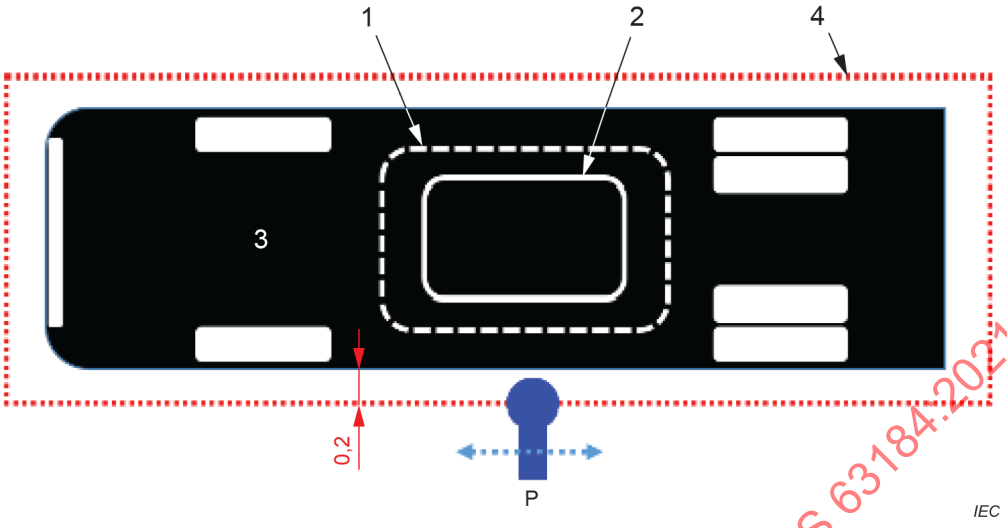

Key

1 Primary device
2 Secondary device
3 WPT bus
4 Virtual area for scanning the worst-case position
P Probe

Figure I.13 – EMF measurement for heavy duty vehicle: top view

Dimensions in metres

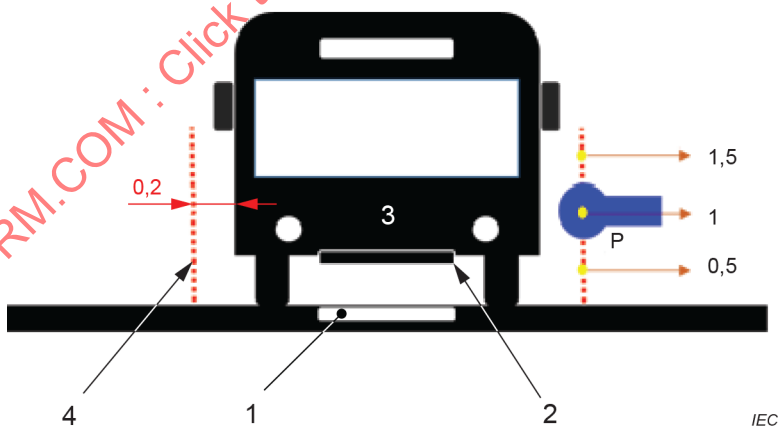

Key

1 Primary device
2 Secondary device
3 WPT bus
4 Virtual area for scanning the worst-case position
P Probe

Figure I.14 – EMF measurement for heavy duty vehicle: side view

I.2.3 Step 2

a) At the positions where there is the maximum reading (worst-case point) during the first step, a final measurement should be performed for a minimum of 10 seconds. The reading at this point should be recorded together with the exact position (x and y) in the test report and should meet the applicable limits.

b) Measurements should be conducted in a nominal position and offset conditions which are defined by system specifications. Measurements should be conducted in the optimum operating position, see also Figure I.13 and Figure I.14.

c) The measurement is indicated as the arithmetic mean of the measured values (i.e. at 0,5 m, 1,0 m and 1,5 m), as depicted in Figure I.14.

d) The measurement values obtained are used to determine whether the fields comply with exposure limits by comparing them with the field limits for general public exposures such as the reference levels or basic restrictions from the ICNIRP, MPE (maximum permissible exposure) from the IEEE or in national regulations.

e) If the measured values are higher than the reference levels, it does not necessarily indicate that the basic restrictions have been exceeded, but a more detailed analysis is necessary to assess compliance with the basic restrictions as stated in the ICNIRP guidelines 1998 [2] and 2010 [3] and IEC 62233 [9].

f) In optimum operating measurement position, the secondary device(s) should be centred on the primary device(s). Manufacturers can use other methods to prove compliance with the limits.

NOTE 1 IEC 62233 provides information about MPE (maximum permissible exposure).

NOTE 2 Exposure limits given in IEC 62233 Annex B (informative) are for information purposes only and they do not represent an exhaustive list of limits. It is the responsibility of the users of this standard to ensure that they use the current version of the limit sets as specified by national authorities.

NOTE 3 The limitation follows the values of ICNIRP Guideline 1998 [2], ICNIRP Guideline 2010 [3] and IEEE Std C95.6-2002 [5], etc.

I.2.4 Step 3

a) At the positions where there is the maximum reading (worst-case point) during the third step, a final measurement should be conducted for a minimum of 10 seconds. The reading at each point should be recorded together with the exact position (x and y) in the test report and should meet the applicable limits.

b) The measurement is indicated as the arithmetic mean of the measured values (i.e. at 0,5 m, 1,0 m and 1,5 m) such as shown in Figure I.15.

c) The measurement values obtained are used to determine whether the fields comply with exposure limits by comparing them with the field limits for general public exposure such as the reference levels or basic restrictions from the ICNIRP, MPE (maximum permissible exposure) from the IEEE or in national regulations.

Dimensions in metres

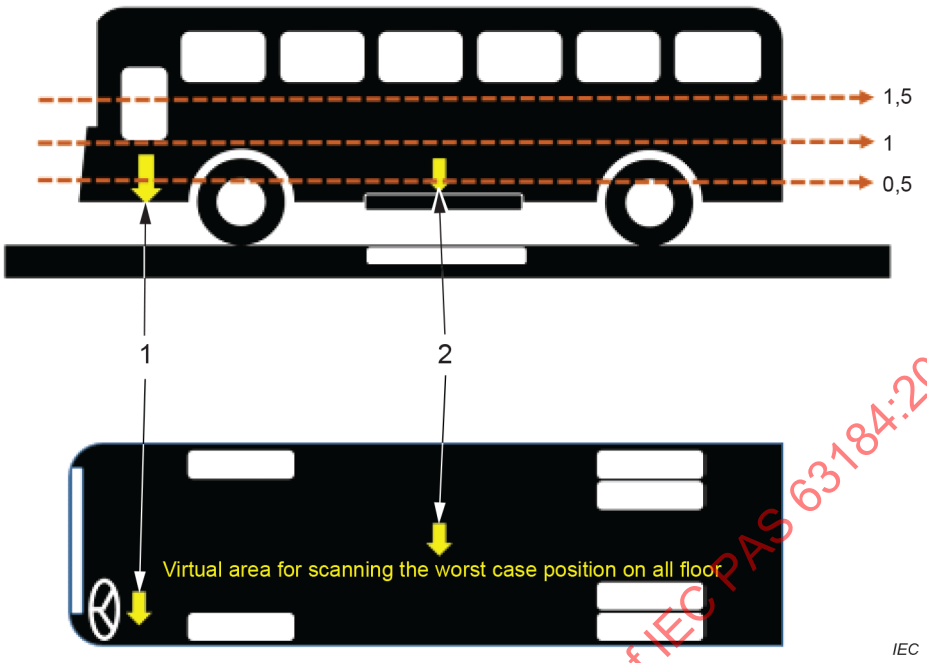

Key

1 Measurement point of driver floor

2 Virtual area for scanning the worst-case position on entire floor

Figure I.15 – Measurement points on the inside floor of WPT bus

I.3 Drone

I.3.1 Introduction

Drones refer to unmanned aerial vehicles (UAV) that can be controlled by radio waves. In general, the operating time of a drone is currently less than 20 minutes to 40 minutes due to limited battery capacity. In order to increase the operating time, the WPT technology is applied to charge the drone. As the WPT systems for drones are used above several tens of watts, human exposure to electromagnetic fields (EMFs) is increasing accordingly. Therefore, the evaluated human exposure to EMFs should conform to electromagnetic exposure guidelines, recommendations, or legislation.

I.3.2 Assessment procedures of WPT system for drone

I.3.2.1 General

a) I.3.2 provides the assessment procedures for considering the direct effects of EMFs from the WPT system for drone. The direct effect deals with the internal electric field or current density, and/or SAR.

b) According to the exposure guidelines both stimulation and thermal effects need to be considered for the WPT system for drone at the frequency range between 100 kHz and 30 MHz, and the stimulation effects are applicable to the WPT system for drone at frequency less than 100 kHz.

c) A human body may be situated close to the WPT system for drone (e.g. 20 cm or less). Therefore, it is possible to assess the exposure in an area at a distance < 20 cm from the WPT system.

I.3.2.2 Assessment of incident field around the WPT system for drone

Testing of the WPT system for drone should be assessed during the maximum charging current state, but consistent with the normal operating conditions as specified by the manufacturer. For evaluating the incident field against reference level, the following procedure should be applied;

- Step 1: Scan with the field-probe over the complete imaginary vertical plane which is located at the normal user distance (d) (e.g. 20 cm or less from the WPT system) and parallel to each side of the WPT system (charging station). Figure I.16 shows the measurement position for the WPT system for drone. The edge of the probe should be on the imaginary surface. At least one point should be measured and recorded in the compliance testing report for each side of the drone.
- Step 2: At the position where there is the maximum reading point (worst-case point), the measurement should be performed. The reading value at this point should be recorded together with the exact position in the compliance testing report.
- Step 3: The maximum field strength is compared to the reference level of the exposure guidelines.
- Step 4: If the electric and magnetic field strength exceed the reference level, proceed to the next evaluation step using the coupling factor k_L or k_G according to 5.2.4.2 and 5.2.4.3.

The spatial averaging may not be practical if only a small part of the body is exposed to the WPT system for drone. Electric and magnetic field strengths may be spatially averaged over the exposed regions of the human body, with the important provision that the basic restrictions for local SAR and current density or internal electric field are not exceeded. The detailed method of spatial averaging is not mentioned in this document.

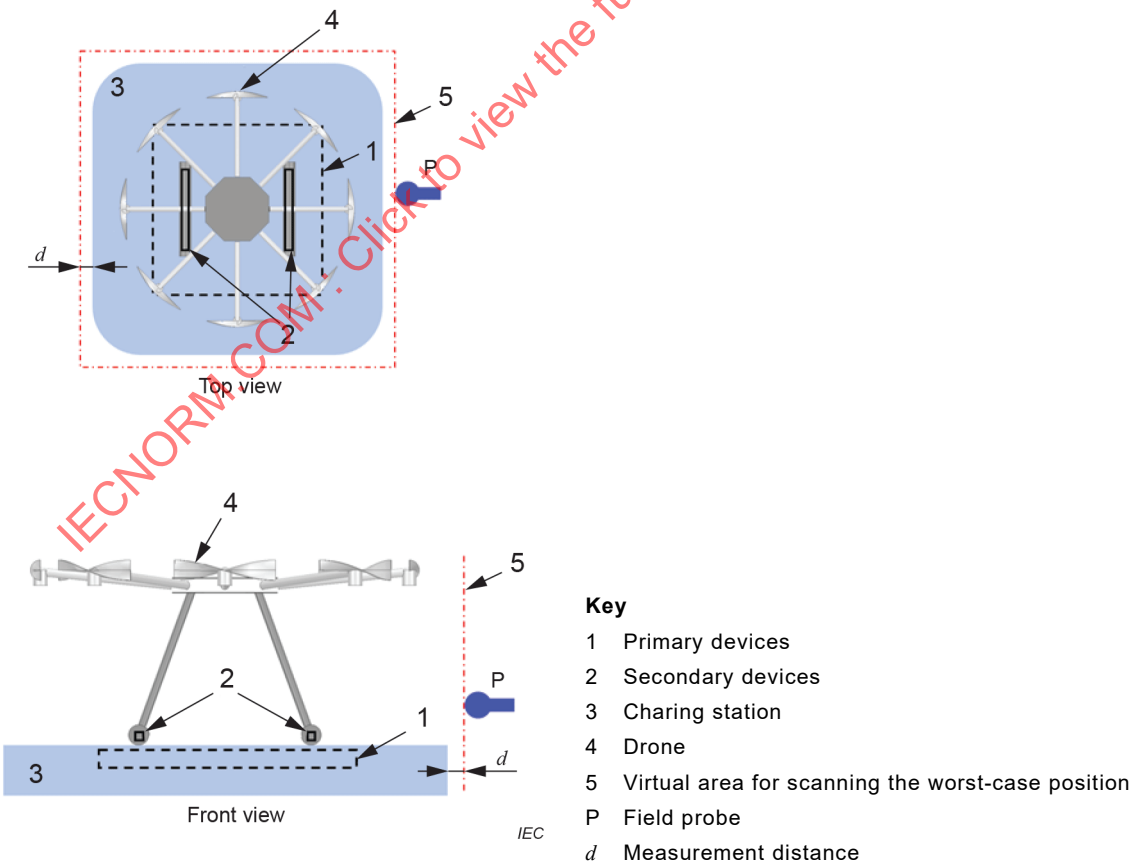

Figure I.16 – Measurement position

I.3.2.3 Assessment of incident field against basic restrictions

I.3.2.3.1 General

As the reference levels are derived from the uniform EMF exposure in a human body model, the evaluation for the incident field may be too conservative for localized WPT exposure. In such a condition, coupling factors can be applied to an evaluation as a corrective method for the non-uniformity of the EMFs.

If the coupling factors are not applicable, proceed to the next evaluation step using basic restrictions.

I.3.2.3.2 Assessment using coupling factor k_L

Coupling factor k_L is specified by the ratio of induced quantities (current density, local SAR, or internal electric field) and incident magnetic field strength. Evaluation conditions such as operating frequency, field distribution, distance to human body, etc., should be equivalent to the condition used in the derivation of the coupling factor.

When the operating frequency of the WPT system for drone is below 100 kHz, the coupling factor for stimulation effects should be used. Between 100 kHz and 10 MHz, the coupling factors for stimulation effects and thermal effects should be used. Above 10 MHz, the coupling factor for thermal effects should be used.

The evaluation procedure using the coupling factor is as follows:

- Step 1: Compute or measure the internal electric field or current density, and/or SAR.
- Step 2: Check the following criteria.
  - Induced quantities, such as an internal electric field, current density or SAR caused by an incident electric field are negligible compared to that by incident magnetic field.
  - The whole-body average SAR is marginal compared to the respective limits and contribution of the local average SAR or the internal electric field is dominant.
- Step 3: Calculate the coupling factors using Formula (3) through Formula (5) described in 5.2.4.2.
- Step 4: The maximum incident magnetic field strength ($H_{inc,max}$) is multiplied by the coupling factor and compared to the reference level:

$$H_{k_{L,J}} = k_{L,J} \times H_{inc,max} \quad \text{(I.1)}$$

$$H_{k_{L,E}} = k_{L,E} \times H_{inc,max} \quad \text{(I.2)}$$

$$H_{k,SAR} = k_{L,SAR} \times H_{inc,max} \quad \text{(I.3)}$$

where

$k_{L,J}$, $k_{L,E}$, $k_{L,SAR}$ are coupling factors for current density, internal electric field, and local SAR, respectively;

$H_{L,J}$, $H_{L,E}$, $H_{L,SAR}$ are computed magnetic field strengths using coupling factors.

- Step 5: If computed magnetic field strengths using the coupling factors exceed the reference level, proceed to the next evaluation step using basic restrictions.

I.3.2.3.3 Assessment using coupling factor k_G

The assessment method using the coupling factor k_G is based on frequency, magnetic flux density magnitude (B_{xyz}) and the local magnetic flux density gradient (G_n) at any point in free space.

The evaluation procedure using the coupling factor k_G is as follows:

- Step 1: Measure the magnetic field gradient (G_n) using a gradient field probe at the closest accessible location around the WPT system for a drone.
- Step 2: Calculate the coupling factors k_G using Formula (7) through Formula (10) (see 5.2.4.3).
- Step 3: The internal electric field, current density and SAR are estimated using Formula (11) through Formula (13).
- Step 4: If the estimated current density, internal electric field, and/or local SAR using the coupling factor k_G exceeds the basic restrictions, proceed to the next evaluation using basic restrictions.

I.3.2.4 Assessment against basic restrictions

SAR can be measured using a small probe in a liquid-filled phantom model simulating the human body, which is exposed to EMFs created by the WPT system for frequencies over 4 MHz, and when the evaluation against basic restrictions such as WPT system for drone using the measurement method may not be practical. Therefore, the current density, internal electric field, and SAR to be compared with basic restrictions, should be evaluated by numerical simulation using the WPT system model and human body model.

The assessment procedure of the WPT system for drone compliance testing with respect to basic restrictions using numerical simulation is as follows:

- Step 1: Select and validate the numerical computation method.
- Step 2: Model the WPT system for drone.

  The requirements for the numerical modelling of the WPT system are listed below, and they should be provided by the manufacturer.

  1) Electrical and physical specifications:
     - operating frequency;
     - geometries of the primary device and secondary device (size of device, shape, alignment);
     - interval of primary device and secondary device;
     - metal and magnetic material.
  2) Operating conditions:
     - maximum amplitude of currents for primary device and secondary device;
     - primary device to secondary device relative phases condition.
- Step 3: Validate the modelling of the WPT system for drone is valid by comparing electromagnetic fields with the numerical computation results and measurement results at the validation data point. The validation method of modelling is described in detail in Clause G.2.
- Step 4: Select the worst-case exposure scenario considering various WPT operational conditions.
- Step 5: Select a numerical human body model and evaluate the induced quantities.
- Step 6: Calculated the induced quantities for comparison with the basic restrictions.